Z.E. Elektronenmikroskopie
Prof. Dr. Paul Walther

and

Institut für Virologie
Prof. Dr. Thomas Mertens

Electron microscopic investigation of cytomegalovirus egress after high-pressure freezing, freeze-substitution and plastic embedding

Dissertation zur Erlangung des Doktorgrades der Humanbiologie
der Medizinischen Fakultät der Universität Ulm

Christopher Buser,
New York, N.Y., USA

2006

Amtierender Dekan: Prof. Dr. Klaus-Michael Debatin

1. Berichterstatter: Prof. Dr. Paul Walther

2. Berichterstatter: Prof. Dr. Thomas Mertens

Tag der Promotion: 8. Dezember 2006

Abstract

Modern cryo-preparation techniques for biological electron microscopy have a great impact on the preservation of the sample structure. Among these, high-pressure freezing, freeze-substitution and plastic embedding of cell cultures for transmission electron microscopy allows new insights into various processes in cell biology due to its superiority over conventional preparation by chemical fixation. On the other side, the recent virological research on herpesviruses and especially on cytomegaloviruses has mainly relied on biochemistry, molecular biology and fluorescence microscopy techniques. Especially the introduction of the viral genome into bacterial artificial chromosomes, thus greatly facilitating the genetic manipulation of the over 200 genes of cytomegaloviruses, allowed the assessment of protein functions in the viral cycle by mutagenesis. Still, deletion of many genes only weakly affects the viral morphogenesis so that the role of the respective proteins has to be investigated at the ultrastructural level. Additionally, this purely morphological characterisation of such phenotypes allows an unbiased approach to identify the potential functions of the respective protein. In this study, the possibilities of genetic manipulation of the virus were combined with the ultrastructural information acquired by cryo-preparation for transmission electron microscopy. To better visualise the stages of morphogenesis, the freeze-substitution protocol was optimised by addition of water to increase the contrast and retention of cellular structures. For substitution media based on acetone the addition of osmium tetroxide and uranyl acetate dissolved in water was found to be optimal, resulting in a mixture of 0.2 % osmium tetroxide, 0.1 % uranyl acetate and 5 % water in acetone. Using this approach the viral morphogenesis of the murine as well as the human cytomegalovirus were reinvestigated in comparison to chemical fixation and the morphogenesis of alphaherpesviruses. In both cytomegalovirus systems it was observed that the viral nuclear egress by budding into the perinuclear space does not occur at the nuclear periphery as postulated. Instead, cytomegaloviruses induce deep tubular infoldings of the inner nuclear membrane, through which nucleocapsids bud to acquire their primary envelope and access the perinuclear space. Also in the cytoplasmic events, especially in the release of intracisternal, mature virions, several structural intermediates were seen that are not adequately explained by current models. Further, the following mutant viruses were investigated for their ultrastructural

phenotypes: In the murine cytomegalovirus morphogenesis, the protein pM97 and pM48.3 were implicated in the nuclear processes of capsid formation and localisation. In the phase of nuclear egress, pM50 was found to have an essential function in the passage through the infolded inner nuclear membranes. In the human cytomegalovirus, pUL97 was suggested to have a similar function in nucleocapsid formation as its homolog pM97. A mutant deleted in all four viral G-protein coupled receptors did not show any defects in morphogenesis. Additionally, the role of the two proteins ppUL35 and pUL35A, both transcribed from the open reading frame UL35, were investigated by mutation of the start codons. According to their localisation, a lack of the nuclear protein pUL35A lead to a defect in early nuclear morphogenesis, while the lack of the cytoplasmic tegument protein ppUL35 caused a cytoplasmic tegumentation defect. Taken together, these results demonstrate the power of the combination of cryo-preparation techniques with genetic manipulation of cytomegaloviruses in elucidating the mechanisms of viral morphogenesis.

Table of Contents

1 Introduction 8
1.1 Sample Preparation Techniques 8
1.1.1 Chemical Fixation 9
1.1.2 Ambient Pressure Freezing Techniques 10
1.1.3 High-Pressure Freezing 11
1.1.4 Freeze-Substitution and Embedding 12
1.1.5 Fixatives for Freeze-Substitution 13
1.1.6 Evaluation of the Preparation Process and Artefacts 14
1.1.7 Cryo-Transmission Electron Microscopy 15
1.2 Cytomegaloviruses 16
1.3 Aim of the Project 21
2 Materials and Methods 22
2.1 Reagents 22
2.2 Cell Culture and Viruses 23
2.2.1 Experiments with Murine Cytomegaloviruses 23
2.2.2 Experiments with Human Cytomegaloviruses 23
2.2.3 Experiment with the Poxvirus Strain MVA 24
2.3 Sample Preparation for Electron Microscopy 25
2.3.1 Preparation of Sapphire Disks and Cell Cultures 25
2.3.2 High-Pressure Freezing 25
2.3.3 Freeze-Substitution, Plastic Embedding and Sectioning 26
2.3.4 Immunogold Labeling 28
2.3.5 Image Analysis 28
2.3.6 Correlative Microscopy of DNA and RNA Distributions 29
2.3.7 Electron Tomography and Stereo Imaging 29
2.4 Biochemistry and Molecular Biology 30
2.4.1 Isolation of Cell Nuclei 30
2.4.2 PCR Amplifications 30
2.4.3 SDS PAGE 31
3 Results 32
3.1 Optimising Freeze-Substitution 32
3.1.1 Influence of the Water Content in Substitution Based on Acetone 32
3.1.2 Other Solvents and Water 38

3.1.3 Duration of Substitution 38
3.1.4 Fixatives and Concentrations 39
3.1.5 Application of HPF / FS on Poxvirus Morphogenesis 41
3.2 MCMV 43
3.2.1 MCMV (Smith Strain) Morphogenesis 43
3.2.2 Phenotypical Characterisation of an M97-Deleted MCMV 51
3.2.3 Phenotypical Comparison of MCMV ΔM97 with MCMV UL97 55
3.2.4 Investigation of MCMV Nuclear Egress by Conditional Expression 55
3.3 HCMV 59
3.3.1 HCMV AD169 Morphogenesis 59
3.3.2 Involvement of Endocytic Compartments in HCMV egress 62
3.3.3 Morphological Analysis of an UL97-Deleted HCMV 63
3.3.4 Imaging of an HCMV lacking 4 viral G-Protein coupled Receptors 64
3.3.5 Analysis of the diverse function of two proteins encoded by UL35 66
4 Discussion 69
4.1 Sample Preparation Technique 69
4.1.1 The Influence of Water during Freeze-Substitution 70
4.1.2 Duration of Substitution 72
4.1.3 Fixatives and Concentrations 73
4.1.4 Visualisation of the Poxvirus Immature Virion Double Membranes 74
4.2 MCMV 75
4.2.1 MCMV (Smith strain) Morphogenesis 75
4.2.2 Phenotypical Characterisation of an M97-deleted MCMV 80
4.2.3 Observation of Conditional MCMV Variants 82
4.3 HCMV 85
4.3.1 HCMV AD169 Morphogenesis 85
4.3.2 Morphological Analysis of an UL97-Deleted HCMV 87
4.3.3 The role of G-Protein Coupled Receptors in HCMV Morphogenesis 88
4.3.4 UL35 and UL35A fulfil Diverse Roles in HCMV Morphogenesis 88
4.4 Model of Cytomegalovirus Morphogenesis 90
4.5 Conclusions 91
5 Literature 92
6 Acknowledgments 98

Abbreviations

AD169	fibroblast adapted HCVM strain, model virus for HCMV infection
CMV	cytomegaloviruses, *betaherpesvirinae*
ER	endoplasmic reticulum
FA	formaldehyde
FS	freeze-substitution
GA	glutaraldehyde
GFP	green fluorescent protein, originating from *Aequora victoria*
GPCR	G-protein coupled receptor
HA	hemaglutinin epitope tag from influenza virus
HCMV	human cytomegalovirus, *betaherpesvirinae*
HFF	human foreskin fibroblast cells
HHV6	human herpesvirus 6
HSV	herpes simplex virus, *alphaherpesvirinae*
HPF	high-pressure freezing
HUVEC	human umbilical vein endothelial cells
kbp	kilobasepairs
ORF	open reading frame
MCMV	murine cytomegalovirus, *betaherpesvirinae*
MOI	multiplicity of infection, [PFU/cell]
MTOC	microtubule organising centre
PCR	polymerase chain reaction
PFU	plaque forming unit, infectious unit in plaque titration assays
p.i.	time post infection
PI(3)K	phosphatidyl inositol (3) kinase
PrV	pseudorabies virus, *alphaherpesvirinae*
pUL…	protein encoded by the UL… ORF
ppUL	phosphoprotein encoded by the UL… ORF
SDS-PAGE	sodium dodecyl sulfate polyacrylamide gel electrophoresis
TB40E	endotheliotropic HCMV strain
TEM	transmission electron microscope (or microscopy)
TGN	trans-Golgi network
vDNA	viral DNA

1 Introduction

Virology and electron microscopy have a long tradition of cooperation. The size of viruses, ranging from 30 to 400 nanometers, predisposes electron microscopy as the tool to visualize and investigate these peculiar “life-forms”. One of the first biological objects imaged with a transmission electron microscope (TEM) was the tobacco mosaic virus [96]. In the last decades this method has been extensively used in biology especially with the development of chemical fixation, plastic embedding and thin sectioning, which allowed the visualisation of biological structures at a resolution of few nanometers and brought cell biology to the eye and the mind of the researcher. This method lead to the discovery of elementary processes in cell biology, e.g. the secretory pathway in pancreatic cells [15]. In recent years, electron microscopy has shown its importance also in pathogen diagnostics, e.g. by the discovery of the coronavirus responsible for the SARS epidemic [30, 46]. It was, however, already noted by Palade in 1951 that the most critical point in biological EM would be the process of fixation [68]. In recent years with developments in molecular biology (e.g. PCR and cloning) and fluorescence microscopy (GFP-tagging, live cell imaging and single particle tracking), electron microscopy has lost a lot of its previous “flair” in virological science and much know-how has been lost. But with the development of new cryo-preparation techniques and the conquest of the third dimension by electron tomography, electron microscopy and virology are again profiting from each other. These sophisticated new techniques make research more and more specialized and it becomes impossible for the researcher to use all technologies available to answer his specific questions. Yet, this situation creates unique opportunities for the interdisciplinary scientist in bringing together different methods to create novel approaches to old and new unanswered questions. The object of virological research in this thesis is the morphogenesis of cytomegaloviruses seen with the use of cryo-preparation techniques for electron microscopy.

1.1 Sample Preparation Techniques

The main limitation in imaging biological specimens in the TEM is that the sample has to be very thin (approximately 60 to 80 nm for standard TEM) for proper image formation as explained below. Accordingly, most samples have to be sectioned,

which is only possible with solid samples. Additionally, standard TEMs operate with high-vacuum conditions with at least 10^{-5} to 10^{-6} mbar. At this low pressure, liquid water evaporates almost instantaneously which would destroy an aqueous sample. For ambient temperature TEM of biological samples, therefore, the sample has to be prepared by removing the water and replacing it with plastic while maintaining the structural features as best as possible. What at the first moment appears to be an impossible task has been solved by substitution of the water first by an organic solvent, which is then exchanged with the liquid plastic monomers that are then polymerised. To retain the specimen structure during this processing, the sample has to be fixed before substitution to reduce the extraction of molecules. An other line of difficulties arises in image formation: In order to produce an image, the beam has to penetrate the sample and has to be scattered by it. The image contrast is mainly formed by scattering of electrons to high angles, which is proportional to the ordering number of the atom (i.e. scattering contrast or amplitude contrast, for in depth information refer to [71]). The light biological elements are very poor scatterers and additionally are embedded in plastic, i.e. mainly carbon. Direct imaging of such a sample would give images of very low contrast. To increase the visibility of the biological structure heavy metal contrasting is performed during sample preparation. The prerequisite that the beam has to penetrate the sample draws further restrictions on the sample geometry.

The reason is that multiple scattering events that blur the image are dependent on the mean free path length of the electrons, which again is dependent on the sample composition, sample thickness and the electron energy. For standard TEMs operating at electron energies of 80 to 120 kV and for heavy metal stained plastic embedded biological specimens the thickness must be around 60 to 100 nm to ensure good imaging conditions. For intermediate-voltage TEMs suitable for electron tomography and operating at 300 kV acceleration voltage the thickness can be increased to approximately 500 nm. Accordingly, the plastic sample has to be sectioned to this thickness with an ultramicrotome. Different preparation techniques to deal with these problems have been designed, all having their specific advantages and limitations.

1.1.1 Chemical Fixation

Chemical fixation is based on the crosslinking abilities of aldehydes, usually glutaraldehyde and formaldehyde, which mainly react with amino groups.

Subsequently, a postfixation with osmium tetroxide is done followed by block contrasting in uranyl acetate, dehydration and plastic embedding. Considerable progress has been made in adapting fixative solutions to the osmotic properties of the specimen, but the inherent problem of chemical fixation remained, i.e. the duration of penetration and reaction of the fixative (in the range of seconds to minutes) is several orders of magnitude slower than the cell biological processes in a living cell we are able to observe (fast processes such as membrane fusion during exocytosis can occur within milliseconds [31]. Accordingly, artefacts can be expected in structures with low fixation potential (e.g. membranes with low protein content) and such behind permeation barriers (e.g. membranous compartments as nucleus, mitochondria etc.). This leads to artefacts which can be identified with the modern cryo-techniques by comparison with chemically fixed specimens. Accordingly, several artefacts are spread and sometimes functionally interpreted in the literature, among others the bacterial mesosome [18], the appearance of the wide mitochondrial cristae and the typical viral DNA-condensation (see below). More subtle differences can be seen in the appearance of most organelles, e.g. the size and tubulation of endocytic vesicles [64], the cisternae of the endoplasmic reticulum (shrinkage after chemical fixation) and general increased extraction and/or fragmentation of membranous compartments (see below). Still, chemical fixation is easy to perform and can be used to fix bulk specimens (> 1 mm^3), which is not feasible with cryo-methods as explained in the following paragraphs.

1.1.2 Ambient Pressure Freezing Techniques

Attempts to circumvent the problems of chemical fixation were made with the introduction of cryofixation techniques. The fixation of biological samples by freezing lead to a great reduction of the immobilization times down to few milliseconds, i.e. in the range of fast cell biological processes such as membrane fusion [31]. On the other hand, freezing brought new problems due to the physical properties of water which is the main constituent in biological samples. Water has a high heat capacity and crystallizes when frozen, which leads to the destruction of the sample structure. Theoretically, their formation can be prevented if the water is cooled so fast that the water molecules do not have time to rearrange in crystals, but instead freeze in an amorphous state. For this, cooling rates above 100,000 K/s have to be achieved [81, 88]. Due to the large heat capacity of water the cooling rate is reduced with increasing specimen thickness which results in good freezing at the surface of the

samples but very poor cooling in the centre thus leading to extensive ice crystal damage.

Several ways of freezing were established and are still used: Spray freezing (by spraying a suspension in liquid propane), plunge freezing (by immersion of the sample into a cryogen), slam freezing (by slamming the sample on a cooled metal block) and propane jet freezing (by spraying the sample with liquid propane). These methods provide adequate freezing into sample depths of a few micrometers. The freezing quality can be enhanced by infiltration of the live specimen with cryoprotectants, which reduce the formation of ice crystals. However, this step abolishes the main advantage of cryo-preparation techniques, i.e. the ability to immobilise a live specimen in a fully physiological state. Accordingly, these techniques are mainly used for freezing thin liquid films adsorbed on EM grids.

1.1.3 High-Pressure Freezing

The low freezing depth with plunge freezing was tackled by the development of high-pressure freezing (HPF). HPF makes use of a property of water: At 2075 bars pressure, the freezing point of water is reduced to -22°C, thus slightly but significantly reducing the temperature difference between the liquid and the solid amorphous phase. Accordingly, the transition time through the crystalline phase is shortened by synchronized application of pressure and liquid nitrogen for cooling, thus reducing the growth of ice crystals. This way biological samples of up to approximately 200 µm thickness can be frozen without visible segregation patterns and this without addition of cryoprotectants. This was developed by Moor, Höchli and Riehle around 1970 [59, 60, 73] and technically realised by Müller and Moor in 1984 [62].

Several practical aspects have to be considered. Since the sample has to be protected from the strong liquid nitrogen jet, a good thermal conductivity has to be ensured and an optimal geometry of the specimen has to be found [81, 88]. Also the support for cell culture monolayers has to be chosen such, that the cells properly grow and adhere to it. Additionally, at the end of the preparation procedure when the cells are in plastic it has to be possible to remove the support without damaging the sample. This was solved by growing cells on round sapphire discs with 3 mm diameter that have been coated with a 20 nm carbon film [11]. Sapphire has been chosen because of its transparency, high stability and the relatively good thermal

conductivity. The carbon layer is added to ensure better growth of the cells and also serves as interfacial layer for easy removal of the sapphire disc from the polymerised plastic sample before sectioning. As protection from the liquid nitrogen jet the sapphire discs are mounted between two aluminium planchettes in a sandwich construction [62], where the upper planchette has a cavity of 100 µm towards the cells (see Chapter 2.3.2). To ensure proper thermal conductivity, the cells with the sapphire disc and the two planchettes are immersed in 1-hexadecene, which has a low heat capacity and is not miscible with water and thus ideal to transmit pressure and cooling without influencing the cellular interior in contrast to cryoprotectants [87].

1.1.4 Freeze-Substitution and Embedding

In order to observe the samples in the vacuum of the conventional microscope the biological sample needs to be solid to prevent evaporation. Accordingly, the water has to be substituted by a solvent and the solvent by the liquid plastic which is then polymerised. With frozen material this is done by immersion of the sample in an organic solvent (usually containing fixatives) pre-cooled to -90 °C, slow warming to approximately 0 °C and followed by embedding. At this temperature the fixatives have to be removed by washing with pure solvent so they do not react with the plastic monomers. The sample is then gradually immersed in plastic / solvent mixtures with increasing plastic content to ensure complete perfusion with the monomers. This is followed by polymerisation by heat or UV-irradiation, depending on the type of plastic used. The embedded samples are then sectioned with diamond knives to sections of approximately 60-80 nm thickness for standard TEM applications and eventually further contrasted with lead and uranium salts, and imaged in the TEM.

The physical processes that ultimately lead to the substitution of the water are fairly understood and pose a difficulty in designing optimal substitution protocols. In addition, the reactivity of the added fixatives also has to be considered in concert with the solvent properties to reduce extraction of cellular molecules during the substitution. Quantification of the substitution capacity of different solvents at constant temperatures was done by Humbel and Müller for diethyl ether, acetone and methanol [37]. As expected, the speed of substitution increases with the temperature and is fastest for methanol > acetone > diethyl ether. They could also show that the addition of water significantly increased the time for complete substitution especially at low temperatures and stronger for acetone than for methanol. Accordingly, one

central dogma of substitution was that the solvent has to be free of water to retain its full substitution capacity. Intriguingly, it has been shown by Walther and Ziegler that the addition of 1 - 5 % water increases the visibility of cellular structures, especially of membranes [92]. In daily use, acetone has proven to be the best solvent in respect to structural appearance of the samples, but also ethanol and methanol are widely used.

1.1.5 Fixatives for Freeze-Substitution

To stabilize the specimen structure during the freeze-substitution process fixatives are added to the solvent, but in spite of their widespread use little is known about their chemical properties while interacting with a biological specimen at low temperatures. The main fixative for samples embedded in Epon traditionally is osmium tetroxide (OsO_4), which is able to cross link C=C double bonds e.g. in unsaturated fatty acids. The osmium is reduced during the process, which probably leads to its retention at the charged interface of the membrane, thus also contributing to membrane contrast [26]. The reactivity of osmium tetroxide starts at approximately –70 °C [93]. This substance greatly contributes to membrane retention and is essential for structural investigations. Unfortunately, is it also highly proteolytic at higher temperatures (around 0 °C) and thus not suitable for most immunolabeling studies. Often osmium tetroxide is combined with uranyl acetate ($UO_2(CH_3COO)_2$) which strongly binds to phosphate and weaker to carbonyl groups by ionic interaction and thus has slight crosslinking and strong contrasting activity (especially for nucleic acids and membranes). There is evidence that uranyl acetate is active at even lower temperatures than osmium tetroxide. A further class of frequently used fixatives are the aldehydes that mainly react with amino groups. In freeze-substitution glutaraldehyde (GA; $HCO\text{-}CH_2\text{-}CH_2\text{-}CH_2\text{-}COH$) is often used in low concentrations (0.1 % or less) to increase the structural retention of samples designated for immuno-labelling without strongly affecting the respective antigens. Due to its two aldehyde groups and the ability to form long polymers GA very efficiently cross links molecules and structures over various distances. During freeze-substitution GA exhibits only moderate crosslinking activity below –50 °C that increases dramatically towards 0 °C [37]. Even addition of 0.01 % greatly increases the structural retention during substitution and thus makes it a good but slightly inferior alternative to osmium tetroxide.

Further fixatives less frequently used for freeze-substitution are among others tannic acid, formaldehyde or potassium permanganate [27, 95]. In summary, many protocols and fixatives can be used depending also on the investigated sample and the specific structure to be imaged.

1.1.6 Evaluation of the Preparation Process and Artefacts

Since the quality of the preparation can only be assessed after completion of the entire process it can only be optimised in an empirical way. A significant problem in this approach is that the freezing process is usually not completely reproducible, which can be seen as variation of quality in samples frozen and substituted under identical conditions. This makes it difficult to address the question of designing optimal substitution protocols, since any flaws seen in the sections might as well reflect inadequate freezing or handling of the samples. Accordingly, many different protocols are available in the literature. In this respect it is important to note, that this work was done with a prototype of the new HPF 01 (Wohlwend Engineering), which greatly increases the reproducibility of the freezing process due to its special design and thus allowed to systematically investigate the substitution process. The different artefacts of chemical fixation mentioned already above were also evaluated empirically. The effect of DNA aggregation during chemical fixation is a good example. When imaging chemically fixed viruses the vDNA often appears as condensed material not completely filling the capsid, in contrast samples prepared by cryo-methods, where the space is completely filled. In clear favour for the authenticity of the cryo-derived structure stands that an increase of the DNA length leads to packaging incompetent DNA in various viral vector systems, thus arguing that there simply is not more space available in the capsid. The condensation with chemical fixation can be explained by osmotic effects during fixation or substitution. Similar effects can be made responsible for the other well-described artefacts. Direct morphometric comparison of chemically prefixed with high-pressure frozen samples without pre-fixation showed drastic effects on shape and size of endosomes [64]. One of the most obvious artefacts in cell monolayers after chemical fixation are the wide cristae of mitochondria that appear as cylindrical tubular structures with diameters of more than 20 nm. In cryo-prepared samples the membranes are usually very tightly apposed with distances of few nanometers in maximum. All these observations are in line with the slightly irregular appearance of almost any

membrane system in chemically fixed samples when comparing them to the usually smooth membranes after cryo-preparation.

1.1.7 Cryo-Transmission Electron Microscopy

An alternative way of imaging biological specimens is by directly viewing the frozen specimen in a special cryo-TEM using a liquid nitrogen or helium cooled specimen stage. Two approaches are possible: i) A whole cell approach by growing cells on a plastic-filmed, carbon coated copper grid, followed by freezing and imaging [48]. Alternatively, suspension samples can be adsorbed on a bare EM-grid and frozen, thus producing thin layers of amorphous ice in the meshes [49]. ii) CEMOVIS (cryo-electron microscopy of vitreous sections), i.e. freezing of the cells, cryo-sectioning of native frozen sections and imaging [2, 57]. In general, these approaches have the advantages that the sample is still in its native environment and that the image is formed by the biological material itself (and not by heavy metals as in substituted plastic sections). This also makes it possible to draw the resolution limit of biological EM further towards the identification of individual macromolecules by their shape [9]. The advantages of these methods are obvious but they also bring new difficulties. Since the sample is maintained in a frozen state any processing is difficult (e.g. cryo sectioning for CEMOVIS) or impossible (e.g. post “embedding” immunolabeling). Also the samples are very sensitive to electron beam damage and the contrast is weak which causes problems in electron tomography. Nevertheless, these methods represent the reference in retaining the most native state of biological samples.

1.2 Cytomegaloviruses

Cytomegaloviruses (CMV) are herpesviruses of the *betaherpesvirinae* subfamily. Their DNA is approximately 220 kbp in size and codes for more than 200 proteins [58, 65]. The genome is organized in two unique regions termed the unique long (UL) and the unique short (US), and the open reading frames (ORF) are numbered accordingly. A second independent nomenclature exists for the viral phosphoproteins, which were named after their mobility in denaturing polyacrylamide gels (e.g. UL83 = pp65, phosphoprotein migrating as 65 kDa protein). In contrast to alphaherpesviruses, cytomegaloviruses exhibit a narrow host range and cellular tropism, which complicates the establishment of animal models for human cytomegalovirus (HCMV). Among the many cell types infected by the virus in vivo are endothelial and epithelial cells, fibroblasts and macrophages / monocytes, where endothelial cells and monocytes probably represent important host cells in natural infection. Several different HCMV strains are in laboratory use, the most prominent being AD169, which is a fibroblast adapted strain that has lost the capacity to infect the endothelial and immune cells due to the loss of genetic material [16]. Accordingly, fibroblast infection with this strain is regarded as a model system, but also as artificial and inefficient. More recently isolated endotheliotropic strains (e.g. TB40E) thus have to be considered closer to the natural infection.

The structure of the virion is complex and consists of approximately 60 [40] proteins. The mature virion consists of the capsid that contains the viral DNA and is surrounded by the tegument protein layer and the lipid envelope that contains the viral glycoproteins **(Fig. 1A)**. The virus replication is divided into three distinct phases of gene expression termed immediate early (IE), early (E) and late (L) [58]. A full replication cycle takes approximately two days for murine cytomegalovirus (MCMV) and three to four days for HCMV, which is slow in relation to the alphaherpesviruses with approximately 16 hours for herpes simplex virus (HSV)[76].The process of CMV morphogenesis is not fully understood and mainly relies on data acquired from the related alphaherpesviruses (e.g. HSV and pseudorabies virus, PrV) [53, 54]. According to this model, herpesvirus egress proceeds via nucleocapsid formation, envelopment and de-envelopment at the nuclear membranes (primary envelopment), tegumentation and budding of the naked cytolpasmic capsids into Golgi-derived

cisternae (secondary envelopment) and finally the release of the mature virion by fusion of the cisternae with the plasma membrane.

In the first step the nucleocapsid is pre-formed from the capsomers with the help of a scaffold structure (HSV UL26.5), probably with the portal (HSV UL6) as nucleation centre [66]. This leads to the formation of the B-capsid, which is free of DNA and shows the typical inner scaffold ring **(Fig. 1B)**. The viral DNA is replicated independently in a rolling circle mechanism by the viral DNA polymerase (HCMV pUL54). Upon loading of the capsid the scaffold protein autoproteolyses and is exchanged by the viral DNA, thus forming the C-capsid **(Fig. 1B)**. Failure of the loading process probably leads to the formation of A-capsids that neither contain DNA nor scaffold **(Fig. 1B)**. Several other proteins are needed during this process, e.g. for processing the DNA from concatemers to single-copy genomes, loading the DNA and sealing the capsid. The main reason that most data about nucleocapsid formation and maturation is based on HSV is because of the availability of a temperature sensitive protease HSV and a cell free capsid maturation system [67]. Interestingly, not all proteins necessary for CMV capsid maturation could be identified, which may already reflect subfamilial differences in spite of the expected conservation of this process in the early phase of the morphogenesis.

The following transition to the cytoplasm is not very well described. It has been shown that two viral proteins, one localized in the nucleoplasm (MCMV pM53 / HSV and PrV pUL31) the other in the inner nuclear membrane (MCMV pM50 / HSV and PrV pUL34), are binding each other and are thought to recruit the nucleocapsids for their primary envelopment [39, 42, 63, 72]. Interestingly, unbalanced expression of BFRF1, the homologue of M50 in Eppstein-Barr virus (EBV), leads to local duplications of the nuclear membranes [20]. A further prerequisite for primary envelopment is that the inner nuclear membrane has to be made accessible for the budding of the nucleocapsids by removal of the nuclear lamina by phosphorylation of the lamins. The responsible kinases may be of viral and cellular origin and are speculated to be recruited to the budding sites by the M50/53 complex. In HCMV it has been shown that the viral kinase pUL97 plays a role in this process by interacting with the cellular protein p32, which leads to phosphorylation and redistribution of the lamins [52]. In alphaherpesviruses its homolog UL13 appears to act in cooperation

with the US3 kinase, which is not conserved in betaherpesviruses, which leads to phosphorylation of UL34 and UL31 in herpes simplex virus infection [39]. UL97 is a focus of interest because it monophosphorylates several nucleoside analogs that are used in therapy of HCMV infection. The monophosphates are then triphosphorylated by cellular enzymes and incorporated in the viral DNA, which leads to a stop in elongation. pUL97 has also been implicated in other processes such as DNA replication and secondary tegumentation [4, 44, 45, 51, 69, 98]. Still, its precise function in these processes has to be elucidated. The same applies for pM97, the homolog in MCMV. In search for a small animal model for HCMV infection and therapy MCMV was considered as a candidate. Unfortunately, phosphorylation of nucleoside analogs by MCMV pM97 was found to be greatly reduced [55, 56, 91]. Also transgenic complementation of an M97-deficient MCMV by insertion of UL97 did not fully restore the wild type phenotype. The structural features of primary envelopment in CMV at the moment are thought identical to alphaherpesviruses [53], i.e. budding occurs at the nuclear periphery by a local depolymerisation of the lamina and passage of a single virion through the generated gap. In conflict to this model stand previous EM analyses by chemical fixation suggesting that HCMV and human herpesvirus 6 (HHV6) further modify the inner nuclear membrane to create vesicular structures involved in primary envelopment [75, 84]. In HHV6 these structures were termed “tegusomes”, but ,as shown later in the results section, the structure was probably misinterpreted due to the dramatic alteration of this structure due to chemical fixation. The same was probably the reason why the identical structures seen in HCMV infected cells were not further investigated or interpreted. Once the nucleocapsids have been primary enveloped, they are thought to fuse with the outer nuclear membrane to be released to the cytoplasm. Interestingly, upon deletion of the PrV kinase US3, this fusion is inhibited and leads to a perinuclear accumulation of enveloped virions [42]. A similar effect was reported upon deletion of HSV UL20 [6], but could not be confirmed in PrV, where it resulted in a retention of secondary enveloped virions in the cytoplasm [23].

Once in the cytoplasm, the capsids acquire the inner layer of tegument which consists of HCMV UL48 and UL47, and are conserved and essential throughout the herpesvirus family (HSV UL36 and UL37) [24, 41]. In HCMV, UL69 forms a complex with UL48 and UL47 [10]. In parallel, the viral glycoproteins are synthesized in the

Golgi complex and transported to the sites of secondary envelopment. On the ultrastructural level budding occurs at cisternal membranes in close proximity to the Golgi-complex, which are supposed to originate from the trans-Golgi network [34] or endosomes [89]. The process of further tegumentation and envelopment, and the release from the cell is fairly understood and relies on redundant interactions between the different tegument components and the glycoproteins, which leads to the wrapping of the cisternae around the tegumented virions and ultimately to an enveloped viral particle inside a vesicle, which can be secreted by the cell. For PrV several interactions between the tegument and the glycoproteins are known [54], but can not be applied to CMVs because of the lack of conservation between the herpesvirus subfamilies. For HCMV several tegument proteins are important during envelopment, e.g. ppUL83 (pp65), ppUL35, ppUL32 (pp150), UL69, ppUL99 (pp28) and ppUL82 (pp71) as well as the glycoproteins gpUL55 (gB), gpUL4 (gp48), UL18, US10, US11 [8], UL132 [86] and the tripartite complex of gpUL75 (gH), gpUL100 (gL) and gpUL74 (gO) [35, 36]. Some of the tegument proteins have important functions in manipulating the newly infected host cell and transcriptional regulation of the immediate-early replication phase, e.g. ppUL82 (pp71), ppUL35A and ppUL69 [7, 13, 29, 50, 97]. Among these UL35 is an interesting ORF, since it codes for two proteins, the full length ppUL35 and a C-terminal fragment ppUL35A (Quote Liu). ppUL35 is a cytoplasmic component of the tegument and also important for virion morphogenesis, while ppUL35A is a nuclear factor involved in modulation of the immediate-early promoter [50, 79].

In contrast, our knowledge about how these factors mechanistically drive the envelopment process is very limited. Herpesviruses are also able to envelope tegument aggregates devoid of capsids, the so-called L-particles or dense bodies. An interesting example illustrating the complexity of secondary envelopment is the role of ppUL83 (pp65) in HCMV. ppUL83 is the major component of the tegument and the dense bodies [90], yet its deletion from the viral genome neither affects viral growth nor changes the ultrastructural appearance of the virions, but abolishes dense body formation [80]. The function of dense bodies is debated, the arguments are ranging from “tissue culture artefact” to important factor in immune evasion by downregulation of the interferon gamma response [1, 14]. In the envelopment process also other non-structural proteins are incorporated into virions, e.g. the four predicted G-protein

coupled receptor homologs (GPCRs) US27, US28, UL33 and UL78 [21, 22]. Also the GPCRs are implicated in immune evasion by binding and internalising chemokines, since they undergo constitutive endocytosis and are internalised into multivesicular endosomes. Still, their exact function has not been tackled until now.

The standard approach to investigate the function of viral proteins is to delete them from the viral genome and to analyse the introduced block in the morphogenesis. This technique has been used extensively in the herpesvirus field, but also has its limitations. A frequent problem arises when deleting essential proteins, what causes a complete block in replication and thus has to be compensated by growing the virus on a complementing cell line. This is often toxic for the cell or causes side effects in the morphogenesis due to too high or low expression levels. Also, the possibility that other unintentionally introduced mutations could also cause a phenotype cannot be definitely reverted. An interesting new development to overcome these limitations is the development of a conditional expression system, in which the protein of interest is introduced at a different position of the genome and controlled by an inducible promoter [77]. Accordingly, the expression of the respective protein is happening in the context of the wild type viral replication and can be regulated by induction. Unfortunately, the promoter may also cause problems through leakage and thus low level expression of the respective protein. This system was enhanced by expression of dominant negative mutant proteins, which are functionally inactive and compete with the wild type protein when expressed. The phenotype generated is almost identical to a deletion of the respective protein. This has been achieved for two MCMV proteins, the small capsid protein (SCP, M48.2) and the M50 protein. The viruses conditionally expressing the respective dominant negative proteins both show severe replication defects in biochemical analyses and were also investigated by HPF / FS as described in the results section.

This complex interplay of viral and cellular proteins poses a great challenge in the mechanistic understanding of the morphogenesis of cytomegaloviruses. In order to approach the many questions we still have, a combination of genomic mutagenesis, biochemistry, fluorescence microscopy and the ultrastructural imaging by electron microscopy is essential, but demands tight collaboration between different fields of research.

1.3 ***Aim of the Project***

This thesis was aimed at establishing and optimising EM after high-pressure freezing, freeze-substitution and plastic embedding as method for cytomegalovirus research. The virological question was to what extent does this cryo-preparation method enable us to ultrastructurally assess the phenotypes generated by mutating the cytomegalovirus genome.

2 Materials and Methods

2.1 Reagents

Acetone	Merck, Germany
Benzil	Sigma, Germany
Benzoylperoxide	Sigma, Germany
Copper grids	Plano, Germany
DAPI (4,6-diamidino-2-pehylindole dihydrochloride)	Sigma-Aldrich, Germany
DMEM	GIBCO, Germany
Doxicycline	Sigma, Germany
Epon	Fluka, Germany
FCS	GIBCO, Germany
Goat anti-mouse antibody 10 nm gold	Aurion, Netherlands
HEPES	[3]
1-hexadecene	Merck, Germany
Iodixanol	Progen, Germany
Lead citrate	Merck, Germany
LR-Gold	London Resin Ltd, England
Magnesium chloride	Merck, Germany
Osmium tetroxide (OsO_4)	Chempur, Germany
PBS (phosphate buffered saline)	[3]
Penicilline / Streptomycine	GIBCO, Germany
Potassium chloride	AppliChem, Germany
Sapphire disks	Brügger, Switzerland
Sucrose	Sigma, Germany
Syto RNASelect	Invitrogen, Germany
Toluidine blue	Sigma-Aldrich, Germany
Tricine	Sigma, Germany
Trypsin	GIBCO, Germany
tubulin m-antibody (mouse anti α-tubulin, T5168)	Sigma-Aldrich, Germany
Uranyl acetate (UAc)	Merck, Germany
Wortmannin	Sigma-Aldrich, Germany

2.2 Cell Culture and Viruses

2.2.1 Experiments with Murine Cytomegaloviruses

MCMV (Smith strain) infections were done with Swiss 3T3 murine fibroblasts or M210B4 murine stroma cells. 3T3 fibroblasts were cultivated in DMEM containing 10% (v/v) fetal calf serum (FCS), 1% Glutamine (w/v) and penicillin / streptomycin, and passaged with trypsin/EDTA. M201B4 were cultivated in MEM containing 10% (v/v) FCS, 1% Glutamine (w/v) and penicillin / streptomycin, and passaged with trypsin.

For infection, cells were seeded on the previous day to approximately 50% confluency, overlaid with virus diluted in complete medium in a low total volume (300 µl per 24-well) with an MOI of 0.5 to 1 PFU / cell for EM or with 0.1 PFU / cell for nuclei isolation and transferred to the incubator for 45-60 minutes. After the internalisation, fresh medium was added.

In the experiments on the role of M97, two additional mutants were used: MCMV ΔM97, an M97-deletion mutant in which the complete M97 ORF was deleted and MCMV UL97, in which the deleted M97 was replaced by UL97, its homolog in HCMV [91].

In experiments in collaboration with Brigitte Rupp and Zsolt Ruzsics from the laboratory of Ulrich Koszinowski (Max von Petterkofer Institut für Virologie, LMU Munich), three viral mutants conditionally expressing viral proteins under control of a tetracycline dependent promoter in addition to the wild type protein [77] were used: MCMV M50HA, which conditionally expresses a hemagglutinine tagged pM50, MCMV ΔP, which expresses a truncated form of M50, and MCMV SCP-GFP, which expresses the small capsid protein (SCP, M48.5) tagged with a green fluorescent protein [77]. All mutants were introduced in the Smith strain genome.

2.2.2 Experiments with Human Cytomegaloviruses

For HCMV infections two different strains and cells were used: Infections with the fibroblast adapted AD169 strain were carried out on human foreskin fibroblasts (HFF) that were grown in DMEM containing 10% (v/v) fetal calf serum (FCS), 1% Glutamine (w/v) and penicillin / streptomycin, and passaged with trypsin / EDTA. HFF were

seeded several days before infection and allowed to grow to confluency. Infections were carried out as described for MCMV experiments.

Also for HCMV different mutants were used: HCMV ΔUL97, in which the complete UL97 ORF was deleted from the AD169 genome, HCMV Quattro, in which the four ORFs US28, UL33, UL78 and US27 that code for G-protein coupled receptors were deleted from the AD169 genome (Jens Holl and Detlef Michel, Inst. for Virology, Ulm). In a further project with Karina Schierling and Michael Winkler, formerly Inst. for Virology, Ulm) on the tegument protein UL35 three mutant AD169 viruses were used, i.e. HCMV ΔUL35 (deletion of the complete UL35 ORF, [79], HCMV UL35RV2026 (mutation of three start codons of UL35A, i.e. M448A, M449A and M465A) and HCMV UL35dATG (mutation of the first start codon of UL35, i.e. M1A).

Gold internalisation experiments and inhibition of PI(3)K were carried out as following: Gold colloids (15 nm, OD_{520} = 1.1) were mixed with complete medium (1 volume Gold with 3 volumes medium) and overlaid on the cells for 4 hours before HPF. The PI(3)K-inhibitor wortmannin was added 4 hours before HPF (at a final concentration of 0.2 µM) [25].

2.2.3 Experiment with the Poxvirus Strain MVA

In collaboration with Jacomine Kijnse-Locker (EMBL Heidelberg) on the morphogenesis of the poxvirus core, HeLa cells (prepared as stated above) were infected with the non-human pathogenic poxvirus strain MVA (provided by Jacomine Kijnse-Locker) and high-pressure frozen at 6 hours p.i.

2.3 Sample Preparation for Electron Microscopy

2.3.1 Preparation of Sapphire Disks and Cell Cultures

The sapphire disks were cleaned by sonication for 15 minutes each in 60% sulphuric acid, soap water and twice in absolute ethanol, and allowed to dry. The disks were then coated with approximately 20 nm carbon by electron beam evaporation in a BAF 300 (Bal-Tech, Principality of Liechtenstein) and dried 8 hours or overnight in an oven at 120 °C to increase the stability of the carbon film. The coated sapphire disks were then carefully immersed in complete medium and the cells were seeded on top and the infections were done as described above.

2.3.2 High-Pressure Freezing

After the specified amount of time post infection (p.i.) the samples were high-pressure frozen with a HPM01 (Engineering Office M. Wohlwend, Switzerland). Two aluminium planchettes (3 mm diameter; Engineering Office M. Wohlwend, Switzerland) were immersed in hexadecene (i.e. 1-hexadecene), the lower one being flat, while the upper one had a cavity of 100 µm. First, the lower planchette was inserted into the sample holder, then the sapphire disk with the adherent cells was removed from the culture dish (usually a 24-well plate) with tweezers, shortly deposited on a filter paper to remove excess medium, immersed in hexadecene and placed in the sample holder. The sandwich construction was then completed with the upper planchette with the 100 µm cavity pointing down towards the cells and high-pressure frozen **(Fig. 1E)**. Since hexadecene is not miscible with water it does not serve as cryoprotectant but instead to properly transfer the pressure and cooling during the freezing process by providing good contact between the planchettes and the sample [11, 62, 88]. The entire mounting process takes approximately 10 to 20 seconds for a trained person to perform. After the freezing the samples are quickly transferred to the cryo-box filled with liquid nitrogen where they can be stored until freeze-substitution.

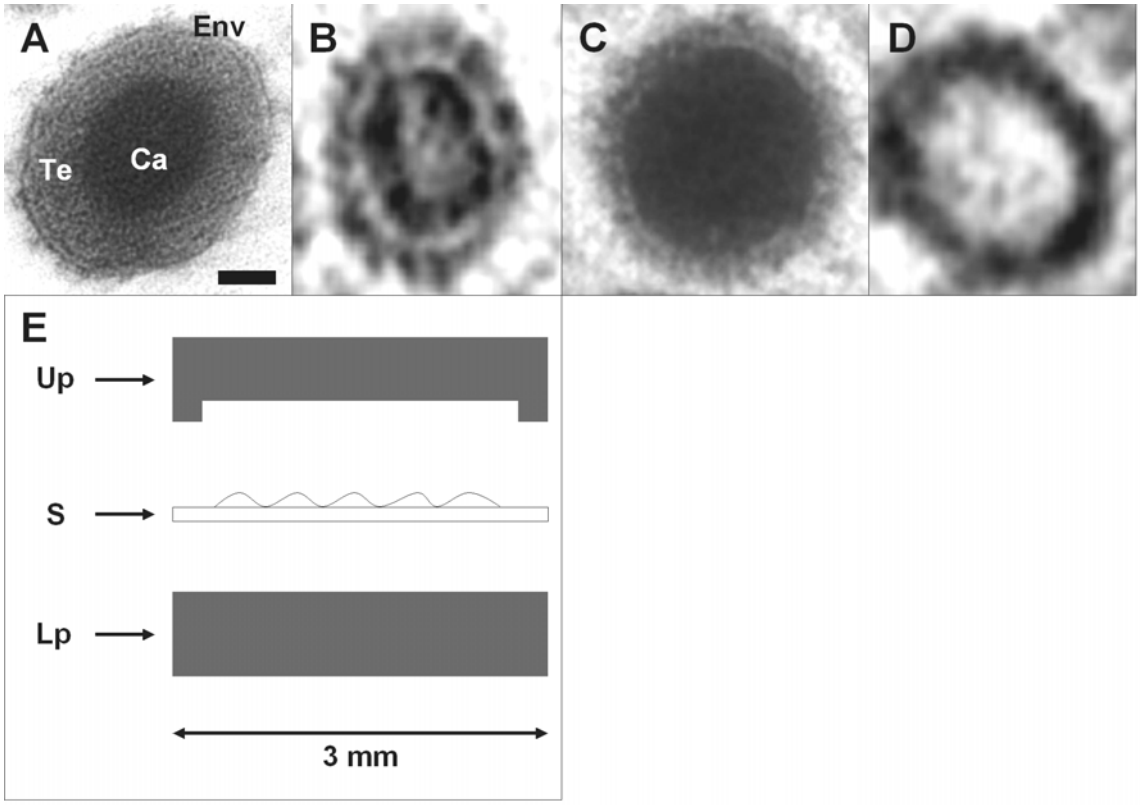

Figure 1: Herpesvirus capsids in TEM and sandwich construction for HPF. **(A)** Appearance of mature herpesvirus virions consisting of the vDNA loaded capsid (Ca), surrounded by the tegument (Te) and the envelope (Env) (bar 50 nm). **(B)** Nuclear B-capsid with visible internal scaffold protein that is autoproteolysed during vDNA encapsidation. **(C)** Nuclear C-capsid fully loaded with vDNA. **(D)** Nuclear A-capsid that probably originates from abortive packaging of vDNA into a B-capsid. **(E)** Sandwich construction used for high-pressure freezing of cell culture monolayers. The cells are grown on carbon-coated sapphire disks (S, 3 mm diameter), immersed in 1-hexadecene, mounted between an upper (Up, 100 µm cavity) and a lower aluminium planchette (Lp, plane) and high-pressure frozen at 2 kbar with liquid nitrogen.

2.3.3 Freeze-Substitution, Plastic Embedding and Sectioning

Before starting the substitution process the sandwich construction first has to be disassembled under liquid nitrogen in order to remove the major part of the hexadecene, since it may react with fixatives during substitution. In parallel the substitution mixture has to be prepared. In this study a mixture based on acetone and osmium tetroxide based on the original protocols by Martin Müller and Bruno Humbel [37] (formerly Facility for Electron Microscopy, ETH Zürich) was used and modified by

addition of water and other fixatives [92] and further optimised as described in the results.

For standard ultrastructural analysis and embedding in Epon acetone containing 1.6 % (w/v) osmium tetroxide, 0.1 % (w/v) uranyl acetate and 5 % (v/v) water was used. The substitution mixture was precooled for 15 minutes to –90 °C in a self-made substitution apparatus (W. Fritz and A. Ziegler, unpublished). The samples were then quickly transferred from liquid nitrogen to the substitution mixture. Substitution was carried out by warming over 16 to 24 hours from –90 to 0 °C with an exponential temperature profile, i.e. with low temperature gradient below –80 °C and increasing gradient at higher temperatures. After the substitution the samples were equilibrated at room temperature for 15 to 30 minutes and washed 3 times with acetone. Infiltration with Epon was done with 50 % (v/v) Epon in acetone (or in other cases the solvent used for substitution) for one hour and pure Epon for 6h. After this the Epon was exchanged once more and polymerised in 1.5 ml Eppendorf tubes at 60 °C for 2 days. Special care should be taken that the samples never fall dry since this leads to collapsing of the structures.

For fluorescent staining or immunolabeling and embedding in LR-Gold substitution was done in acetone containing 0.1 % (v/v) glutaraldehyde, 0.1 % (w/v) uranyl acetate and 5 % (v/v) water. Substitution was carried out from –90 to –20 °C over 16 to 24 hours. The samples were left at –20 °C for 1 hour and washed twice with precooled acetone before infiltration with 50 % LR-Gold in acetone at –20 °C for 2 hours and pure LR-Gold for 1 hour in closed and completely filled 0.5 ml Eppendorf tubes. LR-Gold was prepared with 0.1 % (w/w) benzil and 0.1 % (w/w) benzoylperoxide and covered with nitrogen to remove oxygen. The samples were then transferred to a peltier element and polymerised under UV-light for 24 hours at –20 °C.

The Eppendorf tubes were then cut off and the polymerised samples were immersed in liquid nitrogen to remove the sapphire disk. LR-Gold samples were only immersed very briefly since strong cooling leads to cracks in the plastic. The resulting surface was then trimmed to fit to a microtome diamond and sectioned with a Leica Ultracut UCT (Leica, Germany) to a thickness of 60 to 80 nm for standard TEM applications

or 400 to 500 nm for stereo imaging and tomography. The sections were picked on bare 200 to 300 mesh copper grids in case of Epon sections or on formvar / carbon coated copper grids for LR-Gold samples. For the standard ultrastructural samples embedded in Epon, section contrasting was not necessary, while for immuno-EM samples a slight increase of contrast was seen. Accordingly, these sections were contrasted 2 to 4 minutes with 2 % (w/v) uranyl acetate, washed 3 times, contrasted in 2 % (w/v) lead citrate, washed 3 times and allowed to dry before imaging in a Phillips EM400 (FEI, Netherlands) or Zeiss EM10 (Zeiss, Germany) at an acceleration voltage of 80 kV. Stereo images were recorded on a Zeiss EM902 (Zeiss, Germany) at 120 kV, tomograms either on a Technai F40 (FEI, Netherlands) at 200 KV or on a Titan Microscope (FEI, Netherlands) at 300 kV.

2.3.4 Immunogold Labeling

Anti-tubulin labelling was performed on sections of LR-gold embedded uninfected 3T3-fibroblasts as described above. The labelling reaction was performed according to a protocol by Heinz Schwarz (MPI für Entwicklungsbiologie, Tübingen, Germany). The sections were first blocked with PBG (0.2 % gelatine, 0.5 % BSA in PBS), then incubated with primary antibody (monoclonal mouse anti-tubulin, diluted 1:200 in PBG) for 40 minutes, followed by washing 6 times for 2 minutes in PBG. The gold-coupled secondary antibody (10 nm gold, goat anti-mouse IgG, diluted 1:80) was then applied for 40 minutes, followed by washing in PBG and PBS, 3 times 2 minutes each.

2.3.5 Image Analysis

Images were recorded on negative film, scanned with a Duoscan f40 (AGFA, Germany) and processed with Photoshop (Adobe, USA). In standard TEM images only contrast enhancement was done. For nuclear particle statistics 700 to 1000 nucleocapsids were counted in more than 8 independent nuclear cross sections for each viral mutant. Capsids that could not be unambiguously assigned to a specific type were excluded from the statistics but amounted to approximately 5% in all samples. For the stochastic analysis of MCMV nucleocapsid distributions, individual capsids were manually marked in Photoshop with dots of the corresponding color and analysed (Frank Fleischer and Volker Schmidt, Dept. of Stochastics, Universität Ulm) using the GeoStoch library. Further description of the method can be obtained in [5].

2.3.6 Correlative Microscopy of DNA and RNA Distributions

Serial thin sections were cut from LR-Gold embedded samples as described above. While the first section was prepared for the TEM as described above, the second section was transferred on a glass object carrier for fluorescence microscopy. These sections were then stained with DAPI (1 mg/ml) for DNA staining or Syto RNASelect (500 nM) for RNA staining for 5 to 10 minutes, briefly washed with water and viewed in a Zeiss Axiophot (Zeiss, Germany) equipped with a 100x objective and an SPOT RT Monochrome camera (Diagnostic Instruments, USA). To better identify corresponding cells in phase contrast, a further section was sometimes stained with toluidine blue. The corresponding cells were then imaged and digitally overlaid using Photoshop (Adobe, USA).

2.3.7 Electron Tomography and Stereo Imaging

Tomograms were recorded on a Technai F40 (200 kV, FEG) and a Titan (300 kV, FEG) TEM at 1° step tilt angels from –70 to 70° using a single tilt holder (Fishione, USA) and reconstructed with Xplore3D (FEI, Netherlands) using an iterative back-projection algorithm for alignment (SIRT) or with the IMOD package [43]. Stereo images were recorded at an angle of ±6 ° using a Zeiss 902 operated at 120 kV (Zeiss, Germany).

2.4 Biochemistry and Molecular Biology

2.4.1 Isolation of Cell Nuclei

Swiss 3T3 murine fibroblasts were grown in 3 T175 flasks each and infected with MCMV wt or MCMV ΔM97 at an MOI of 0.1 PFU/cell. At 48 hours p.i. the cells were washed with PBS, trypsinised and pelleted with 1200 rpm for 5 min. The pellet was washed with 10 ml cold PBS (phosphate buffered saline) and 10 ml swelling buffer (0.1 M Hepes / 0.1 M magnesium chloride / 1 M potassium chloride) and carefully resuspended in 10 ml fresh swelling buffer. After swelling for 60 minutes the cells were dounced and pelleted with 1200 rpm for 5 min. The pellet was resuspended in 1 ml 2 M sucrose / 1 M potassium chloride / 0.1 M magnesium chloride / 1 M tricine and mixed with 1 ml 50 % iodixanol / 0.2 M potassium chloride / 0.02 M magnesium chloride / 0.2 M tricine. 2 ml of the suspension were under layered with 4 ml 30 % iodixanol and 4 ml 35 % Iodixanol in ultracentrifuge tubes (14x95 mm, ultraclear; Beckmann, Germany) and centrifuged for 8000 rpm for 20 min in an SW41 rotor in a Beckmann Ultracentrifuge (Beckmann, Germany). The band forming at the gradient interface containing the nuclei was collected. The concentration of nuclei in both wt- and ΔM97-preparations was estimated in a counting chamber, adjusted to the same value and used for PCR.

2.4.2 PCR Amplifications

For the estimation of the viral DNA, nuclei were treated with proteinase K for 30 min at 56 °C, boiled for 5 min at 95 °C and analysed by PCR amplification of a fragment of the unrelated M96-gene using the primers M96p (5´-AGAGTGCGCTGCTC AAGGAC-3´) and M96m (5´-GTCAGTCACACCTCCTCACTG-3´). Estimation of encapsidated viral DNA was performed by micrococcal nuclease digestion and subsequent proteinase K-treatment of isolated nuclei as described in [83], followed by PCR of the M96-fragment.

As second method to verify that equal amounts of nuclei were used we also performed PCR on actin using the primers actin P(4) (5'-GGATGTCCACGT CACACTTCATGATGG-3') and actin M(5) (5'-AGCCATGTACGTAGCCATCCAGGC-3').

2.4.3 SDS PAGE

SDS PAGE was performed using 12 % polyacrylamide gels. 10 µl purified nuclei were mixed with an equal volume loading buffer (100 mM Tris-HCl, 200 mM DTT, 4 % SDS, 20 % glycerol, 0.2 % bromphenol blue), boiled for 5 minutes at 95 °C, loaded on the gel and run at 200 V for 30 minutes in running buffer (25 mM Tris, 190 mM glycine and 0.1% SDS). The gels were then stained for 1 hour with Comassie-blue (0.1 % Comassie blue, 50% methanol, 7% acetic acid in ddH_2O) and destained over night (in 50% methanol, 7% acetic acid in ddH_2O). The gel was wrapped once in transparent foil and scanned with a Duoscan f40 (AGFA, Germany).

3 Results

3.1 Optimising Freeze-Substitution

The approach by high-pressure freezing, freeze-substitution and plastic embedding is a young technique and its development has mainly been hampered by the low reproducibility of freezing and the spreading of a multitude of empirical substitution protocols in the literature. Still, our understanding of the chemical processes occurring during freeze-substitution is minimal and systematical investigations are scarce. The high reproducibility of high-pressure freezing with the HPM01 makes it possible to systematically assess the effects of different substitution conditions on the visibility and/or retention of ultrastructural details in the samples. The basic protocol used at the beginning consisted of acetone with 2 % (w/v) osmium tetroxide to provide good membrane fixation and staining. Further addition of 0.1 % (w/v) uranyl acetate slightly increases the contrast. An interesting observation was that water in the substitution medium increases the visibility of membranes [92], while previous protocols took great care in avoiding any “contamination” of the organic solvent by water. All substitution media used in this study are summarised in Table 1.

The aim of this chapter was to optimise the current protocols to obtain a better ultrastructural representation of the samples and to find a rationale for designing the according substitution medium using adherent mammalian fibroblast cell monolayers.

3.1.1 Influence of the Water Content in Substitution Based on Acetone

In these experiments the water content of the substitution mixture was varied while keeping the other components and the substitution process constant. Accordingly, the substitution media had the composition 1.6 % (w/v) osmium tetroxide, 0.1 % (w/v) uranyl acetate and X % (v/v) water in acetone, the substitution time was kept at 16 hours and embedding was done in Epon as described in chapter 2.3.3.

Figure 2 shows representative views of Swiss 3T3 cell cultures substituted with water concentrations of 0 % **(Fig. 2A)**, 1 % **(Fig. 2B)**, 5 % **(Fig. 2C and D)**, 10 % **(Fig. 2E)** and 20 % **(Fig. 2F)** water. Note the slight increase in structural visibility from 0 to 1% water and the strong difference between 1 and 5 % water. Interestingly, further addition of water did not influence the sample structure in any way and thus

did not promote any visible recristallisation of the sample even at 20 % water content. When starting the substitution process at –90 °C, the added water was visible as milky precipitate (small ice crystals) at the bottom of the acetone-filled Eppendorf tubes and is gradually dissolved in the acetone while warming. The same improvement of the sample quality between 5 % water and water free substitution mixtures was seen when using 0.1 % glutaraldehyde instead of 1.6 % osmium tetroxide. These samples could be used for immunolabeling as tested with an anti-tubulin antibody **(Fig. 3)**.

Fixatives [%]	Water [%]	Solvent	Figures
1.6 % OsO_4, 0.1 % UAc	0	acetone	2A
1.6 % OsO_4, 0.1 % UAc	1	acetone	2B
1.6 % OsO_4, 0.1 % UAc	5	acetone	2C/D,5F,7-16
1.6 % OsO_4, 0.1 % UAc	10	acetone	2E
1.6 % OsO_4, 0.1 % UAc	20	acetone	2F
0.1 % GA, 0.1 % UAc	5	acetone	3A /B
1.6 % OsO_4, 0.1 % UAc	0 / 5	acetone	4A/B
1.6 % OsO_4, 0.1 % UAc	0	ethanol	5A
1.6 % OsO_4, 0.1 % UAc	5	ethanol	5B
1.6 % OsO_4, 0.1 % UAc	0	methanol	5C
1.6 % OsO_4, 0.1 % UAc	5	methanol	5D
1.6 % OsO_4, 0.1 % UAc	0	2-butanol	5E

TABLE 1: Composition of substitution media tested.

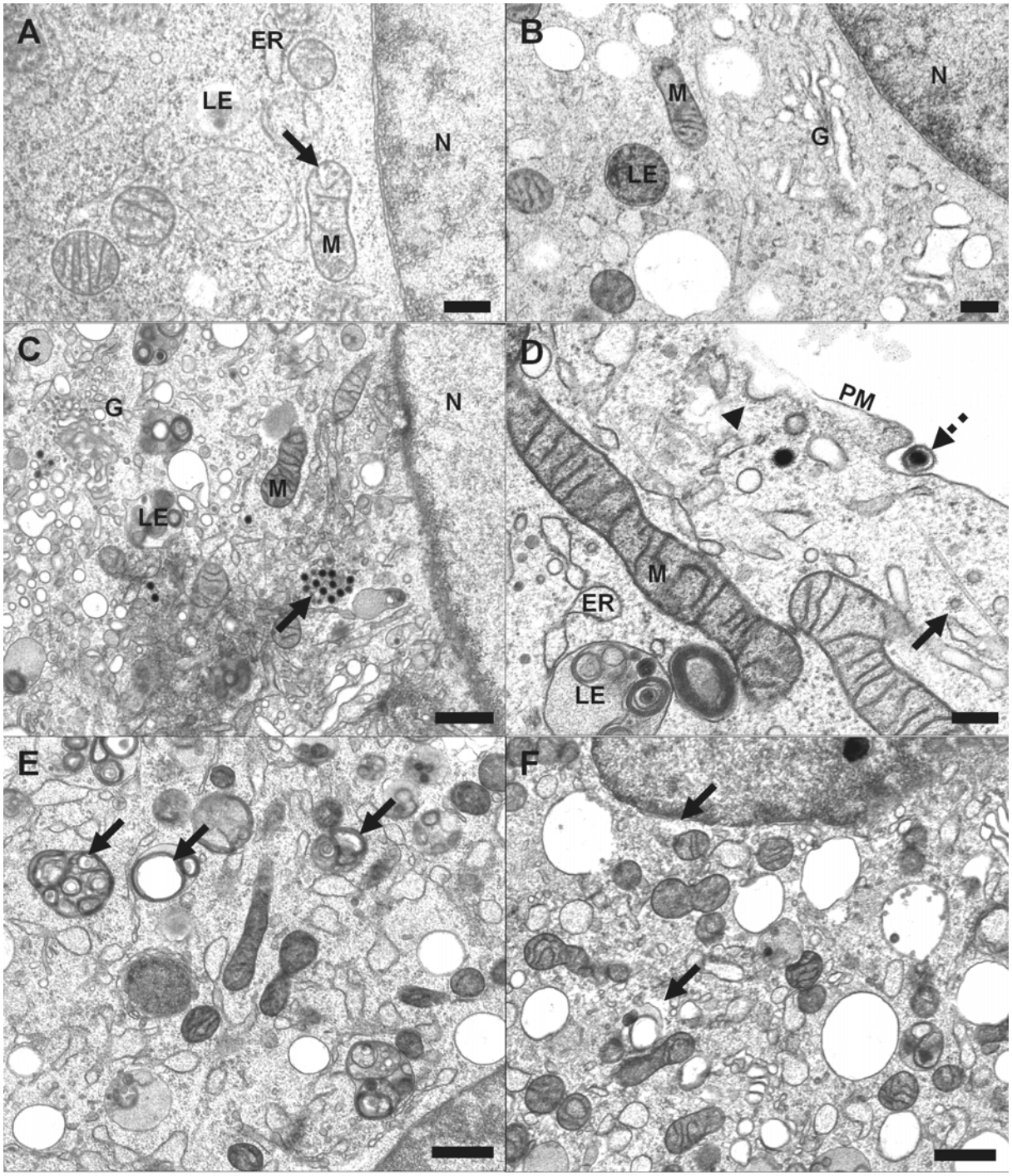

Figure 2: Influence of the water content on the sample quality with media based on acetone with 1.6 % OsO_4 and 0.1% UAc. (A) Without water added, the sample contrast was low and small holes were visible indicating extraction of cellular material (arrow). Note that the mitochondrial membranes appeared well retained, while the matrix contrasted weakly (bar 200 nm). **(B)** Addition of 1 % water already slightly increased the overall contrast and the visibility of fine structures. Also the extraction patterns were not present any more (bar 200 nm). **(C)** Addition of 5 % water greatly enhanced the sample quality. All cellular

membranes were well retained and continuously visible especially in mitochondria (M) and multivesicular late endosomes (LE). A Golgi-complex with many secretory vesicles was also well retained (G) together with a cytoplasmic cluster of MCMV capsids embedded in tegument material (arrow) (bar 500 nm). **(D)** Also, using 5 % water many fine structural details were well visible, among these a clathrin-coated pit (arrowhead), two coated vesicles moving along a microtubule (arrow), the release of a murine cytomegalovirus reminiscent of a primary enveloped virion (dotted arrow) and again the lamellar structure of a late endosome (LE) and mitochondria (M) (bar 200 nm). **(E)** When adding 10 % water, no deterioration of the sample quality was seen except for the emergence of plastic perfusion problems especially in the centre of multilamellar endosomes resulting in “holes” in the sample (arrows). Still, all fine structure was retained (bar 500 nm). **(F)** Even addition of 20 % water did not influence the sample appearance except for the more frequent problems in plastic perfusion (arrows) (bar 500 nm). ER endoplasmic reticulum, G Golgi-complex, LE late endosome, M mitochondria, N nucleus, PM plasma membrane.

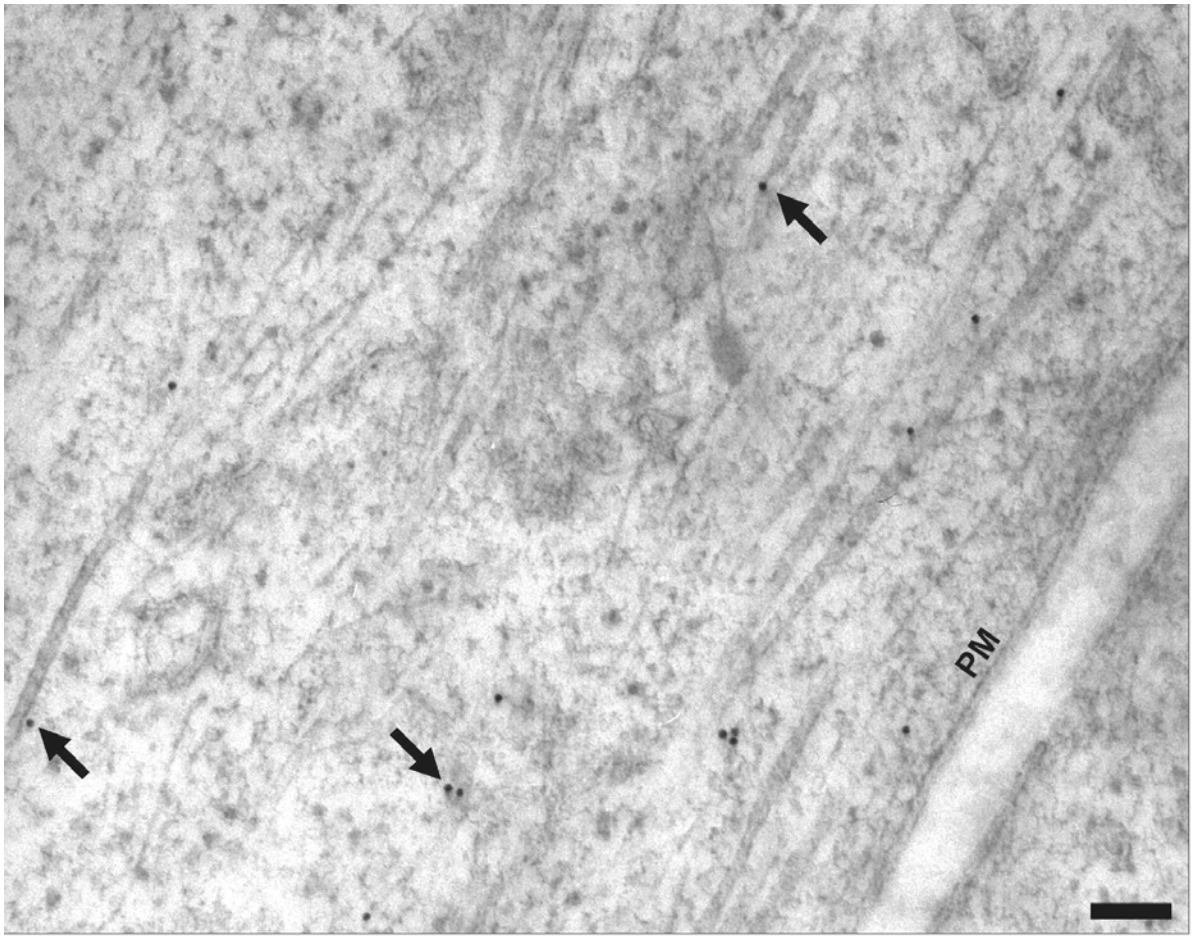

Figure 3: Anti-tubulin labelling on fibroblasts substituted in 0.1 % glutaraldehyde, 0.1 % uranyl acetate and 5 % water in acetone and embedded in LR-Gold. In this basal section through the cell several microtubules were labelled with a primary mouse-anti-tubulin antibody and a secondary gold-coupled goat-anti-mouse antibody (10 nm gold). Also here, the sample quality was good while maintaining the antigenicity of the sample. It was obvious that the tubulin was best accessible for the antibody when the microtubule was running out of the section (arrows) (bar 200 nm). PM plasma membrane.

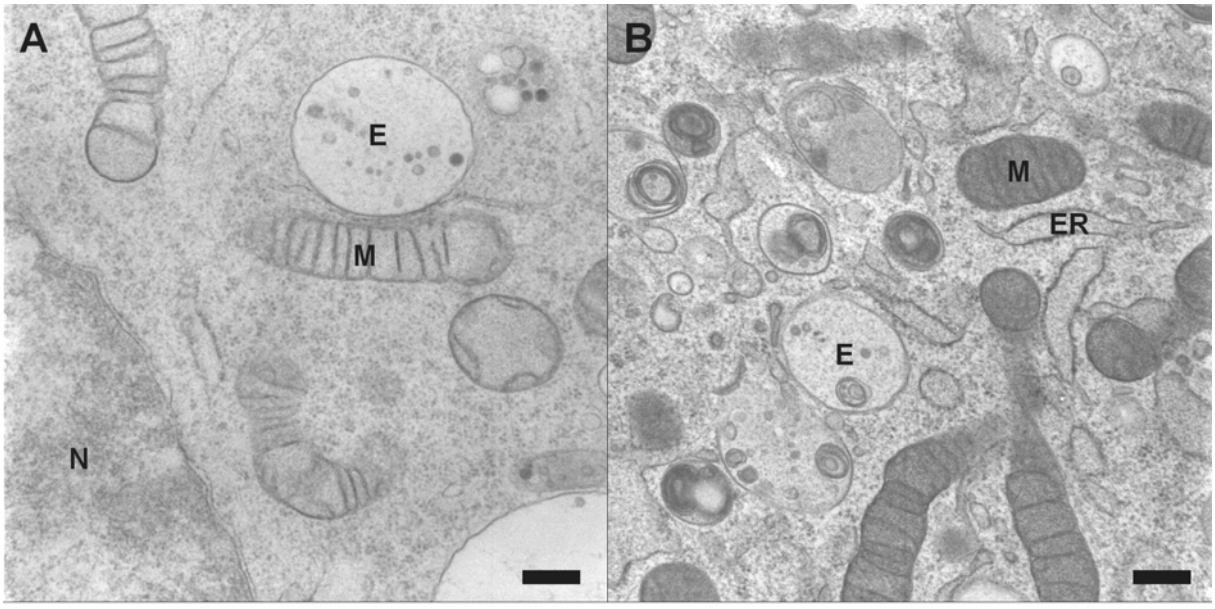

Figure 4: Effect of water in the early and late phase of substitution. (A) When 5 % water was only present in the early phase of substitution from –90 to –60 °C the samples appeared similar to samples substituted in water free acetone (see Fig. 2A). Mitochondria (M) and late endosomes (LE) were retained, but exhibited weak contrast (bar 200 nm). **(B)** With 5 % water present from –60 to 0 °C, the contrast was greatly enhanced as seen for samples where water was present throughout the entire substitution process (bar 200 nm). ER endoplasmic reticulum, LE late endosomes, M mitochondria, N nucleus.

To further investigate the time point during freeze-substitution when the added water has an effect on the sample quality, substitution was performed in parallel with two different protocols: In the first, substitution proceeded with 5 % water from –90 °C to –60 °C and continued without water to 0 °C, while the second was opposite, i.e. water was not present in the initial phase, but added at –60 °C. The result was that samples encountering water in the initial phase appeared similar as samples substituted without water. If the water was present at warmer temperatures the structures was indistinguishable from samples where water had been present during the entire process **(Fig. 4)**. To clarify if the effect of water was based on an interaction with the fixatives, samples were substituted in pure acetone without any fixatives but with increasing water concentrations. Using pure acetone without water, the cells were weakly visible and the ultrastructural details (e.g. membranes) were

lost even after on section contrasting. Intriguingly, any addition of water completely destroyed the cells by heavy extraction and collapsing so that only debris remained.

3.1.2 Other Solvents and Water

Many substitution protocols are based on solvents other than acetone, especially on methanol and ethanol. Samples were thus substituted in methanol and ethanol again containing 1.6 % (w/v) osmium tetroxide, 0.1 % (w/v) uranyl acetate and either without or with 5 % (v/v) water and embedded in Epon as previously. Ethanol without water gave results comparable to acetone, but with increased signs of extraction, so that membranes were not visible **(Fig. 5A)**. Upon addition of 5 % water the membranes were partially retained, but still some signs of extraction could be seen **(Fig. 5B)**. The sample quality after substitution with methanol without water was very bad due to strong extraction. Additionally, halo-like voids typical for shrinkage were seen around cellular organelles **(Fig. 5C)**. Accordingly, organelles were barely identifiable (e.g. mitochondria) and membranes were not visible. Addition of 5 % water could not eliminate the shrinkage, but was able to increase the retention of ultrastructural details **(Fig. 5D)**. Since the strength of extraction correlated with the polarity of the solvents, i.e. methanol > ethanol > acetone it was evident to try substitution in a solvent with a lower polarity than acetone. This solvent additionally had to be liquid at –90 °C and of low toxicity. 2-Butanol appeared to be a good candidate with a melting point of –115 °C. As control solvent with very low polarity n-hexane was chosen. As expected, n-hexane with or without 5 % water did not substitute the water in the sample and also lead to insufficient perfusion of Epon during embedding. 2-butanol without water substituted the samples with quality comparable to ethanol but with low reproducibility and subsequent problems with embedding **(Fig. 5E)**. Addition of 5 % water lead to extreme extraction of the samples such that only a “skeleton” remained.

3.1.3 Duration of Substitution

Also for the temperature profile and the duration of substitution, various protocols are available, some even arguing for keeping the samples at –90 °C in the solution for several days [19]. Here, substitution was usually performed over night for practical reasons using an exponential warming (see 2.3.3), which lead to an approximate duration of 16 to 24 hours. Since no difference in quality of these samples was

observed, in this experiment substitution was shortened drastically to 3 hours with the same embedding procedure as above. To our great surprise, the sample quality was almost the same as for substitution over 20 hours, except for subtle differences in nuclei, eventually representing small ice crystals **(Fig. 5F)**. As already stated, this applies to cell monolayers and will probably not be the case for thicker samples as tissues because of the greater dimensions.

3.1.4 Fixatives and Concentrations

The original protocol used for freeze-substitution was based on 2 % osmium tetroxide. Since this represents a major factor in cost and disposal in the entire preparation a reduction in osmium consumption would be desirable. Accordingly, the osmium concentration was gradually reduced to 0.2 % (w/v), which had no visible effect on the fixation quality and only slightly reduced the contrast. Since 5 % water is added to the substitution medium, both osmium tetroxide and uranyl acetate can now be dissolved in water in a stock solution containing 4 % (w/v) osmium tetroxide and 2 % uranyl acetate which is stable at 4 °C and can then be diluted 1:20 in acetone to yield the final substitution medium of 0.2 % (w/v) osmium tetroxide, 0.1 % (w/v) uranyl acetate and 5 % (v/v) water in acetone. This mixture gives identical results as the original protocol using 2 % osmium and reduces costs and waste. In a further step also uranyl acetate was replaced by lead citrate, which has comparable affinities to charged groups in biomolecules and gives structural contrast very similar to the standard protocol.

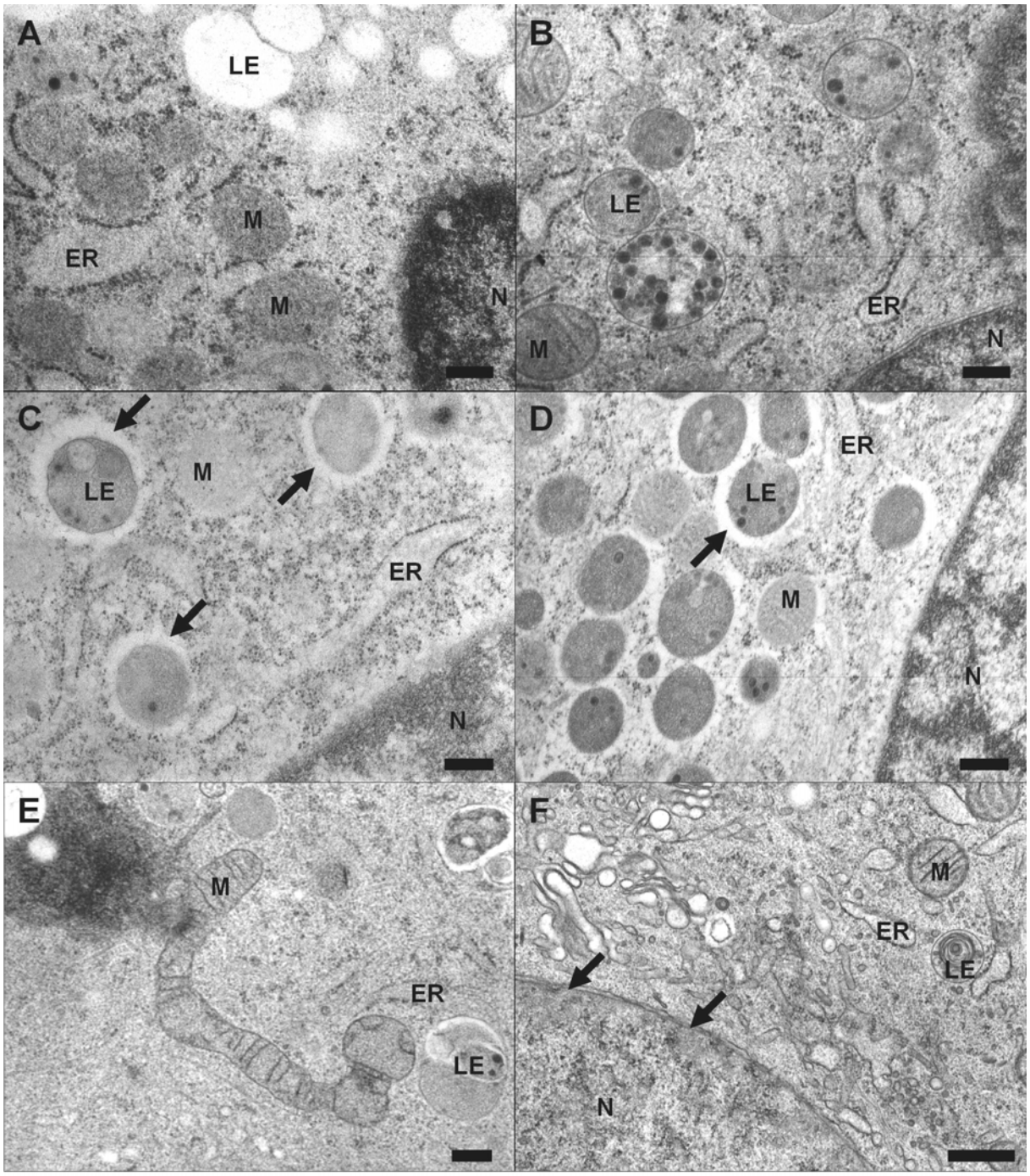

Figure 5: Substitution with different solvents and fast warming. (A) After substitution in ethanol containing osmium tetroxide and uranyl acetate without water, cellular membranes were not visible, neither in mitochondria (M), the endoplasmic reticulum (ER) or in late endosomes (LE). In contrast, ribosomes on the ER were strongly contrasted (bar 200 nm). **(B)** When 5 % water was added to the ethanol medium, all membranes became well visible and the general contrast was increased (bar 200 nm). **(C)** Replacement of ethanol by methanol without water, resulted in even stronger extraction and shrinkage of organelles (arrows).

Membranes were not visible and mitochondria (M) almost not identifiable (bar 200 nm). **(D)** Upon addition of 5 % water to the methanol medium, the visibility of membranes was slightly increased, but the extraction artefacts (arrow) remained (bar 200 nm). **(E)** As additional solvent, 2-butanol was tested. Without water the sample quality was comparable to ethanol with water (bar 200 nm). **(F)** Shortening the substitution time from approximately 16 hours to 3 hours in the standard acetone medium containing osmium tetroxide, uranyl acetate and water resulted in surprisingly good structural preservation and the cytoplasm was free of obvious ice crystal segregation patterns. Interestingly, only at the inner nuclear membrane the structure appeared diffuse, probably due to ice crystal damage (arrows) (bar 500 nm). ER endoplasmic reticulum, LE late endosomes, M mitochondria, N nucleus.

3.1.5 Application of HPF / FS on Poxvirus Morphogenesis

A special field of virological and cell biological interest is the long lasting discussion on the structure of the poxvirus core membrane. Since several years it is disputed if the so called crescent shaped membranes are single membrane bilayers open at their ends or if they actually represent membrane cisternae where the membranes are so tightly apposed that the bilayer structure is barely seen. Several approaches to this question have been done by scanning and transmission EM [32, 74]. In collaboration with Jacomine Krijnse-Locker (EMBL Heidelberg) HeLa cells were infected with the poxvirus MVA and high-pressure frozen at 6 h p.i. At this time point the first crescent shaped membranes were observed. As already suggested by Risco et al. [74], they consisted of a bent cistern in which the two tightly apposed bilayers were apparently connected by a dense material. Also already fused, double-membraned vesicular cross sections were observed **(Fig. 6 A and B)**.

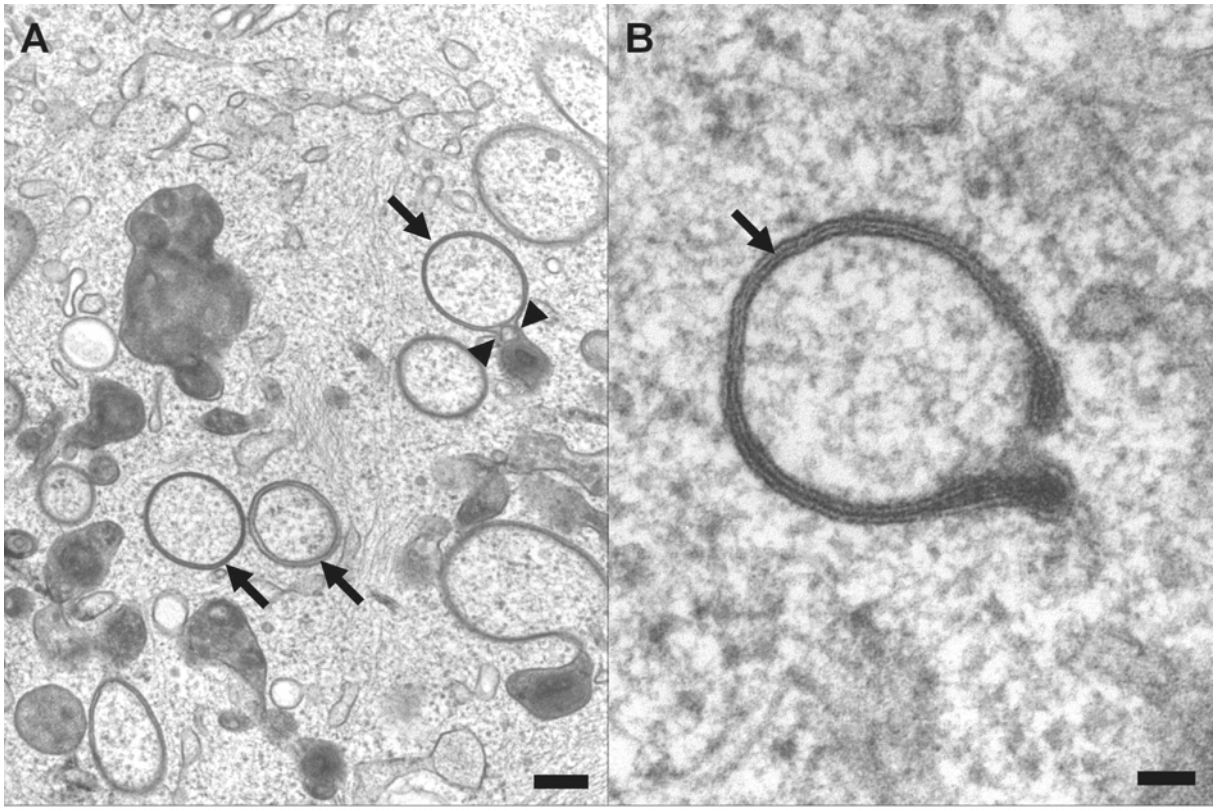

Figure 6: Immature virion morphogenesis of poxviruses. (A) The overview image of the cytoplasm of an MVA-infected HeLa cell at 6 h p.i. shows several double membraned cisternae and “vesicles” induced by the virus (arrows), one being connected with a assumed later stage in core formation (arrowheads) (bar 200 nm). **(B)** The magnification of a “crescent shaped membrane” clearly shows that it consists of a double membraned cistern connected by a dense material. The membranes are so tightly apposed that the connected leaflets of the membrane are barely visible as thin line (arrow) (bar 50 nm).

3.2 MCMV

As MCMV is considered as an approximate model system and in terms of morphogenesis is similar to HCMV first experiments especially on the role of UL97 / M97 in the viral replication was done in this system. This investigation of the egress of MCMV with the HPF / FS approach in general confirms the egress pathway described in the literature, but adds new structural features to the current model.

3.2.1 MCMV (Smith Strain) Morphogenesis

The first structure of this process visible in the electron microscope is the formation of the different capsid types. The capsid is preformed in the infected nuclei as B-capsid **(Fig. 1B)** with an internal scaffold structure and subsequently loaded with vDNA to from the mature C-capsid **(Fig. 1C)**, while the empty A-capsid is probably formed by abortive packaging of the vDNA **(Fig. 1D)**. In nuclei infected with the wild type Smith strain the particle ratios were 1.3 % A, 20.3 % B and 78.4 % C-capsids at 48 hours p.i. (n=929) **(Fig. 7)**.

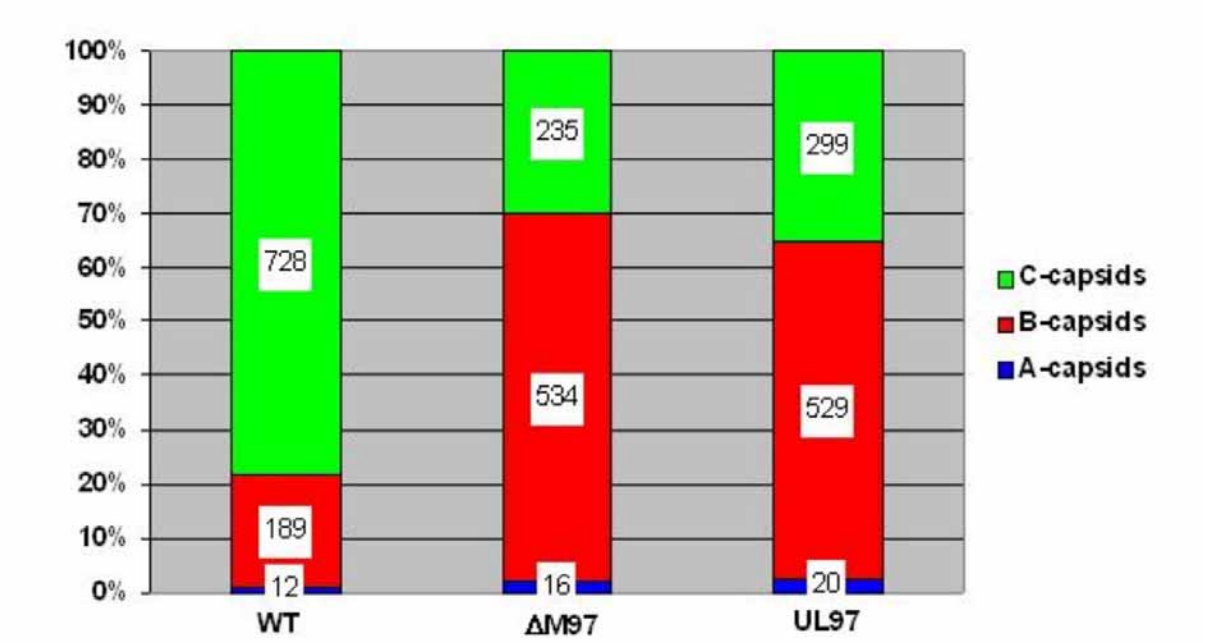

Figure 7: Nucleocapsid particle ratios in 3T3 fibroblasts infected with the respective MCMV mutants as counted in the TEM. 3T3 fibroblast cells were infected with either wild type MCMV (WT), the M97-deletion MCMV (ΔM97) or the virus where M97 was replaced by HCMV UL97 (UL97) and prepared for TEM. In thin sections infected nuclei were identified and the nucleocapsid types (depicted in Fig. 1B-D) were counted, i.e. A-capsids (empty capsids; blue), B-capsids

(capsids only containing the scaffold protein; red) and C-capsids (mature, vDNA-filled capsids; green). The numbers in the columns represent the total particles counted over >8 independent nuclei for each virus. Comparing columns of WT and ΔM97 it can be seen that upon deletion of the M97 ORF of MCMV the relative amount of B-capsids drastically increases on expense of C-capsids, while the fraction of A-capsids remains constant. The third column shows that this phenotype is not rescued by insertion of the UL97 ORF from HCMV.

When viewing these samples a startling structure could be seen in infected nuclei: Clearly resolved single membranes were visible that were of a tubulo-vesicular shape. In addition, nucleocapsids were in close contact with these membranes and several budding profiles in different stages were present **(Fig. 8A and B)**. Some of the membranes were continuous in section with the inner nuclear membrane while others appeared vesicular.

To assess the topology of these membranes serial sectioning (not shown) and stereo imaging of 400 nm thick sections **(Fig. 8C)** was performed. These experiments showed that the apparently vesicular membranes were cross-sectioned tubular infoldings of the inner nuclear membrane. These tubules were up to 4 µm long and 500 nm wide and their intranuclear surface was apparently free of nuclear lamina in contrast to the peripheral inner nuclear membrane **(Fig. 8D)**. Accordingly, the lumen of the tubule is continuous with the perinuclear space.

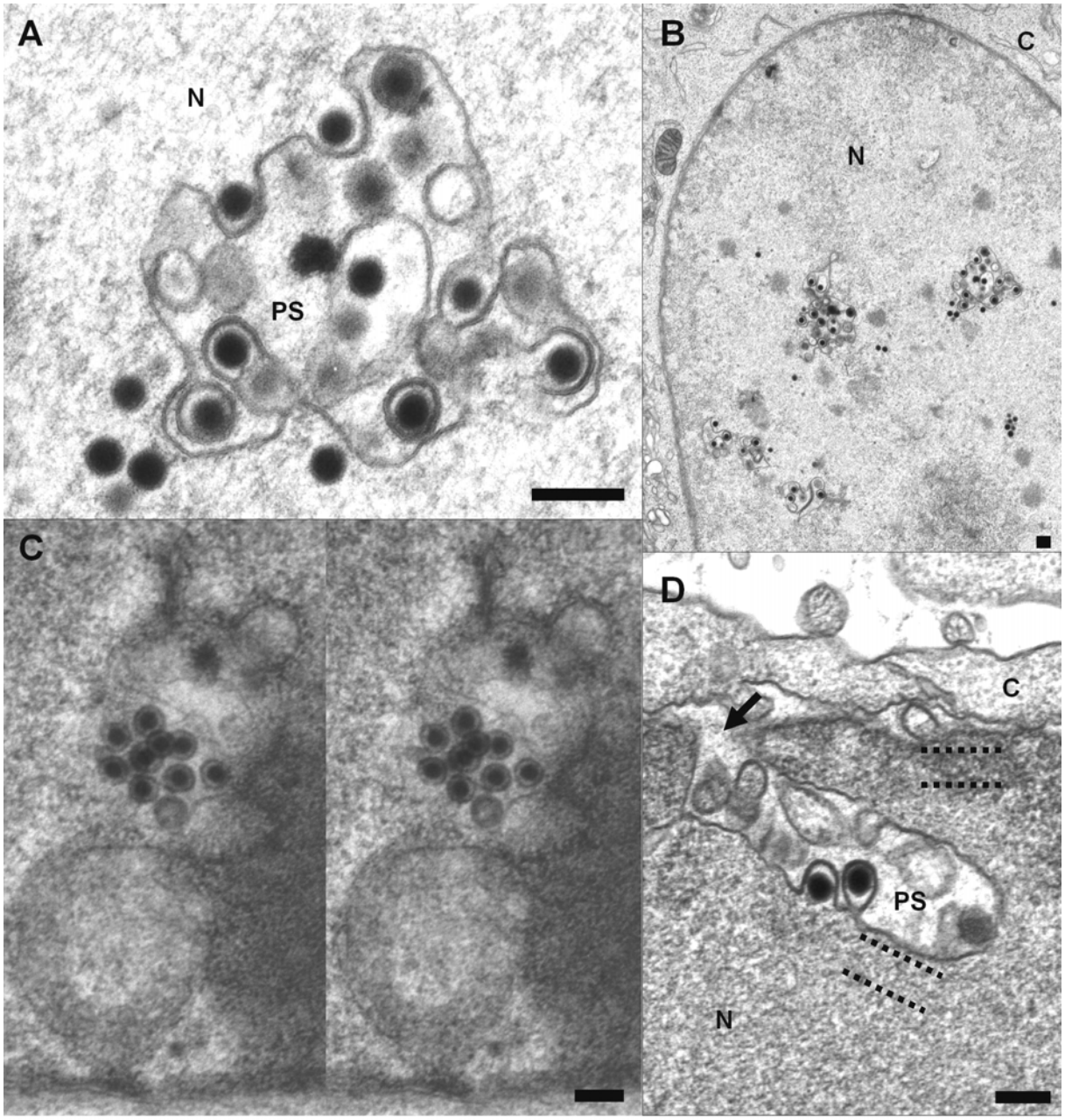

Figure 8: MCMV induces deep infoldings of the inner nuclear membrane for its primary envelopment. (A) A thin section through a fibroblast infected for 48 hours shows intranuclear single membranes involved in primary envelopment of nuclear C-capsids. All intermediate stages of budding can be seen (bar 200 nm). **(B)** Overview images of an infected nuclei reveal several such infoldings that approximately amount to a dozen per nucleus (bar 200 nm). **(C)** Stereo imaging (viewed with stereo glasses) of 400 nm thick sections shows that the apparently vesicular profiles are in fact cross-sectioned tubulo-vesicular infoldings of the inner nuclear membrane with a complex 3D architecture (bar 200 nm). **(D)** Longitudinal sections show that the infoldings had lengths of up to 3 µm and diameters of up to

500 nm and were also free of visible lamina when compared to the nuclear periphery (dotted lines). The lamina was apparently depolymerised locally, thus forming the narrow neck of the infolding (arrow). Accordingly, the lumen of the infoldings is continuous with the perinuclear space (PS) (bar 200 nm). C cytoplasm, N nucleus, PS perinuclear space.

The budding process into the infoldings also showed interesting aspects. In all MCMV samples (including all mutant viruses) budding at the inner nuclear membrane was initiated almost exclusively by C-capsids and very rarely by B-capsids. Almost nothing is known about the mechanism, which leads to budding, but a primary tegument is postulated to make the contact between the capsid and the viral membrane proteins of the inner nuclear membrane. At the moment the proteins pM50 and pM53 are probable candidates in this process, but may not act alone. Also in this question, the power of the HPF/FS approach can be seen, since it was possible to visualize an electron-dense material, probably representing the primary tegument, at the capsid-membrane interface during budding and in the primary enveloped particle in both thin sections and virtual sections through a reconstructed tomogram **(Fig. 9)**.

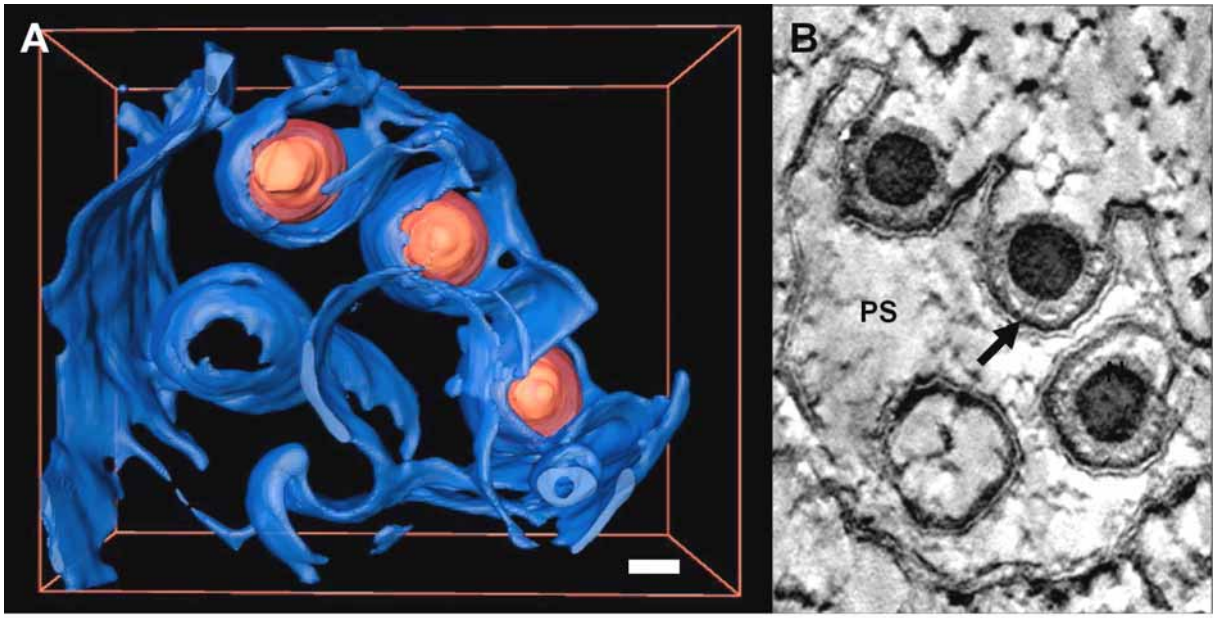

Figure 9: Tomography of MCMV primary envelopment at an infolded inner nuclear membrane. (A) In the 3D model of the tomogram membranes are represented in blue and viral particles in red. The image shows 3 nucleocapsids budding into the lumen of an infolding (bar 50 nm). **(B)** A virtual cross-section through the reconstructed tomogram shows the presence of an electron-dense material at the interface of the capsids with the membrane, probably representing the primary tegument (arrow). PS perinuclear space. Reconstructed by Ch. Kübel (FEI, Eindhoven).

The subsequent step in nuclear egress would be the fusion of the primary envelope with the outer nuclear membrane to release the naked capsid to the cytoplasm. While cytoplasmic particles could sometimes be seen in close apposition to the outer nuclear membrane, a fusion intermediate was never observed. In the cytoplasm, the capsids were distributed among the following structures: cytoplasmic clusters of naked capsids, single naked capsids, heavily tegumented capsids being “wrapped” by cisternal elements, and fully enveloped and tegumented virions in the lumen of cisternae and vesicles **(Fig. 10A and B)**. In accordance with the exclusive primary envelopment of C-capsids almost all cytoplasmic particles were loaded with vDNA. In proximity of the nucleus, naked capsids were sometimes seen aligned along microtubules **(Fig. 10C)**. Secondary envelopment usually to place in the region of one specific Golgi-complex / trans-Golgi network (TGN) which contained several additional membrane cisternae active in secondary envelopment of virions, while the other Golgi-areas morphologically appeared as in uninfected cells. Secondary

envelopment often proceeded by wrapping of several heavily tegumented capsids by a single cistern resulting in multiple capsids within a single membrane **(Fig. 10D)**. The tegument seemed to be condensed during this process. The multicapsid virions were also observed in multilamellar vesicles where membrane rearrangements seemed to take place **(Fig. 10B)**. At later time points, i.e. 50 hours p.i. virions were sometimes also seen in large (several micrometers in diameter), predominantly translucent vesicles (often referred to as “vacuoles” in the literature, **(Fig. 10E)**. Fully mature single capsid virions were frequently observed in small vesicles and cisternae from which they are believed to be released into the extracellular space.

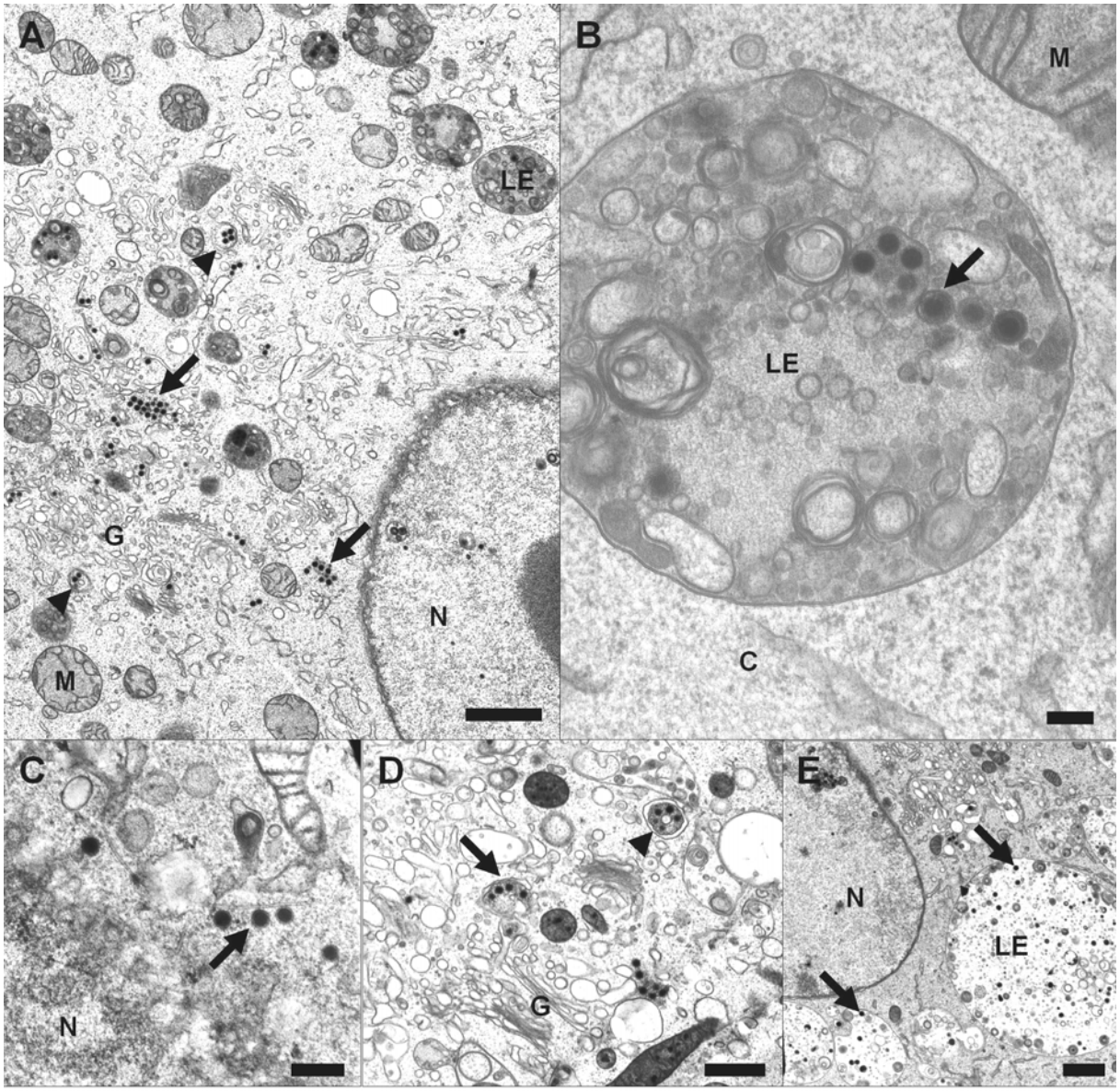

Figure 10: Cytoplasmic stages in MCMV morphogenesis. (A) Overview over the cytoplasm of a fibroblast infected with MCMV. Cytoplasmic capsids accumulate in clusters embedded in tegument material (arrows). Multiple capsids are then enveloped by cisternae (arrowheads) in proximity to a Golgi-complex (G) (bar 1 µm). **(B)** Unexpectedly, enveloped virions were also observed in late endosomal compartments (LE) as judged by their internal membranes. Additionally, multicapsid virions were observed to have a dynamic limiting membrane reminiscent of budding events (arrow) (bar 200 nm). **(C)** In the cytoplasm naked capsids were seen aligned along microtubules (arrow) in close proximity to the nucleus (N) (bar 200 nm). **(D)** The secondary envelopment of capsids occurred in proximity to a Golgi-complex (G). The envelopment proceeded

by wrapping of cisternae around single or multiple tegumented capsids (arrow) leading to the formation of a multicapsid virion (arrowhead) (bar 500 nm). **(E)** In late stages of infection the formation of very large, probably late endosomal vesicles (LE, termed “vacuoles” in the literature) was observed that contain several virions (arrows) (bar 1 µm). C cytoplasm, G Golgi-complex, LE late endosomes, M mitochondria, N nucleus.

3.2.2 Phenotypical Characterisation of an M97-Deleted MCMV

As introduced before, the deletion of M97 from the viral genome leads to a reduced replication of the virus but the function of pM97 (and its HCMV homolog UL97) remains debatable. 3T3 fibroblasts were therefore infected with the MCMV ΔM97 mutant and prepared for EM with HPF / FS at 48 h p.i. and compared to the wild type Smith strain. In these samples several nuclear phenotypes of the deletion were observed. The most obvious was a relative increase of B-capsids on expense of C-capsids in infected nuclei. The ratios were 2.0 % A, 68.0 % B and 30.0 % C-capsids (n=785), which represents an increase of B-capsids by 48 % compared to the wild type virus **(Fig. 7)**. A further observation was that nuclei infected with the mutant virus showed large subnuclear areas with a particular fine structure that was clearly different from the normal nuclear architecture. To better visualize effects on these processes, overview images of nuclei were taken and the capsid types were digitally labelled in Adobe Photoshop **(Fig. 11A and B)**. This lead to the finding that in cells infected with the MCMV ΔM97, the nucleocapsid distribution and the nuclear architecture were changed as following: The large subnuclear areas were apparently excluding all capsids and while the C-capsids were mainly accumulating at the periphery of the subnuclear areas, the B-capsids were now randomly dispersed within the nucleoplasm. Additionally, the typical clustering effect seen with wild type strain was strongly reduced **(Fig. 11A and B)**. Further statistical analysis (collaboration with F. Fleischer and V. Schmidt, Dept. of Stochastics, Universität Ulm) showed that clustering was strongly reduced for C-capsids and abolished for B-capsids, as seen in the point pair density diagrams **(Fig. 11C and D)**. To elucidate the composition of the subnuclear areas, correlative fluorescence and electron microscopy was performed by serial sectioning and overlaying of the images. It turned out that the subnuclear areas seen in the TEM were free of DAPI (staining of DNA) **(Fig. 11E and F)** and Syto RNAselect (RNA) signal **(Fig. 11G)**, and even appeared to displace the cellular chromatin. Since these findings suggested the accumulation of a protein component, cell nuclei were isolated from infected cell cultures and SDS-PAGE was performed. These gels had a complex band pattern unexpectedly showing the disappearance of two protein bands after deletion of M97 **(Fig. 11I)**.

To investigate if the reduction of C-capsids after the deletion of M97 was due to a defect in packaging of vDNA that in this case would be expected to accumulate, nuclei were isolated and the vDNA content was estimated by a twofold dilution series using PCR for detection. To discern between packaged and unpackaged vDNA, one nuclei sample was digested with micrococcus nuclease (from which the encapsidated DNA is protected). Comparing the ratios of encapsidated to total vDNA in both wild type and deletion mutant infected samples showed that the ratio was not changed after deletion of M97, arguing for normal packaging of vDNA **(Fig. 11K)**.

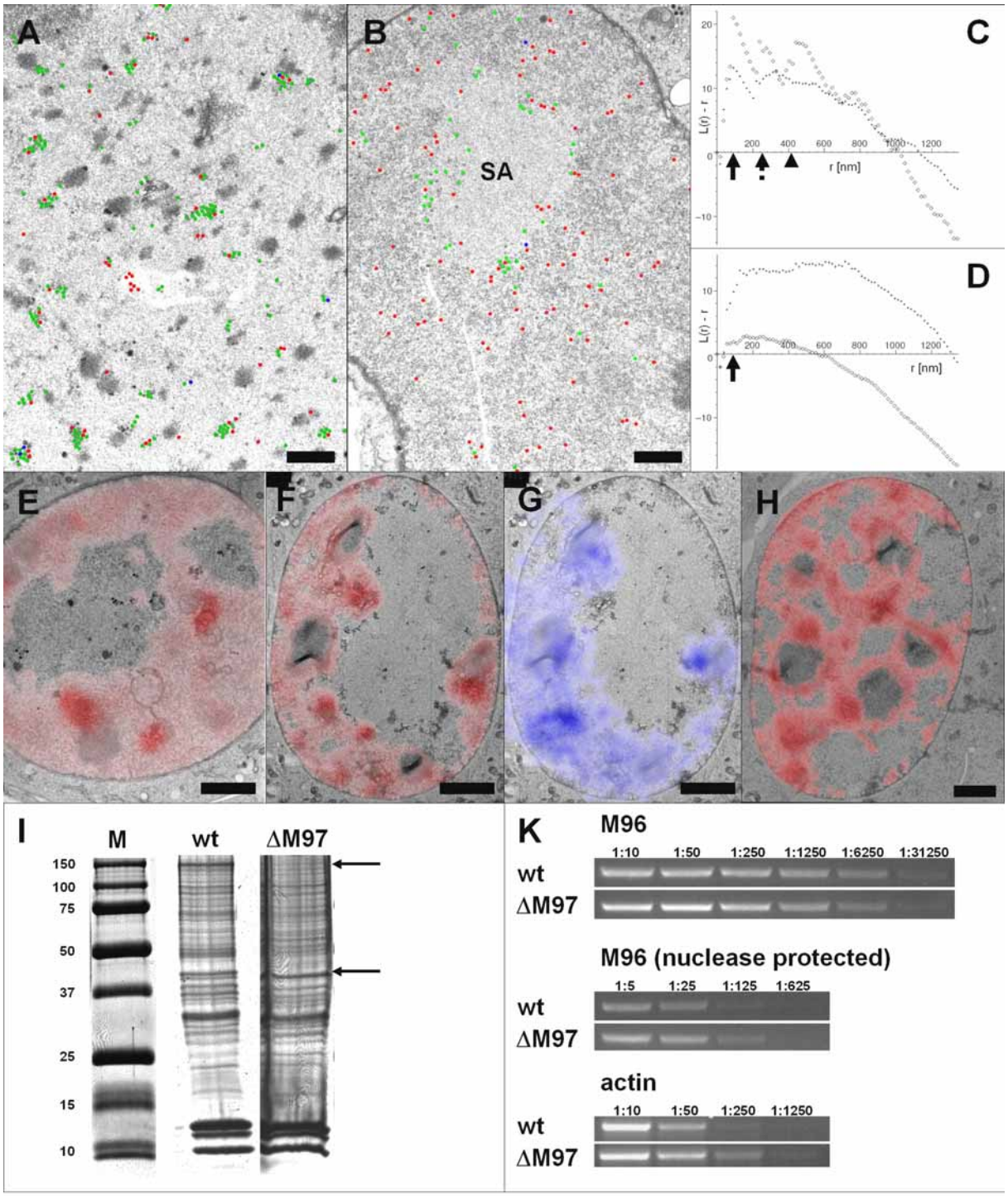

Figure 11: Analysis of the ΔM97-phenotype in MCMV. (A) In an overview of a nucleus infected with the wild type MCMV the nucleocapsid types were colour coded (A-capsids blue, B-capsids red, C-capsids green). MCMV wt shows the typical nucleocapsid clustering and a high amount of C-capsids (see Fig. 6) (bar 1µm). **(B)** The overview of a nucleus infected with the MCMV ΔM97 shows a reduction of C-capsids, a rather random capsid distribution and the emergence of differently structured subnuclear areas (SA) (bar 1 µm). **(C)** This stochastic

analysis of 10 independent nuclei infected with the wild type MCMV shows the density of point pairs (corresponding to the function L(r) – r) versus the distance between the two points in nanometers (r), so that a clustering can be seen by a positive slope in the curve at the distance of the particles in the cluster. C-capsids (crosses) as well as B-capsids (diamonds) can be seen to cluster at distances of approximately 80 to 100 nm (arrow), 240 to 280 nm (dotted arrow), and B-capsids additionally cluster at a distance of 400 to 440 nm (arrowhead). **(D)** The stochastic analysis of 9 nuclei infected with the MCMV ΔM97 instead only shows a weak clustering of C-capsids again at 80 to 100 nm (arrow), while the clustering of B-capsids is completely abolished. **(E)** Correlative electron and fluorescence microscopy of nuclei infected with MCMV wt and stained with DAPI (red) show, that the wild type MCMV forms small DNA free areas (bar 2 µm). **(F)** In nuclei infected with the MCMV ΔM97 the large subnuclear areas are formed that are free of DNA and appear to displace the cellular chromatin and the nucleocapsids (bar 2 µm). **(G)** When staining with SytoRNAselect it can be seen that the subnuclear areas are also free of RNA (blue) (bar 2 µm). **(H)** Also in uninfected cells the distribution of DNA is not homogenous but the DNA free areas are significantly smaller than in (F) (bar 2 µm). **(I)** Unexpectedly, SDS-PAGE of isolated nuclei shows that after deletion of M97 two protein bands disappear (arrows). **(K)** To confirm that the deletion of M97 does not lead to an accumulation of vDNA, the vDNA content of isolated nuclei was tested by a fivefold dilution series and detected by PCR of the unrelated M96. Detection of total vDNA did not show significant differences between the two strains, neither did detection of nuclease protected (i.e. already encapsidated) vDNA. The last lanes show the actin loading controls.

3.2.3 Phenotypical Comparison of MCMV ΔM97 with MCMV UL97

Since no animal model is available to study the effects of ganciclovir therapy on the organismic level, it was an aim to genetically engineer a MCMV virus to exhibit sensitivity to ganciclovir. Since M97 is only very weakly activating this drug, the M97 deletion virus modified to carry the homologous UL97 ORF of HCMV, thus effectively replacing M97 by UL97. Unfortunately, this MCMV UL97 still exhibited a replication defect of 10- to 100-fold [91]. Analysis by EM showed that the capsid ratios were still in the range of the MCMV ΔM97 with 2.3 % A-, 62.4 % B- and 35.3 % C-capsids (n=848, **Fig. 7**), concluding that UL97 failed to rescue the deletion of M97.

3.2.4 Investigation of MCMV Nuclear Egress by Conditional Expression

Due to the common interest in MCMV nuclear egress a collaboration was started with the group of U. Koszinowski (LMU Munich), which established a system to express modified viral (or cellular) proteins in the context of infection by integrating an inducible expression cassette in the viral genome [77].

A first candidate protein in nuclear egress was pM50, which is a transmembrane protein located mainly in the inner nuclear membrane and thought to recruit the nucleocapsid to the budding site together with pM53. By using a random mutagenesis approach and selecting on growth inhibiting mutants, which were then screened for a dominant negative phenotype by conditional expression in the context of the wild type virus infection (to be published). The MCMV M50ΔP is such a construct that without induction exhibits normal viral growth but when induced with doxicycline expresses the dominant negative M50ΔP protein and shows 100-fold reduced growth. To further clarify the position of the block in viral egress samples were prepared by HPF / FS for EM. The samples infected for 48 hours in presence of doxicycline showed a very peculiar phenotype. Firstly, the block in viral egress was obviously in primary envelopment, since no virions were found in the cytoplasm or in the perinuclear space **(Fig. 12A)**. Additionally, the previously described infoldings of the inner nuclear membrane had folded up on each other and showed a lettuce-like morphology. The lumen of the infoldings were reduced to approximately 30 to 80 nm and the space connecting two adjacent cisternae appeared to have a constant

distance of approximately 15 nm and filled with an electron dense material **(Fig. 12B)**. In the cytoplasm of these cells similar multilayered cisternae of the rough endoplasmic reticulum (ER) **(Fig. 12C)** could be observed together with irregular accumulations of membranes reminiscent of smooth ER **(Fig. 12D)**. Also here the cisternae showed the same spacing and intercisternal material. Control experiments with the uninduced MCMV M50ΔP showed wild type morphogenesis, a normal nucleus and, rarely, double-stacked rough ER cisternae, arguing that the inducible promoter was slightly leaky.

To clarify if this phenotype might just be linked to overexpression of pM50 an experiment with a virus conditionally expressing an HA-tagged M50 (MCMV M50HA) was performed. In induced samples, the viral morphogenesis appeared to proceed normally and no intranuclear membrane stacks were found. Interestingly, the cytoplasmic stacks of rough ER were still present, but no accumulation of smooth ER-like membranes could be observed **(Fig. 12E)**.

In order to follow the process of nuclear egress, the conditional expression system was also used in an approach to fluorescently label capsids within the nucleus. For this a variant conditionally expressing a GFP-tagged version of the small capsid protein M48.5 (i.e. MCMV SCP-GFP) was constructed. Unfortunately, expression of this protein lead to a strong reduction of viral titers. The position of the block was again investigated by EM. Since the SCP binds to the pentons of the capsid, it was expected that a step in nuclear egress was defective and thus would lead to a nuclear accumulation of DNA loaded C-capsids. Imaging of these samples showed an unexpected effect. In the induced specimens, large clusters of nuclear B-capsids were observed (not shown). As expected the cytoplasm of the cells was devoid of any viral particles, while uninduced samples showed normal viral morphogenesis.

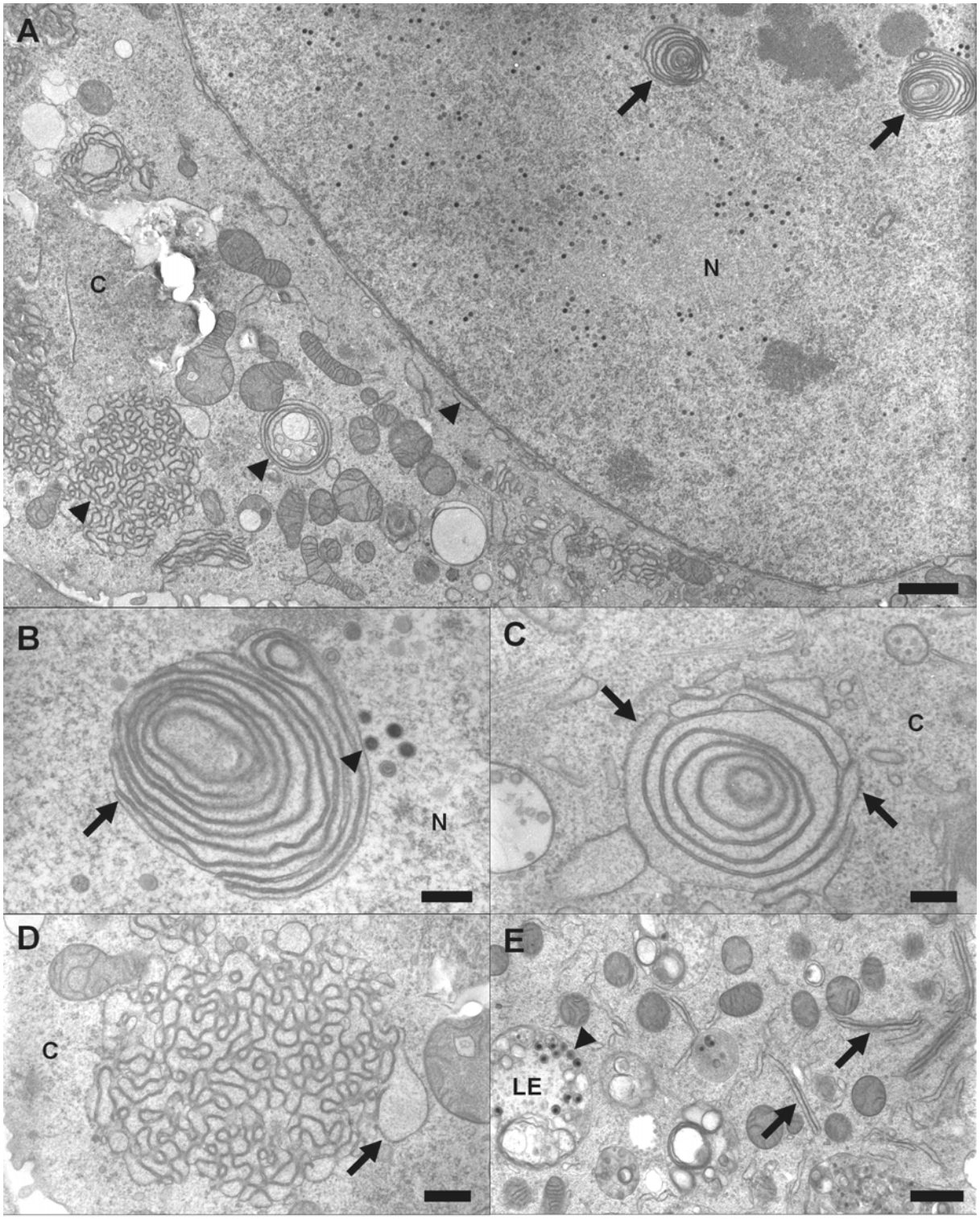

Figure 12: MCMV variants conditionally expressing pM50 proteins. **(A)** Induction of the dominant negative MCMV M50ΔP resulted in lamellar inner nuclear membrane infoldings (arrows), which apparently prevented the capsids from undergoing primary envelopment. Additionally, it also induced the accumulation and stacking of cytolpasmic and outer nuclear membranes (arrowheads) (bar 1µm). **(B)** At higher magnification it can be seen that the

lamellae consist of stacked cisternal infoldings of the inner nuclear membrane (arrow) that are joined by an electron-dense material. Apparently, capsids are still able to contact the membrane but do not undergo budding (arrowhead) (bar 200 nm). **(C)** Also in the cytoplasm cisternae are stacked that can be identified as rough ER by the presence of ribosomes (arrows). The same phenomenon is visible at the outer nuclear membrane in (A). Also the spacing of the stacks is identical with the nuclear lamellae (bar 200 nm). **(D)** Additionally, the adherence of an irregular membrane compartment was observed, which probably represents smooth ER due to the connectivity with rough ER (arrow). Also here the spacing was willed with electron-dense material (bar 200 nm). (E) Induction of the MCMV M50HA, which corresponds to an overexpression of pM50, also induced stacking of cytoplasmic ER membranes (arrows), but not of inner nuclear membrane infoldings. Also, the nuclear egress of the capsids was not blocked so that virions were normally enveloped (arrowhead) (bar 1µm). C cytoplasm, LE late endosomes, N nucleus.

3.3 HCMV

MCMV and HCMV are regarded as very similar in their morphogenesis. In the main aspects this is true but still several aspects of the process appear structurally different. The main difference is the production of so called “dense bodies” (non-infectious enveloped tegument aggregates) by HCMV strains thus adding a structural component to the egress pathway. Other subtle distinctions remarked in the following chapters might as well reflect differences in the viruses as well as in the respective cell lines used. Additionally, most of the work concerning the egress pathway was done with the AD169 strain (at 4 to 5 d p.i.), which represents a fibroblast adapted laboratory strain that has lost its capacity to infect endothelial and epithelial cells which constitute the most important natural host cells. Thus, the overall picture of HCMV egress can be concluded from these images but fine structural details mentioned in the following chapters apply to human foreskin fibroblast cells (HFF) infected with AD169 and might differ in other “wild type” strains, especially in endotheliotropic strains. Also the direct comparison with the

3.3.1 HCMV AD169 Morphogenesis

The first nuclear stages of the morphogenesis structurally appear very similar to MCMV. The capsid is pre-formed as B-capsid and subsequently loaded with DNA to form the C-capsid. The first differences to MCMV are that the relative amount of C-capsids is markedly reduced and that the capsid clustering typical for MCMV is less prominent **(Fig. 13A and B)**. Nuclear capsid ratios were 8.2 % A-capsids, 67.7 % B-capsids and 24.1 % C-capsids (n=1092). Also with HCMV infoldings of the inner nuclear membrane were observed but were usually smaller than for MCMV **(Fig. 13 A and B)**. Interestingly, in this system also B-capsids were performing primary envelopment thus leading to the presence of B-capsids in the entire later pathway. The hypothetical primary tegument was very well visible in perinuclear virions **(Fig. 13B)**. The cytoplasm of infected cells appeared significantly different when compared to MCMV, mainly due to the dense bodies **(Fig. 13 A and C)**. These were present in larger amounts and size than virions. Early stages of dense body formation were visible as diffuse aggregation of electron dense material (the secondary tegument proteins) in close proximity to bent cisternae **(Fig. 13C)**. During the wrapping process the protein mass was condensed and ultimately pinched off into the cistern. Single cisternae were observed to support two or more wrapping events of capsids or dense

bodies at different locations. Different membrane structures carrying virions and dense bodies were observed in thin sections, i.e. long cisternal elements, single particles in tightly fitting vesicles and vesicles harbouring several viral particles **(Fig. 12C)**. As for MCMV, in later time points (5 d p.i.) large vesicles were observed carrying many virions. Electron tomography of these samples shows that the membranes involved in secondary envelopment are interconnected and possess a complex 3D-structure **(Fig. 13D)**.

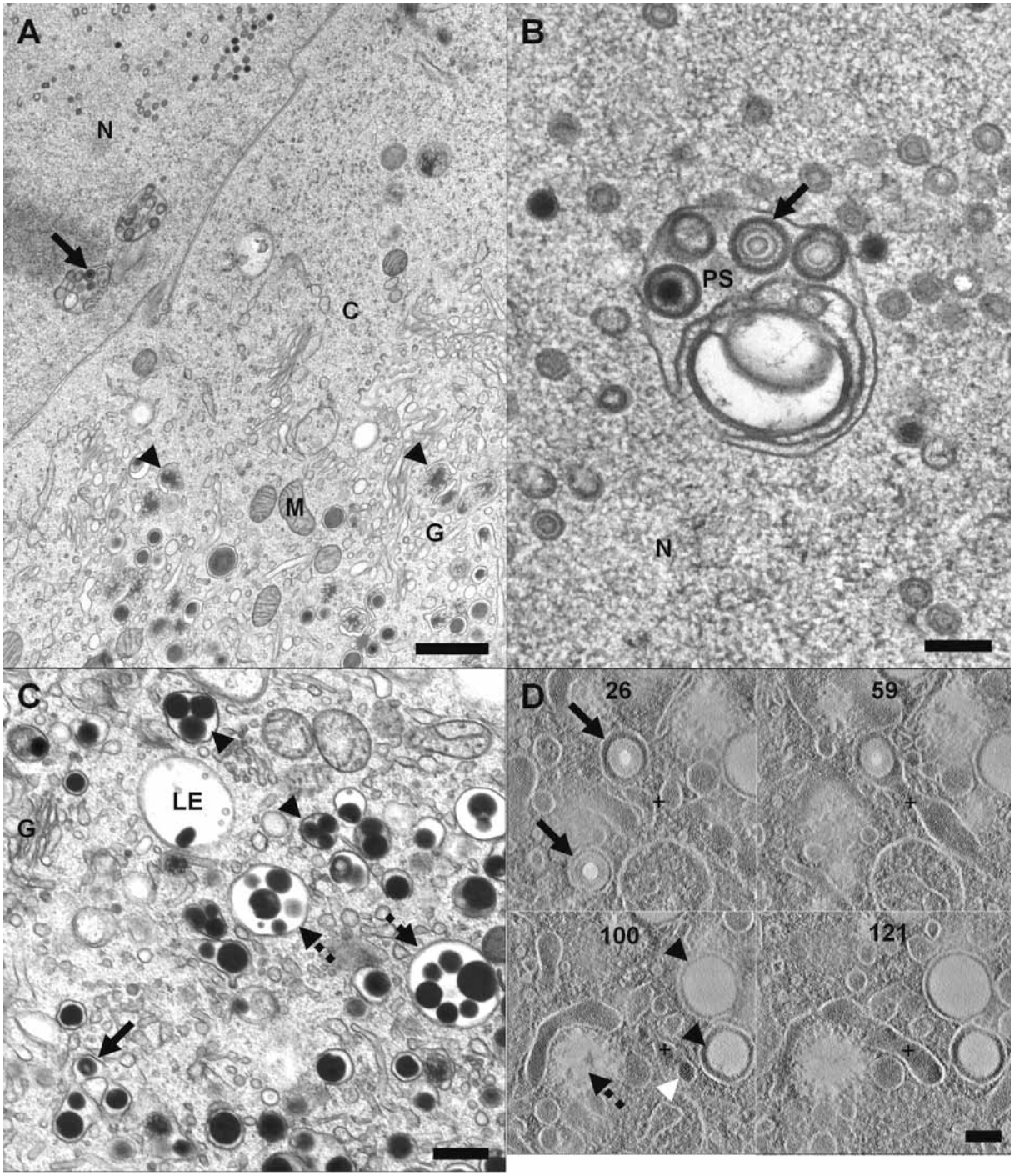

Figure 13: Egress of HCMV AD169 in HFF at 4 days p.i. (A) Overview of an AD169 infected cell shows the nucleocapsid formation, the passage of primary enveloped virions through the infolded perinuclear space (arrow) and the subsequent envelopment processes in the proximity of the Golgi-complex (G) (bar 1 µm). **(B)** The passage to the cytoplasm also occurs through infoldings of the inner nuclear membrane. In contrast to MCMV, also B-capsids are able to undergo primary envelopment. Also here the putative primary tegument is well visible (arrow) (bar 200 nm). **(C)** Enveloped virions and many dense bodies are present in different membrane compartments, i.e. cisternae (arrow), tightly fitting vesicles (arrowheads) and larger apparently endosomal vesicles (dotted arrows) (bar 500 nm). **(D)** Virtual sections (above: section number, section thickness is approximately 2 nm) through a reconstructed tomogram acquired with scanning TEM (inverted contrast) show the 3D complexity of the envelopment process. Two virions (arrows), two dense bodies (arrowheads) and the envelopment of a dense body (dotted arrow) are visible. Interestingly, the cistern enveloping the dense body is continuous with the cistern containing the upper virion through vertical tubular connections (white arrow). The cross marks identical positions in the sections (bar 100 nm). C cytoplasm, G Golgi-complex, LE late endosomes, M mitochondria, N nucleus, PS perinuclear space.

3.3.2 Involvement of Endocytic Compartments in HCMV egress

In infected samples at several days p.i. it cannot be excluded that single virions within cisternae observed under the aspect of viral egress might actually be endocytosed vial progeny. Additionally, endosomal compartments were also implied in viral envelopment in the literature. To investigate the frequency of endocytic compartments associated with virions cells were fed with 15 nm colloidal gold 4 hours before high-pressure freezing. In the respective sections few gold particles were seen, most associated with endosomal compartments as identified by their small internal vesicles. Gold was only seen together with virions or dense bodies in larger vesicles reminiscent of early and late endosomes in which the virions were not tightly enclosed by the vesicular membrane. The small vesicles containing single particles or the tubular cisternae were never observed to carry gold colloids **(Fig. 14A)**.

To further image the process of viral transport to the plasma membrane and the release to the extracellular space, a way had to be found to arrest different post-envelopment steps and thus enrich them in higher amounts. It has been published that in dendritic cells phosphatidylinositol-3 kinases (PI3K) play a role in transport of loaded MHC II complexes from multilamellar bodies to the cell membrane by tubular transport. Also in endosomal processes leading to the formation of internal vesicles in late endosomes PI3Ks have an important function. Since the process of CMV egress could rely on similar mechanisms, cells were treated with wortmannin (a PI3K inhibitor) 4 hours before high-pressure freezing in the hope to delay viral release. Unfortunately, no effect could be observed on viral egress, except for the expected reduction of internal membrane vesicles in endosomes **(Fig. 14B)**.

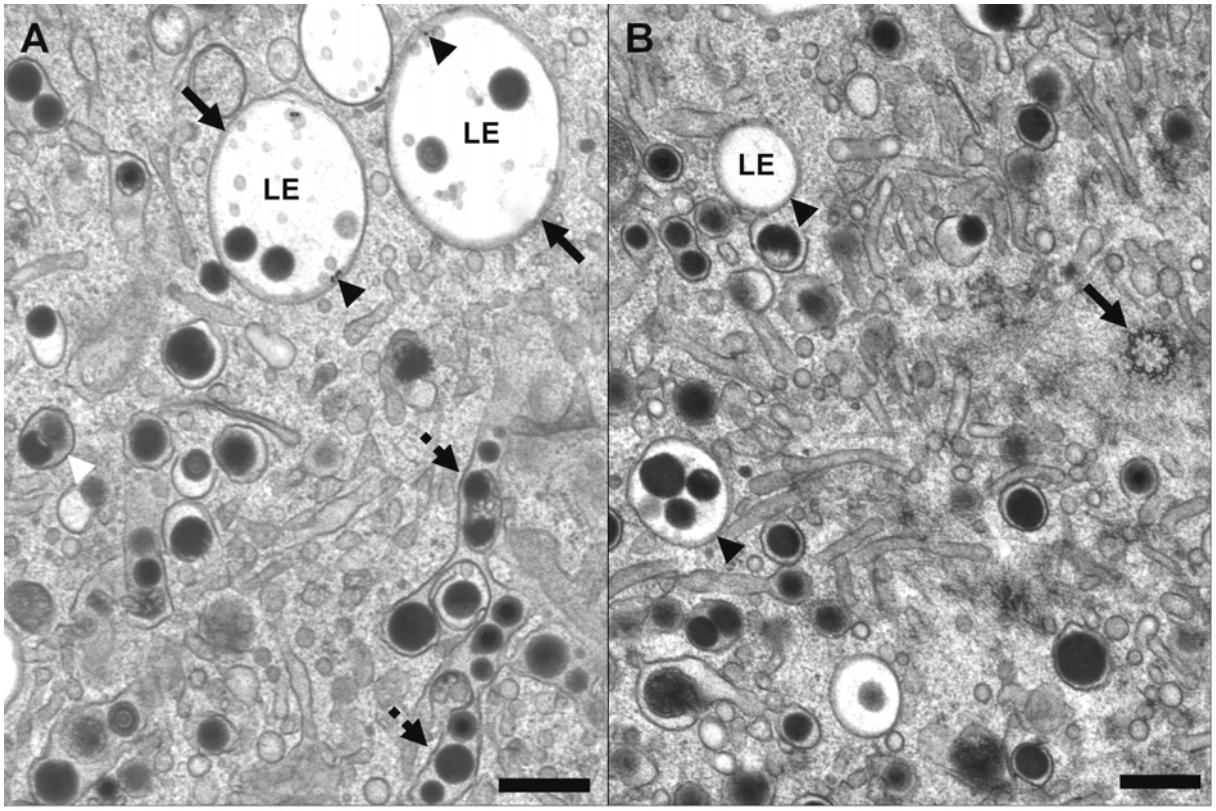

Figure 14: Identification of endocytic vesicles in HCMV AD169 egress. **(A)** Infected HFF were fed with 15 nm gold colloids for 4 hours. As expected, large vesicles containing internal membranes, virions and dense bodies (arrows) also contained gold (arrowheads), identifying them as late endosomes (LE), while cisternae (dotted arrows) and tightly fitting vesicles did not (white arrowhead) (bar 500 nm). **(B)** Inhibition of PI3K by wortmannin for 4 hours did not influence virion morphogenesis, but expectedly reduced the amount of late endosomal internal vesicles (arrowheads). Note the proximity of the envelopment processes to the MTOC (arrow) (bar 500 nm).

3.3.3 Morphological Analysis of an UL97-Deleted HCMV

In a preliminary experiment to investigate the phenotypical relation of the deletion mutants in MCMV M97 with HCMV UL97, fibroblasts were infected with a UL97 deleted AD169 virus and fixed at 4 d p.i. The most obvious defect observable after the deletion of UL97 was the emergence of large (up to several micrometers) enveloped electron dense aggregates in the cytoplasm of infected cells that appeared to be enlarged dense bodies. Also same the effects observed after deletion of M97 from MCMV could be qualitatively inferred from these samples, e.g. a high

number ob nuclear B-capsids and the appearance of a subnuclear structure **(Fig. 15A)**. To confirm these results further experiments have to be performed.

3.3.4 Imaging of an HCMV lacking 4 viral G-Protein coupled Receptors

A further phenotypical analysis of a mutant HCMV was done on the topic of G-protein coupled receptors (GPCRs). HCMV encodes for 4 known GPCRs, US28, UL72, UL33 and US27. It has been published for US28 that it is able to bind various cytokines [47] and US28, US27 and UL33 have been localized to multilamellar endosomes [21, 22], but their function in the viral infection is unclear. A deletion mutant lacking all four GPCRs has been constructed (termed “Quattro”) and prepared for EM at 4 d p.i. to investigate if any step in viral morphogenesis is disturbed. This was not the case, since all morphogenetic processes appeared to proceed as for the wild type and no accumulation of capsids could be observed in any step **(Fig. 15B)**. Quantification of nucleocapsid ratios gave an increase of C-capsids in expense of A- and B-capsids, i.e. 4.1 % A-capsids, 60.8 % B-capsids and 35.2 % C-capsids (n=1796).

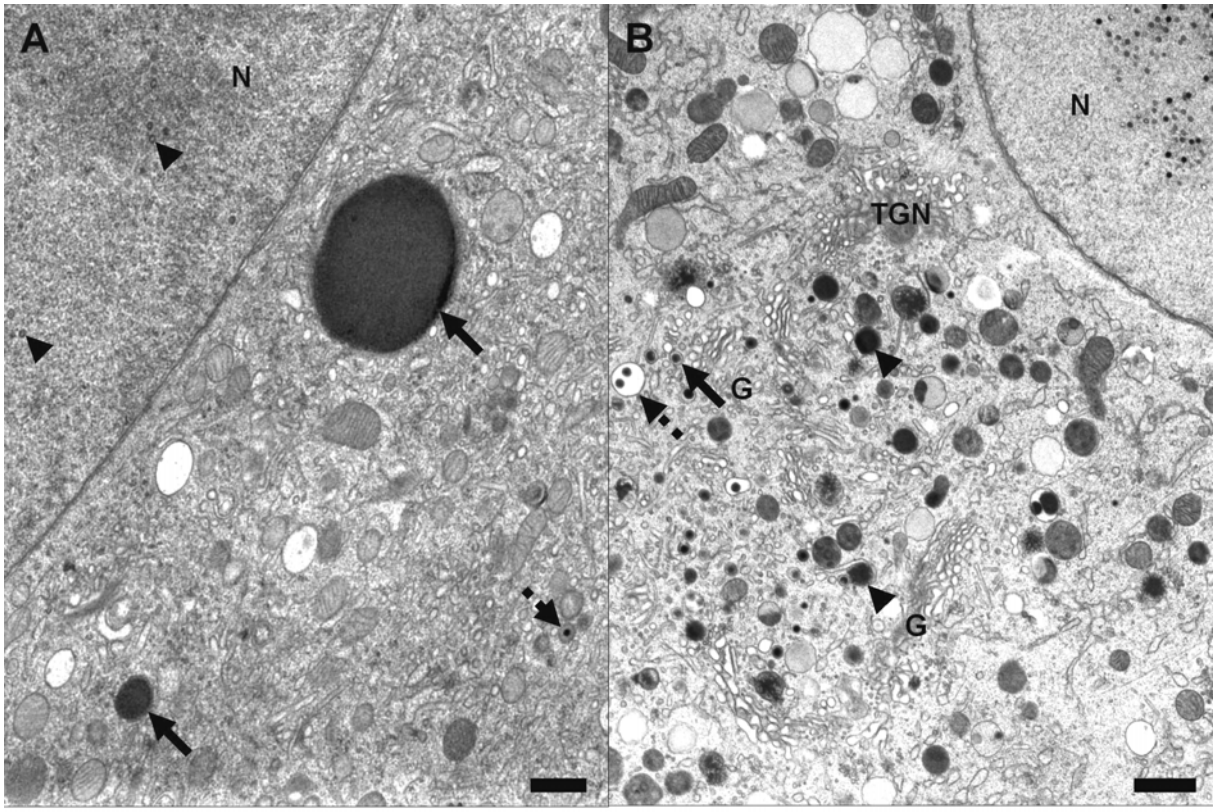

Figure 15: Further HCMV mutants. (A) The morphogenesis of HCMV ΔUL97 is disturbed and shows many nuclear B-capsids (arrowheads), few cytoplasmic virions (dotted arrow) and an irregular nuclear structure as seen for the MCMV ΔM97 (Fig10B). Additionally, large dense bodies (arrows) are formed (bar 500 nm). **(B)** The HCMV Quattro mutant lacking all four G-protein coupled receptors does not show any defects in morphogenesis. All stages are visible in normal amounts, i.e. nucleocapsids, virions in small (arrow) and large vesicles (dotted arrow) and dense bodies (arrowheads) (bar 1 µm). G Golgi-complex, N nucleus, TGN trans-Golgi network.

3.3.5 Analysis of the diverse function of two proteins encoded by UL35

UL35 is a tegument protein that also possesses transactivation capacity. The UL35 ORF contains four translation start codons, that all use the same stop and polyadenylation site. Transcription using the first (M1) leads to the UL35 full-length protein, while usage of the three downstream ones (M448, M449 and M465) leads to three short forms of similar length termed UL35A. To discern the roles of the different forms in the morphogenesis of HCMV, three viral mutants were constructed: i) AD169 ΔUL35, in which the entire UL35 ORF was deleted so that neither UL35 nor UL35A are expressed [79]. ii) AD169 RV2026, in which the three downstream methionines were mutated, so that only the full length UL35 is made. iii) AD169 UL35dATG, in which the first start codon was mutated from methionine to alanine, so that only UL35A is expressed. HFF were infected with the viruses and high-pressure frozen at 4 d p.i.

The phenotype described for the AD169 ΔUL35 could be reproduced, i.e. the emergence of electron dense aggregates in infected nuclei that were surrounded by nucleocapsids and the lack of dense bodies in the cytoplasm **(Fig. 16A)**. In general, enveloped virions were rare but appeared structurally unaffected. Additionally, an unidentified fibrillar electron dense material could be observed in the cytoplasm **(Fig. 16B)**. Cells infected with the AD169 RV2026 also showed nuclear aggregates, a lack of dense bodies and a strongly reduced amount of cytoplasmic enveloped virions (as described for AD169 ΔUL35) **(Fig. 16C and D)**. Additionally to the full-length deletion mutant the cytoplasm showed accumulations of small vesicles in connection with electron dense material **(Fig. 16D)**. In contrast, AD169 UL35dATG samples appeared to have a phenotype similar to the AD169 ΔUL97 mutant, i.e. the appearance of subnuclear areas of different structure and the presence of enlarged dense bodies in the cytoplasm **(Fig. 16E and F)**. Additionally, large unenveloped tegument aggregates were present. In spite of these effects the enveloped virions were structurally unaffected.

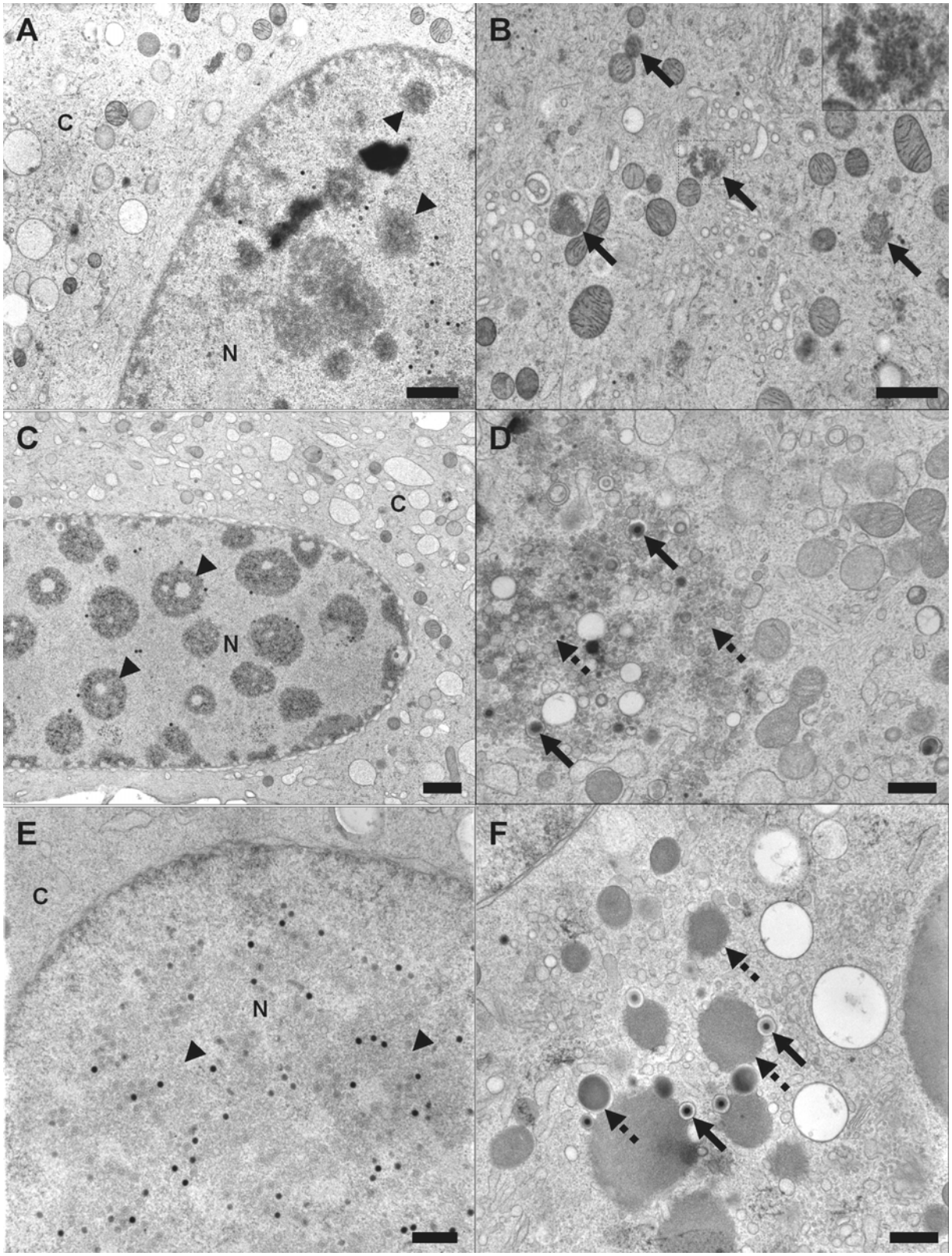

Figure 16: HCMV UL35 mutants. (A) Overview of a nucleus infected with HCMV ΔUL35, in which the complete ORF (i.e. UL35 and UL35A) is deleted. The nuclei accumulate electron-dense aggregates (arrowheads) that are surrounded by nucleocapsids (bar 1 µm). **(B)** The cytoplasm of a cell infected with HCMV ΔUL35

shows few virions and no dense bodies. Additionally, electron-dense accumulations are visible that exhibit a regularly spaced, “chequered” structure (arrows) and presumably consist of viral protein material (bar 1 µm). **(C)** Nuclei infected with the HCMV RV2026 that only expresses the tegument protein ppUL35, but not the nuclear ppUL35A, show the same nuclear aggregates of which some appear “hollow” (arrowheads) (bar 1 µm). **(D)** In the cytoplasm, HCMV RV2026 shows few enveloped virions (arrows), no dense bodies and the emergence of small vesicular membranes embedded in a presumably protein material (dotted arrows) (bar 500 nm). **(E)** Nuclei infected with the HCMV UL35dATG, which only expresses ppUL35A but not the tegument protein ppUL35, the nucleus appears similar to wild type HCMV AD169, except for the slightly irregular nuclear structure (arrowheads) (bar 500 nm). **(F)** In the cytoplasm, the HCMV UL35dATG shows wild type amounts of morphologically normal enveloped virions (arrows), but causes the formation of enlarged, enveloped and nonenveloped dense bodies (dotted arrows), similar as the HCMV ΔUL97 (see Fig. 14A) (bar 500 nm). C cytoplasm, N nucleus.

4 Discussion

The aim of this study was to re-evaluate the morphogenesis of CMVs and, on this basis, to structurally analyse various mutant CMV strains with establishment of a routine modern cryo-preparation method for cell culture systems. As a first step, the technique had to be adapted and optimised for its application in virological research. An essential aspect is the optimal retention and visibility of cellular structures. Accordingly, the first chapter of the discussion will deal with the findings in the optimisation of sample preparation, especially in freeze-substitution. The further chapters will discuss the application of the technical findings to the field of virology.

4.1 Sample Preparation Technique

The general difficulty in sample preparation by high-pressure freezing, freeze-substitution and plastic embedding is the compromise between the need for removal of the water without inducing extraction or aggregation of structural components (proteins and membrane lipids). Since complete dehydration of the sample is a necessity, this problem can be solved by a reduction of extraction or an increased fixation of the structural components. Additionally, the structural features are made visible by heavy metal contrasting during freeze-substitution. The evaluation of the preparation quality is difficult for several reasons: i) Our knowledge of the underlying physical and chemical processes of fixation and dehydration at low temperatures are at best rudimentary, also due to the complexity of the chemical composition of a biological sample. ii) The success of the preparation can only be judged qualitatively at the end of the entire process, thus showing a superposition of all previous processes influencing the sample appearance, i.e. from the quality of the living sample, over the quality of handling, freezing, substitution, fixation, extraction, contrasting and embedding to the quality of thin sectioning. iii) Until recently, the freezing process was not entirely reproducible, which lead to a significant variation of freezing quality. Fortunately, with the use of the HPM01, this problem has been greatly reduced. Accordingly, this work was focused on optimising freeze-substitution with the aim to increase the visibility and retention of cellular and viral structures.

4.1.1 The Influence of Water during Freeze-Substitution

Previous empirical experience lead to a freeze-substitution protocol based on acetone and containing osmium tetroxide for membrane fixation and uranyl acetate for stain deposition. As already noted by Walther and Ziegler on yeast samples [92], already the presence of small amounts of water substantially increases the visibility of membranes. The results shown here provide data that in acetone addition of 1 % water already leads to an increased contrast and visibility of cellular structures **(Fig. 2B)**. With the addition of 5 % water the effect is more pronounced and shows an optimal representation of cellular organelles **(Fig. 2C and D)**, while addition of up to 20 % does not influence the sample quality at all **(Fig. 2F)**, but may cause technical difficulties when embedding the sample, because after the substitution incomplete removal of water during washing disturbs the penetration of the Epon. Still, the effect of water is apparently saturable at 5 % in acetone, which argues for an involvement of a mixing equilibrium between the acetone and the water. The same effects were observed when replacing the osmium tetroxide by 0.1 % glutaraldehyde when 5 % water was added, yielding samples suitable for immunolabeling **(Fig. 3)**. What process the water actually influences can only be speculated. The original dogma in freeze-substitution was that addition of water would delay the substitution effect of the solvent, so that addition of large amounts would delay above the recristallisation temperature of amorphous water to hexagonal ice (approximately –80 °C) and thus lead to crystal growth and destruction of the sample structure. Obviously, this was not the case. To understand at which temperature the water was exerting its function during the substitution process, the substitution medium was exchanged from 5 % water to water free, or vice versa, at –60 °C. Interestingly, the effect was stronger when water was present during the warmer temperatures above –60 °C **(Fig. 4)**. Accordingly, an effect in crystallisation processes can again be excluded since these occur at lower temperatures. Contradictory to these findings comes that substitution with acetone containing just uranyl acetate and rising concentrations of water without fixatives only gives fair results without water, while already 1 % of water leads to destruction of the sample structure, probably due to extraction and aggregation. This shows that fixation has to occur if water is used, but again the reason for this effect remains elusive.

To assess the possibility that the water specifically interacts with the acetone to create the effects described above, substitution was carried out with ethanol and methanol with 5 % water and without **(Fig. 5)**. Without addition of water it was clearly seen that methanol lead to stronger extraction than ethanol, while ethanol was stronger than acetone, which corresponds to an increase of the polarity of these solvents and accordingly also to their miscibility with water, i.e. methanol > ethanol > acetone. Also with these solvents a clear favourable effect of the water could be seen on the retention of structural details. Interestingly, the improvement was again more pronounced for methanol > ethanol > acetone when adding the same percentage of water. To investigate the role of solvent polarity on the substitution quality, a solvent slightly more apolar than acetone was needed. Furthermore, this solvent had to be liquid at –90 °C. 2-butanol fitted to the profile and was used for substitution. As control, the apolar n-hexane was also used. As expected, n-hexane did not substitute the water and lead to aggregation and destruction of the sample structure, whereas 2-butanol with 1.6 % osmium tetroxide and 0.1 % uranyl acetate gave results similar to water free ethanol. Unfortunately, 2-butanol is very viscous at -90 °C and is also difficult to remove after substitution and thus caused problems in embedding of the samples. Surprisingly, addition of 5 % water to this substitution medium again lead to complete destruction of the sample structure. Thus, 2-butanol is not suitable as substitution solvent, but the results suggested that the polarity of acetone is close to optimal for substitution and that the effect of water seems to be connected to this chemical property.

The following mechanisms are the most plausible to explain the effect of water on the visbility of structures: i) Its addition could have an stabilizing influence on the cellular architecture during the substitution process thus reducing the amount of extracted structural components. ii) The water could also just play a role in solubilising uranyl acetate, which is one of the main contrasting constituents in this substitution medium and is very badly soluble in acetone. Thus the added water could act as simple carrier for uranyl acetate and lead to an increased stain deposition in the sample. iii) The water might also influence the chemical reactions of the fixatives with the sample. The last option seems not very convincing, since samples substituted with both osmium tetroxide and glutaraldehyde show the same structural improvement after addition of water in spite of their very different reaction mechanism. During the

reaction of amines with glutaraldehyde water is actually released and not consumed. The crosslinking reaction of osmium tetroxide with C=C double bonds on the other hand leads to the formation of an osmium ester (or even diester, [26]), which can be hydrolysed. Furthermore, osmium tetroxide probably reacts as first fixative at very low temperatures (probably below –80 °C) when the water is presumably still frozen to a large extent. Additionally the experiments have shown that water mostly exerts its function at temperatures above –60 °C. The second point mentioned very probably plays a role in the process of heavy metal deposition, but cannot be the sole explanation for the increased structural visibility, since uranyl acetate is very well soluble in methanol and ethanol alone which both show a poor sample quality after substitution. Accordingly it is obvious to think of water having a much stronger effect on structural retention than on pure stain deposition. Thus, the first hypothesis appears the most plausible one. This stabilizing effect could be based on the presence of the “structural” water. Complete removal of the water, especially the interfacial water on the lipid membranes, would strongly reduce the strength of hydrophobic interactions and accordingly destabilise the membrane and other structures based on the hydrophobic effect. This might eventually lead to an increased extraction of membrane lipids and thus to a decreased visibility of membranes. The addition of water could saturate the solvent and thus reduce the extractive force on the interfacial water. The success of the substitution process would then be based on a precise balance of water solubilisation (which is essential for the substitution of water) and the extractive force imposed on the cellular components (which should be minimized). If the results of the experiments with the different solvents really reflect this balance, substitution with acetone and 5 % water could actually already be the optimal condition, since a slight increase (ethanol) or decrease (2-butanol) of the solvent polarity already leads to a suboptimal sample quality.

4.1.2 Duration of Substitution

A further way to reduce extraction is the reduction of the sample residence time in the substitution solvent. The question in this respect is how long the process of water substitution takes, since a premature warming of incompletely substituted amorphously frozen water would lead to recristallisation and the destruction of the structure. To test this, high-pressure frozen cell monolayers were substituted in the standard medium (1.6 % (w/v) osmium tetroxide, 0.1 % (w/v) uranyl acetate and 5 %

(v/v) water in acetone) from –90 °C to 0 °C in only 3 hours (instead of >16 hours). It was strongly expected that in this time substitution would be incomplete and lead to severe crystal formation. Surprisingly, no segregation patterns were observed and overall the samples appeared as if substituted for 16 hours **(Fig. 5F)**. A slight difference was observed in the appearance of the nuclear periphery. In contrast to standard substitution times, a slightly more diffuse, grainy pattern typical for the growth of small ice crystals was present in close apposition to the inner nuclear membrane, which itself was also not clearly retained. Due to its position in the centre of the cell the nucleus is the last structure to be substituted and thus is the position where segregation patterns are to be expected first. Still, the low extent of segregation patterns shows that for cell monolayers the duration of substitution is much less sensitive than expected from previous publications and again stresses the superlative importance of proper and reproducible high-pressure freezing for the sample quality.

4.1.3 Fixatives and Concentrations

The addition of water also simplified the preparation of the substitution mixtures, since the uranyl acetate could just be added from a 2 % (w/v) stock solution in water. A further reduction in cost, waste disposal and exposition to the very toxic osmium tetroxide was achieved by reducing the osmium content of the substitution mixture from 1.6 % (w/v) down to 0.2 % (w/v) by including the osmium in a stock solution of 4% (w/v) osmium tetroxide and 2 % (w/v) uranyl acetate in water, which is stable at 4 °C for weeks and can be diluted 1:20 in acetone to result in a substitution medium with 0.2 % osmium tetroxide, 0.1 % uranyl acetate and 5 % water in acetone. The sample quality after substitution in this medium was identical to samples substituted with 1.6 % osmium tetroxide. A further reduction of toxicity and waste disposal could be achieved by replacement of uranyl acetate with the less problematic, non-radioactive lead citrate with comparable results. Also in this respect, further variations could be interesting to investigate in order to modify the staining properties of the substitution to better visualise other structural elements, e.g. by the use of monovalent metal cations (e.g. silver) or even negatively charged metal complexes (e.g. hexacyanoferrate). This would be a step back to reintegrate the “old” and often forgotten histochemical methods [26] into the new technique of freeze-substitution.

4.1.4 Visualisation of the Poxvirus Immature Virion Double Membranes

In contrast to CMV, the poxvirus field is far from being a white spot concerning cryo-methods. Still, one basic debate about the complex morphogenesis remains: Do poxviruses break a dogma of cell biology by creating “open ended” membranes during their envelopment? The morphogenesis of the poxvirus core starts by the formation of so called crescent-shaped membranes, which then fuse at their tips to yield the immature virion (IV, [61]). The question is, if these crescents are consisting of a bent cistern with tightly apposed membranes or of a bent single bilayer stabilised by a high protein content. Results in favour of the first have, among others, come from previous freeze-substitution data [74], while recently support for the second came from deep-etch electron microscopy [32]. Here again the high-pressure freezing, freeze-substitution shows its power and also how the technique has advanced in the recent years. The results shown here clearly supported the previously published view, that the crescents consist of a bent cistern in which the lumen has collapsed completely, so that the individual membrane bilayers are in close proximity and barely recognisable **(Fig. 6B)**. This example shows the excellent preservation of very fine structures achieved with a substitution protocol based on acetone and 5 % water.

4.2 MCMV

The aim of these experiments was to assess MCMV morphogenesis and phenotypes of different viral mutants with the new cryo-preparation methods, since all data available until now were acquired with classical chemical fixation. The hope was to image previously badly characterised intermediates of the morphogenesis process and to be able to define mutant phenotypes more precisely due to the increased information available in cryo-prepared samples. One general problem in this respect is exactly the amount of information visible in only a small area of a 60 nm section of a cell. Looking at just a single image of such a section reveals a myriad of organelles, vesicles, cisternae, filaments and many more that are implemented in a 3-dimensional context. It thus becomes obvious that we are far away to grasp the cellular system underlying viral morphogenesis. Still, we are able to draw general conclusions and to judge by experience of analysing hundreds of images what a special structure could mean in the context of viral egress. These points should be kept in mind during the following discussion of the results presented above.

4.2.1 MCMV (Smith strain) Morphogenesis

Already in the analysis of the formation of nucleocapsids cryo-preparation shows one of its advantages, i.e. the lack of DNA condensation artefacts occurring during chemical fixation. Accordingly, the different capsid types can be distinguished with higher precision, thus leading to better particle statistics. Still, some capsids are only partially in section, which often makes the assignment to a specific type difficult. Accordingly, the precision of these results are in the range of estimated +- 5 %. The interpretation of specific particle ratios is difficult, since we are looking at an image of a steady state equilibrium, thus an increase of a specific capsid form may be the result of an increased production or a decreased “outflow”. Accordingly, the statistics are only valid in direct comparison with mutants prepared under identical conditions. Still, it can be said that in MCMV under wild type conditions, very few A-capsids are formed (approx. 1-2 %, **Fig. 7**), which is in agreement with their status of abortive packaging events, but alternatively they could also represent a short-lived intermediate between the autoproteolysis of the scaffold and the subsequent loading with vDNA. It can also be said that fully loaded C-capsids outnumber the B-capsids by approximately fourfold. This is probably due to a very efficient formation process which will become clear when comparing the wild type virus with the M97-deletion

mutant in the next chapter. An other observation was the clustering of nucleocapsids **(Fig. 11A)**. Mixed clusters of B- and C-capsids were frequently visible in these samples, but the underlying mechanism is completely unclear and will be discussed later.

The most startling structure seen in infected nuclei were the tubular infoldings of the inner nuclear membrane and their involvement in the primary envelopment **(Fig 8 and 9)**. The infoldings have several important structural characteristics. They i) are continuous with the perinuclear space and thus contain a mainly liquid environment ii) have a long (up to 4 µm) and narrow (maximum of 500 nm) tubular shape iii) are free of visible lamina on their nuclear face and thus possess a large free membrane surface iv) do not influence the structure of the outer nuclear membrane. What does the virus profit from their formation? Budding into a such tubular infolding might have several advantages in nuclear egress. The delaminated infolding offers a large, fully accessible membrane surface. Once inside the lumen, the movement of the primary enveloped capsids is not disturbed by chromatin as in the nucleoplasm. Additionally, the movement is restricted to one dimension (i.e. along the tubule) in contrast to the 3D movement possible to naked nucleocapsids in the nucleoplasm. This might result in an increased speed of transport to the nuclear periphery under the assumption of brownian movement. Last, the overall structure of the nucleus is not destabilised since the lamina only is dissolved at a dozen positions. In comparison, the mechanism proposed by the old model where single budding sites are created by depolymerisation of the lamina by recruitment of kinases by the viral particle itself would be inefficient, since only very small patches of inner nuclear membrane would be freed of lamina. Additionally, the transport of a 90 nm particle through the dense chromatin to the nuclear periphery would be difficult. Also the many holes in the lamina would probably destabilise the nuclear structure and ultimately also its function. The envelopment-deenvelopment process at the nuclear membranes also has interesting characteristics. In MCMV infected cells only C-capsids were budding into the infoldings. A possible explanation is that only mature capsids are able to acquire a component of the primary tegument visible in primary enveloped virions in thin sections and tomograms **(Fig 9B)**. A potential candidate protein could be M53, the interaction partner of M50, which will be discussed later. The next step of fusion of primary enveloped particles with the outer nuclear membrane could not be seen in

any of the samples until now. This was surprising since the time resolution of the high-pressure freezing technique should be in the range of a few tenth milliseconds. On the other hand, naked cytoplasmic capsids that were probably freshly released were observed in close apposition to the outer nuclear membrane and primary enveloped virions were never observed in ER-cisternae. This draws the conclusion that the fusion event must be very fast and thus close to the resolution time of high-pressure freezing. Based on this data a new model of cytomegalovirus nuclear egress is proposed **(Fig. 17)**. This model also brings up some questions. What is the mechanism of formation of the infoldings and which proteins are involved? How does a primary enveloped viral particle in the lumen of an infolding discern between back-fusion with the inner nuclear membrane and correct fusion with the outer nuclear membrane? These questions remain to be answered. Also in this respect the power of the high-pressure freezing / freeze-substitution approach is evident. Previous publications on human cytomegalovirus and human herpesvirus 6 done with chemical fixation actually imaged these infoldings, but failed to recognise the importance of this structure. Probably, the main reason was that most infoldings collapsed due to the large membrane artefacts induced by the fixation technique [75, 84]. Accordingly, these results were forgotten and not further mentioned in the recent literature.



Figure 17: Model of cytomegalovirus egress. The C-capsids are formed by loading of B-capsids with vDNA. Independently, the nuclear lamina (La) is locally depolymerised to allow the inner nuclear membrane to fold into the nucleus, creating delaminated budding sites for the C-capsids. The primary enveloped capsids are then transported along the tubule to the outer nuclear membrane, where they probably fuse with it and release the naked capsids into the cytoplasm. After acquiring the inner tegument, the particles are enveloped in close proximity to a Golgi-area by cisternae and transported through unidentified vesicular intermediates to the plasma membrane, where they are released to the extracellular space. C cytoplasm, G Golgi-complex, La nuclear lamina, N nucleus, TGN trans-Golgi network.

Also the following cytoplasmic steps of the morphogenesis are complex, especially because the cytoplasm is structurally much more complex than the nucleus. To finish the assembly of the infectious virion the naked cytoplasmic capsids first have to be tegumented. The acquisition of the inner tegument layer is assumed to take place as soon as the capsids pass to the cytoplasm followed by binding of the large tegument protein M48 (as shown for its HSV and PrV homolog UL36 [17, 24]). It is then

believed that the large tegument protein serves as docking station for all the following tegument proteins. Accordingly, deletion of UL36 in PrV leads to accumulation of cytoplasmic capsids and practically abolishes viral tegumentation and envelopment. In MCMV infected cells we could also observe capsids in close proximity of the nucleus that were tightly apposed to microtubules, thus suggesting that microtubule-mediated transport of herpesviruses does not only play a role in viral entry [85], but also in transport of cytoplasmic capsids to the locations of secondary envelopment in the Golgi-area. Considering that the attachment to minus-end directed microtubule motor proteins has been shown to be mediated by inner tegument in HSV [99], it can be speculated that the same protein also mediates the transport in viral egress. If the same process applies for egress it would lead to an accumulation of capsids around the microtubule organising centre (MTOC). In HCMV, the viral tegumentation was also appeared to take place near the MTOC by immunofluorescence microscopy [78]. Strikingly, naked cytoplasmic MCMV capsids are also seen in clusters of different sizes, in which the capsids are embedded in an electron dense material, and in the in the surroundings of one Golgi-complex in close proximity to cisternae, where they undergo envelopment. Interestingly, the envelopment appears to take place preferentially at one Golgi-complex, while other seem structurally unaffected (not shown). Eventually, this might be the most proximate one to the MTOC. Envelopment was usually observed to proceed by wrapping of one or more capsids by a cistern with similar morphological characteristics as Golgi or TGN membranes **(Fig. 10A and 13C)**. These were always in close proximity to the Golgi / TGN, but a clear connectivity was never observed. Thus, we cannot see if the originating compartment of the cisternae really is the Golgi and not some endosomal organelle. During the secondary envelopment tegument material attached to the capsids seemed to be condensed. The final result of the process was a multicapsid virion with one limiting membrane inside an elongated cistern. Identical multicapsid virions together with single capsid virions were also observed in multivesicular late endosomes, in which their limiting membrane appeared more tightly apposed to the individual tegumented capsids, reminiscent of a budding process **(Fig. 10B)**. This finding is very confusing, since it would call for a crosstalk between the cisternal elements and endosomal compartments. Alternatively, these particles could represent endocytosed progeny virions. This would be surprising because of their large fraction inside the cells, which would call for a large amount of these virions in the extracellular space that is not to

be expected at 48 hours p.i. This question will be discussed further when covering the gold internalisation experiments done with HCMV AD169. Fully mature single capsid virions were also seen in larger translucent vesicles that are probably identical with the “vacuoles” found in the literature **(Fig. 10E and 13C)**. Again, how the transition of the virions from cisternal to vesicular compartments is achieved remains elusive. The last step of viral release to the extracellular space is rarely observed and could be mixed with viral endocytosis **(Fig. 2D, dotted arrow)**.

4.2.2 Phenotypical Characterisation of an M97-deleted MCMV

As described in the introduction, the role of M97 and its HCMV homolog UL97 in the replication cycle is a matter of debate and has been assigned to almost every step of viral morphogenesis (see below). This first morphological analysis of the egress of MCMV ΔM97 presented here shows several major alterations of the nuclear events and structures. The striking nuclear reduction of C-capsids by 48 % is the most prominent effect of the deletion **(Fig. 7)**. Since in this system only C-capsids are leaving the nucleus, the amount of cytoplasmic particles is reduced accordingly (not quantified), but the C-capsids are still able to reach the cytoplasm. After the analysis of the capsid distribution, the other defects were obvious, i.e. the reduced capsid clustering and the emergence of a differently structured subnuclear area **(Fig. 11 B, C and D)**. The next question was how these different effects can originate from the deletion of M97 alone. Obviously, a defect in the formation of C-capsids was present, while one educt of the DNA loading process, the B-capsid, was present in large numbers. Accordingly, the block had to be either in replication, processing or encapsidation of the vDNA. In HCMV it has been shown that pUL97 phosphorylates pUL44, the processivity factor of the viral polymerase. Accordingly, the hypothesis was that the vDNA was not replicated properly. In case of a defect in either processing or encapsidation an accumulation of vDNA would be expected in infected nuclei. To assess this, infected nuclei were isolated and their vDNA content (encapsidated vs. free) was estimated by twofold serial dilution, nuclease digestion and PCR amplification. Within the range of precision of the method, no difference could be seen between encapsidated and free vDNA or the total vDNA (standardised on actin) after deletion of M97 **(Fig. 11K)**. A crucial problem of this assay is how well the entire preparation can be standardised and how big an accumulation effect would be. Unfortunately, several aspects play a role in this, especially standardisation of

infection, nuclei isolation and preparation of the dilutions. As rough estimate, a 48 % reduction in C-capsids would lead to a twofold reduction of encapsidated vDNA, which is very close to our detection limit using twofold dilutions. Taken together with the difficulties of preparation, these results have to be considered an approximation. To test the findings acquired by PCR and to clarify the composition of the subnuclear structures infected cells were analysed by correlative microscopy of serial sections by fluorescently labelling DNA and RNA **(Fig. 11 E to H)**. The results clearly showed that the subnuclear areas do not consist of either DNA or RNA and thus consist of protein mass. Surprisingly, also wild type infected nuclei possess these subnuclear structures, although of smaller sizes. Recently, a similar phenotype has been characterised in HCMV infected cells where the UL97 kinase activity was prevented either by deletion of by drug inhibition [69]. These accumulations were mainly consisting of the two tegument proteins ppUL83 (pp65) and UL25. The function of these tegument proteins in the nuclei of infected cells and the connection to UL97 remains unclear. Accordingly, it is very probable that the homologous proteins in MCMV are the main mass forming the subnuclear structures. The function of these proteins in the nuclei is not clear, but as they are components of the secondary tegument, they might as well be involved in primary tegumentation. Thus, their accumulation would just reflect the reduced amount of capsids undergoing nuclear egress. The third phenotype, the reduction in capsid clustering, is the most elusive effect of the deletion of M97, mainly because the underlying mechanism of clustering is not known. Seen by eye, the clustering appears completely abolished in the M97 deletion mutant, but the stochastic analysis shows that the effect is stronger for B- than for C-capsids. This defect itself could be explained in different ways: i) Let us assume that capsid clustering reflects an aggregation of several capsids to one long concatemeric vDNA by their binding to packaging sequences. If we further assume that the missing phosphorylation of the processivity factor M44 leads to premature termination of the vDNA replication and accordingly to shorter vDNA concatemers or even fragments, this “beads on a string” mechanism of vDNA packaging would explain the reduction of capsid clustering very elegantly. ii) M97 could purely play a role in a process of vDNA packaging without influencing the vDNA. Accordingly, vDNA would accumulate in infected nuclei, which does not seem to occur in large amounts, if one trusts the results of the dilution series PCR. iii) The last and most speculative explanation would be that the clustering is an effect independent of vDNA

encapsidation and processing, but instead reflects that capsids are actively transported to specific sites in the nucleus for processing, eventually along a putative nucleoskeleton. A nucleoskeleton consisting of actin of a special conformation has been postulated for a long time, but the role of actin in the nucleus is enigmatic [33]. Still it has been shown indirectly by labelling Cdc14B that HSV modulates a nucleoskeleton-like structure [82]. Of all three explanations, the first one appears the best, since it explains both the increased amount of B-capsids and the reduction of capsid clustering. According to this hypothesis, the 10-fold reduction of viral replication at MOI of 1 PFU/cell (here MOIs of 0.1 to 0.5 PFU/cell were used) after deletion of M97 [91] would purely be the result of these nuclear defects and not of a defect in nuclear egress or later cytoplasmic processes. The attempt to rescue the M97 deletion phenotype by cis-complementation with HCMV UL97 obviously failed, since the particle ratios observed in the nuclei of infected cells were corresponding to the deletion mutant MCMV **(Fig. 7)**. This again shows the presence of significant differences within the betaherpesvirus subfamily.

Due to the large amount of B-capsids in the nuclei of cells infected with the M97 deletion virus a point concerning nuclear egress can be made. Wild et al. [94] have shown that in HSV infected cells the nuclear pores are disrupted and thus propose that the nucleocapsids are also able to bypass the nuclear membranes by this mechanism. In MCMV infected cells these disrupted pores were also observed (not shown). Contradictory to the proposed model stands the fact that in a large majority of cells infected with the MCMV ΔM97 the cytoplasmic virions were almost exclusively of the C-capsid type at 48 hours p.i. in spite of the large nuclear fraction of B-capsids. Only in the few cells in which dilated nuclear pores are observed also cytoplasmic B-capsids appear in larger amounts. Accordingly, in MCMV morphogenesis the occurrence of dilated nuclear pores apparently only plays a role in very late stages of infection and thus should not be regarded as standard pathway of nuclear egress.

4.2.3 Observation of Conditional MCMV Variants

The approach to identify the functions of viral proteins by simple deletion of the respective genes has its limitations, especially since revertant viruses constructed by reinsertion of the deleted ORF often show slight growth defects, so that random

mutations in an other essential gene during the genetic manipulations can never be fully excluded. Additionally, when hitting an essential viral gene, the viral replication has to be rescued by trans-complementation, which often raises problems with transfection and protein expression (expression levels and toxicity). Rupp et al. [77] have established a system which allows insertion of a gene of interest into the viral genome under control of an inducible promotor. Thus, expression of the protein can be regulated conditionally and always happens in the context of viral infection. This system has been enhanced recently by selecting dominant negative (DN) mutants of viral proteins and expressing them conditionally, in order to block the specific action of the respective factors. As already described above, pM50 was an interesting candidate to block by the DN-approach, which was achieved with the MCMV M50ΔP mutant. Expression of this DN-protein results in a block of nuclear egress and an accumulation and stacking of the infoldings of the inner nuclear membrane **(Fig. 12 A and B)**. Additionally, also cytoplasmic rough ER cisternae were stacking and a further nonidentified membrane, presumably smooth ER, was accumulating **(Fig 12 C and D)**. Interestingly, only the rough ER membrane stacking phenotype could be reproduced by conditionally expressing an HA-tagged M50, thus representing an M50 overexpression phenotype **(Fig. 12 E)**, but in contrast to DN mutant the viral morphogenesis appears as for the wild type MCMV. It can therefore be concluded that the stacking of the inner nuclear membrane is an effect of the deletion of the proline-rich domain in the M50ΔP virus. The function of this domain is unknown, but it is not involved in binding of pM50 to pM53 (Zsolt Ruszics, personal communications). It could thus be speculated that this domain is needed for the recruitment of a protein responsible for the primary envelopment of nucleocapsids, thus explaining the nuclear egress phenotype of the respective DN mutant. The doubling of the rough ER cisternae has already been described for EBV when complementing the BFRF1 - knockout EBV in trans (BFRF1 is the positional homolog of M50 in EBV, [20, 28]). This probably corresponds to the overexpression phenotype achieved with the MCMV M50HA. The mechanism by which pM50 achieves the membrane stacking is elusive, but considering the amount of dense material allocated between the stacking membranes, the involvement of further proteins has to be expected **(Fig. 12 B and C)**. An other interesting phenotype was observed with the MCMV SCP-GFP that is conditionally expressing a GFP fusion protein with the small capsid protein (SCP, M48.3) [12]. When trying to label the capsids by conditionally expressing this GFP

fusion protein, a dominant negative phenotype was observed, i.e. the viral replication was massively reduced [12]. Due to the location of the protein on the capsid surface it was expected that the binding to structural components needed for primary tegumentation and envelopment was inhibited by the presence of the GFP. Surprisingly, preliminary EM analysis showed large accumulations of B-capsids, which cannot be explained by an egress phenotype, but rather points at a defect in vDNA encapsidation or eventually the sealing of the capsids to retain the vDNA.

4.3 HCMV

As stated above, the morphogenesis of HCMV and MCMV are similar, but already here differences within the betaherpesvirus subfamily are obvious, one main point being the production of dense bodies by HCMV that are not present with MCMV or the approximately doubled duration of the replication cycle of HCMV compared to MCMV [58]. From recent work on HCMV strains other than AD169 in our lab it is also becoming clear that already switching viral strain or cell type may have influences on details of the morphogenesis, especially particle distribution and numbers. Accordingly, generalisations like “herpesviral morphogenesis” or even “cytomegalovirus morphogenesis” have to be considered as greatly simplified views of an overwhelmingly complex process. Within these limitations and due to the lack of EM data gathered with HPF / FS from other MCMV and HCMV strains I will compare the MCMV Smith strain with HCMV AD169 to make general points about the efficiency of morphogenetic processes.

4.3.1 HCMV AD169 Morphogenesis

As shown in the results section, HCMV AD169 infection of HFF shows differences already at the stage of nucleocapsid formation and nuclear egress. The nuclear capsid ratios of 8.2 % A-capsids, 67.7 % B-capsids and 24.1 % C-capsids (n=1092) show a large amount of A- and B-capsids, which might already reflect inefficiencies in vDNA replication and encapsidation and capsid sealing probably due to the long passaging of the virus in fibroblast cell culture. Especially the high percentage of A-capsids that represent a abortive side product are a clear indication in this direction. A further observation is that the typical capsid clustering observed in MCMV infection is not visible by eye in nuclei infected with AD169 **(Fig. 13A and B)**, but since the mechanism of clustering is not known no conclusions on viral fitness can be made at this point. In the step of nuclear egress HCMV AD169 also envelopes **(Fig. 13B)** and releases B-capsids to the cytoplasm, which is further reducing the particle to PFU ratio released from the infected cells. In the cytoplasm few naked capsids were seen, instead most virions were observed inside of cisternae and vesicles. Strikingly, the number of enveloped virions was exceeded by dense bodies by an estimated factor of 5- to 10-fold **(see Fig. 13C)**. Accordingly, also dense body envelopment events were very frequent and also showed characteristics described for MCMV virion envelopment, i.e. the tegument material was first present as diffuse material and

condensed during the envelopment. The tomogram of the secondary envelopment process **(Fig. 13D)** shows that the 3D structure of the cisternae is more complex than expected from images of thin sections and showed a tubulo-vesicular structure and several connections to neighbouring cisternae and vesicles. Still, the vesicles containing dense bodies appeared separated from the rest. This again shows that fission processes have to take place after the secondary envelopment has succeeded. The analysis of these connections will be difficult, since the 3D information is essential and can only be acquired by electron tomography. Also in this respect the sample preparation protocol is critical since it determines the contrast and visibility of the respective structures. Also with HCMV the later events in virion transport to large vesicles and the release from the cell are very poorly understood.

Due to the late time points investigated also the uptake of progeny virions has to be considered, which might be confused with viral egress. In this respect the presence of virions in endocytic compartments was investigated by gold internalisation. A subset of virions and dense bodies was actually observed to localise to the same vesicular compartments as internalised gold colloids, which appear structurally identical to the large vesicles often including several virions and dense bodies as mentioned above **(Fig. 14A)**. Two explanations are possible for this observation: Either these vesicles represent late endosomes into which viral progeny particles have been internalised or they represent an endosomal compartment that is hijacked by the virus for viral release. Interestingly, the HCMV glycoprotein gB has been shown to colocalise with Golgi and TGN markers and also with Rab3, a marker for secretory vesicles, but not with any endosomal or lysosomal markers [34]. Unfortunately, the ultrastructural data on these vesicles is scarce. It could be speculated that the secretory vesicles are identical large vesicles containing virions and gold colloids. In an attempt to block eventual membrane-linked events of virion release, inhibition of PI3K by addition of wortmannin was done. It was already shown that HCMV DNA replication can be inhibited by blocking PI3K [38], but its effects on the morphogenesis were not studied. Inhibition of PI3K leads to the alteration of endocytic and exocytic pathways, e.g. to the inhibition of the formation of endosomal internal vesicles [25]. The application of wortmannin for 4 hours had no obvious effect on the viral morphogenesis and did not cause any accumulations of virions in a specific compartment **(Fig. 14B)**. Accordingly, PI3K seem not to play a role in these

processes. Nevertheless, many more interesting targets for inhibition experiments are available, e.g. the Rab and other GTPases, microtubules and other phosphatidyl inositol metabolites.

4.3.2 Morphological Analysis of an UL97-Deleted HCMV

The UL97-kinase is of great interest because of its ability to phosphorylate the nucleoside analogue ganciclovir, which is the drug of choice in anti-HCMV therapy. The role of UL97 in HCMV morphogenesis is still a matter for debate due to great differences in the results among different labs. Wolf et al. [98] claim that the deletion of UL97 leads to a reduced vDNA replication and an accumulation of A-capsids, thus arguing for a defect in replication and packaging of the vDNA. Krosky et al. [44] suggest a defect in nuclear egress, but also show that UL97 phosphorylates the processivity factor UL44 [45], which was also published by Marschall et al. [51]. Recently, Marschall et al. [52] published that UL97 interacts with the cellular p32, which then recruits UL97 to the lamin B receptor at the inner nuclear membrane where UL97 then phosphorylates the lamins to dissolve the nuclear lamina. Prichard et al [69] reported recently that the UL97 kinase activity was required for the proper intranuclear distribution of the tegument protein UL83 (pp65). Finally, it was presented that UL97 also regulates the localisation of tegument proteins [4], the deletion thus leading to enlarged dense bodies. From the preliminary results with the HCMV ΔUL97 shown above **(Fig. 15A)** already some information can be gathered. In accordance with the observations of MCMV ΔM97 infected cells, a large amount of B-capsids is present in the infected nuclei, but the most striking (and eventually misleading) change is the appearance of massively enlarged dense bodies. Still, the phenotype of the HCMV ΔUL97 appears similar to the deletion of M97 in MCMV, i.e. a massive increase of nuclear B-capsids and a decrease of cytoplasmic virions. Accordingly, the cytoplasmic phenotype is probably just a downstream effect of the nuclear defect. Due to the reduced production of C-capsids less capsids are present in the cytoplasm, while the synthesis of tegument and glycoproteins is normal. This probably leads to an increased aggregation of tegument proteins that are then enveloped as enlarged dense bodies. Also here the reason why UL83 (pp65) and UL25 accumulate in the nucleus is not clear. One possible hypothesis might be that they are components of the primary tegument and accumulate in the nucleoplasm

because they are not transported to the cytoplasm with the capsids by nuclear egress.

4.3.3 The role of G-Protein Coupled Receptors in HCMV Morphogenesis

HCMV also encodes four GPCRs (UL33, UL78, US27 and US28), from which at least US28 has been shown to specifically bind different chemokines [47]. The function of these proteins is not known and their deletion has only mild effects on viral replication in tissue culture. US28, US27 and UL33 have all been localised to endocytic compartments, especially to multivesicular late endosomes [21, 22]. The HCMV mutant used here was deleted in all four GPCRs, which resulted in a slight, approximately 10-fold reduction of viral titers (Detlef Michel, personal communications). The investigation by EM did not show any significant effects of these deletions on the viral egress **(Fig. 15B)**. Accordingly, these proteins do not play a vital role in HCMV morphogenesis and might only be important for immune evasion in the natural infection.

4.3.4 UL35 and UL35A fulfil Diverse Roles in HCMV Morphogenesis

The UL35 ORF codes for 2 proteins, the ppUL35 (75 kDa) and ppUL35A (22 kDa), which is translated using an internal start codon and the same stop codon [50]. Accordingly, the ppUL35A is composed of the C-terminal part of ppUL35. While ppUL35 is a cytoplasmic tegument protein incorporated into the virion, ppUL35a is nuclear factor that decreases the activation of the major immediate-early promotor by ppUL82. In a previous publication the effects of the deletion of the complete UL35 ORF (HCMV ∆UL35) on viral egress was investigated by biochemistry and chemical fixation EM [79]. We found that the deletion reduced the immediate-early gene expression and also disturbed the viral morphogenesis. In the nuclei of infected cells large aggregates were present, surrounded by capsids. In the cytoplasm, no dense bodies were present in these cells, but instead more diffuse electron dense aggregates. The reinvestigation presented here had a more specific approach. Two new viral mutants were constructed, one only expressing the full length tegument component ppUL35 (HCMV UL35RV2026), the other only expressing the nuclear factor ppUL35A (HCMV UL35dATG). Comparing these mutants with the original HCMV ∆UL35, it could be observed that a mainly nuclear phenotype was produced when ppUL35A was absent, while the absence of ppUL35 yielded a purely cytoplasmic phenotype **(Fig. 16A to F)**. The mutant lacking UL35A showed the

nuclear aggregates surrounded by capsids, very few cytoplasmic virions and accumulations of electron dense material, eventually tegument proteins, but no dense bodies. The composition of the nuclear aggregates is not known, but is much denser than the protein accumulations seen after deletion of UL97 and M97. Interestingly, these aggregates seemed to have a lighter core, which appeared similar to the general nuclear architecture. On the other side, the deletion of the long form ppUL35 did not cause any obvious nuclear defects, and also the cytoplasmic virions appeared normal. The only effect were greatly enlarged dense bodies. These two phenotypes obviously reflect the localisation of the two proteins missing in the respective viruses. Interestingly, the mutant lacking UL35A also showed a reduction in nuclear egress, but, in contrast to the UL97 deletion mutant, this did not cause enlarged dense bodies. Instead, dense nuclear aggregates were formed and no dense bodies were present in the cytoplasm. This leads to the hypothesis, that the nuclear aggregates mainly consist of UL83 (pp65), which would be a similar effect as published for the deletion of UL97. However, the appearance of cells infected with the ΔUL97 and the UL35RV2026 viruses was completely different and the same might apply for the mechanisms ultimately leading to these phenotypes. The mutant lacking the long form ppUL35 instead showed a typical tegumentation defect phenotype, similar as the mutant PrV or HSV deleted in UL36, the major tegument protein [17, 24]. This shows that ppUL35 is an essential structural component for proper tegumentation and eventually links a component of the tegument to the virions, so that its absence lead to an accumulation of tegument proteins, which were then packed in dense bodies. The fact that the virions still appeared normal in size and shape is astonishing, but a similar effect was observed after deletion of UL83 (pp65), the major component of the tegument [90]. Deletion of this ORF abolishes dense body formation but leaves the appearance of the virion tegument unaffected [80]. This finding suggests that other tegument proteins are able to replace the structural function of UL83, which might as well be the explanation for the phenotype of the HCMV UL35dATG.

4.4 Model of Cytomegalovirus Morphogenesis

All the results stated above can be condensed to a hypothetical working model of cytomegalovirus morphogenesis based on the results gained with the high-pressure freezing and freeze-substitution technique **(Fig. 17)**. At first, the concatemeric vDNA is packed into B-capsids in a concerted process of vDNA binding ("beads on a string"), cleavage and capsid sealing (M48.3). Failures in this process lead to the formation of A-capsids. Meanwhile, local dissolution of the nuclear lamina leads to the infoldings of the inner nuclear membrane, in which pM50 is present. A complex of primary tegument and pM53 binds to the capsid and recruits it to the inner nuclear membrane, where it clusters pM50 and initiates the primary envelopment. The enveloped virion then travels to the outer nuclear membrane along the infolded tubule and fuses with the outer nuclear membrane to release the capsid into the cytoplasm. There, the capsid is rapidly tegumented by the large tegument protein (M48 / UL48), which then binds to minus end directed microtubule motor proteins and is transported to the MTOC, where it dissociates from the motor protein and forms clusters. In parallel, cisternae are formed in the Golgi area and loaded with the viral glycoproteins. The cisternal glycoproteins offer binding sites for the outer tegument proteins, to which then the capsids bind by the inner tegument proteins. Failures to properly engage inner and outer tegument binding leads to an accumulation of self-nucleating tegument proteins, which are then enveloped as dense bodies. The greater the lack of cytoplasmic capsids, or the overproduction or binding defect of the tegument is, the larger the dense bodies. Secondary envelopment then proceeds via wrapping of single or multicapsid virions at multiple points on a cistern and further condensation of the tegument during the process. Finally, the tips of the bending cisternae fuse and release the mature virions into the lumen of the cisternae. With multicapsid virions, the limiting membrane is eventually pulled closer by the tegumented capsids, which would lead to budding events within the cisternae. The cisternae fuse with and release the virions into secretory vesicles / multivesicular endosomes (which might be identical and carry internalised gold colloids, as for MHCII antigen loading in dendritic cells [25]). In these vesicles, the virions accumulate and are ultimately released to the extracellular space by fusion of the vesicle membrane with the plasma membrane.

This model of herpesvirus egress leads to several questions: i) What components are needed for the primary envelopment and which are the primary tegument proteins seen in thin sections? ii) Once inside an infolded tubule, by what membrane protein does the virion discern the inner from the outer nuclear membrane to prevent back-fusion? And what protein initiates the fusion process? iii) Once in the cytoplasm, how is the microtubular transport regulated, so that the virions and the cisternae appear at the same location? iv) How and from which compartment are the cisternae formed and what machinery do they acquire to accomplish their transport functions? v) We are generally talking about membrane fusion and fission events during viral egress, but what are the factors and mechanisms making these processes possible? Are they of viral or cellular origin? These are just questions arising from the general view of CMV morphogenesis, much more are there to ask about the interplay of all viral proteins to achieve optimal viral replication. These riddles will only be solved by a broad approach to the problem with biochemical and imaging methods in combination.

4.5 Conclusions

The use of high-pressure freezing, freeze-substitution and plastic embedding in cytomegalovirus research not only enables a detailed characterisation of viral phenotypes, but due to the tremendous amount of unbiased structural information also uncovers mechanisms that are missed with other techniques (e.g. the passage through endosomal compartments during viral egress). Accordingly, this method delivers new observations for the understanding of the viral morphogenesis and eventually the development of new antiviral therapies.

Many questions, few answers… the scientists favourite lookout point. More to see, more to learn.

5 Literature

1. Abate, D.A., S. Watanabe, and E.S. Mocarski, *Major human cytomegalovirus structural protein pp65 (ppUL83) prevents interferon response factor 3 activation in the interferon response.* J Virol, 2004. **78**(20): p. 10995-1006.
2. Al-Amoudi, A., et al., *Cryo-electron microscopy of vitreous sections.* Embo J, 2004. **23**(18): p. 3583-8.
3. Ausubel, F.M., et al., eds. *Current Protocols in Molecular Biology*. Current Protocols in Molecular Biology, ed. V. Benson Chanda. 1995, John Wiley and Sons, Inc.
4. Azzeh, M., et al. *The role of human cytomegalovirus UL97 kinase in cellular localization of viral tegument proteins*. in *30th International Herpesvirus Workshop*. 2005. Turku, Finnland.
5. Baddeley, A.J., et al., *Case studies in spatial point process modelling* Springer Lecture Notes in Statistics. Vol. 185. 2006, Berlin: Springer.
6. Baines, J.D., et al., *The UL20 gene of herpes simplex virus 1 encodes a function necessary for viral egress.* J Virol, 1991. **65**(12): p. 6414-24.
7. Baldick, C.J., Jr., et al., *Human cytomegalovirus tegument protein pp71 (ppUL82) enhances the infectivity of viral DNA and accelerates the infectious cycle.* J Virol, 1997. **71**(6): p. 4400-8.
8. Baldick, C.J., Jr. and T. Shenk, *Proteins associated with purified human cytomegalovirus particles.* J Virol, 1996. **70**(9): p. 6097-105.
9. Baumeister, W. and A.C. Steven, *Macromolecular electron microscopy in the era of structural genomics.* Trends Biochem Sci, 2000. **25**(12): p. 624-31.
10. Bechtel, J.T. and T. Shenk, *Human cytomegalovirus UL47 tegument protein functions after entry and before immediate-early gene expression.* J Virol, 2002. **76**(3): p. 1043-50.
11. Bittermann, A., *Beiträge zur Lokalisation von Integrinen auf der Oberfläche von Fibroblasten*. 1995, ETH: Zürich.
12. Borst, E.M., et al., *Genetic evidence of an essential role for cytomegalovirus small capsid protein in viral growth.* J Virol, 2001. **75**(3): p. 1450-8.
13. Bresnahan, W.A. and T.E. Shenk, *UL82 virion protein activates expression of immediate early viral genes in human cytomegalovirus-infected cells.* Proc Natl Acad Sci U S A, 2000. **97**(26): p. 14506-11.
14. Browne, E.P. and T. Shenk, *Human cytomegalovirus UL83-coded pp65 virion protein inhibits antiviral gene expression in infected cells.* Proc Natl Acad Sci U S A, 2003. **100**(20): p. 11439-44.
15. Caro, L.G. and G.E. Palade, *Protein Synthesis, Storage, And Discharge In The Pancreatic Exocrine Cell. An Autoradiographic Study.* J Cell Biol, 1964. **20**: p. 473-95.
16. Cha, T.A., et al., *Human cytomegalovirus clinical isolates carry at least 19 genes not found in laboratory strains.* J Virol, 1996. **70**(1): p. 78-83.
17. Desai, P.J., *A null mutation in the UL36 gene of herpes simplex virus type 1 results in accumulation of unenveloped DNA-filled capsids in the cytoplasm of infected cells.* J Virol, 2000. **74**(24): p. 11608-18.
18. Ebersold, H.R., J.L. Cordier, and P. Luthy, *Bacterial mesosomes: method dependent artifacts.* Arch Microbiol, 1981. **130**(1): p. 19-22.
19. Edelmann, L., *Freeze-substitution and the preservation of diffusible ions.* J Microsc, 1991. **161 (Pt 2)**: p. 217-28.

20. Farina, A., et al., *BFRF1 of Epstein-Barr virus is essential for efficient primary viral envelopment and egress.* J Virol, 2005. **79**(6): p. 3703-12.
21. Fraile-Ramos, A., et al., *The human cytomegalovirus US28 protein is located in endocytic vesicles and undergoes constitutive endocytosis and recycling.* Mol Biol Cell, 2001. **12**(6): p. 1737-49.
22. Fraile-Ramos, A., et al., *Localization of HCMV UL33 and US27 in endocytic compartments and viral membranes.* Traffic, 2002. **3**(3): p. 218-32.
23. Fuchs, W., et al., *The UL20 gene product of pseudorabies virus functions in virus egress.* J Virol, 1997. **71**(7): p. 5639-46.
24. Fuchs, W., et al., *Essential function of the pseudorabies virus UL36 gene product is independent of its interaction with the UL37 protein.* J Virol, 2004. **78**(21): p. 11879-89.
25. Futter, C.E., et al., *Human VPS34 is required for internal vesicle formation within multivesicular endosomes.* J Cell Biol, 2001. **155**(7): p. 1251-64.
26. Geyer, G., *Ultrahistochemie*. 2nd Edition ed. 1973, Stuttgart, Germany: Gustav Fischer Verlag.
27. Giddings, T.H., *Freeze-substitution protocols for improved visualization of membranes in high-pressure frozen samples.* J Microsc, 2003. **212**(Pt 1): p. 53-61.
28. Gonnella, R., et al., *Characterization and intracellular localization of the Epstein-Barr virus protein BFLF2: interactions with BFRF1 and with the nuclear lamina.* J Virol, 2005. **79**(6): p. 3713-27.
29. Hayashi, M.L., C. Blankenship, and T. Shenk, *Human cytomegalovirus UL69 protein is required for efficient accumulation of infected cells in the G1 phase of the cell cycle.* Proc Natl Acad Sci U S A, 2000. **97**(6): p. 2692-6.
30. Hazelton, P.R. and H.R. Gelderblom, *Electron microscopy for rapid diagnosis of infectious agents in emergent situations.* Emerg Infect Dis, 2003. **9**(3): p. 294-303.
31. Heidelberger, R., *Adenosine triphosphate and the late steps in calcium-dependent exocytosis at a ribbon synapse.* J Gen Physiol, 1998. **111**(2): p. 225-41.
32. Heuser, J., *Deep-etch EM reveals that the early poxvirus envelope is a single membrane bilayer stabilized by a geodetic "honeycomb" surface coat.* J Cell Biol, 2005. **169**(2): p. 269-83.
33. Hofmann, W.A. and P. de Lanerolle, *Nuclear actin: to polymerize or not to polymerize.* J Cell Biol, 2006. **172**(4): p. 495-6.
34. Homman-Loudiyi, M., et al., *Envelopment of human cytomegalovirus occurs by budding into Golgi-derived vacuole compartments positive for gB, Rab 3, trans-golgi network 46, and mannosidase II.* J Virol, 2003. **77**(5): p. 3191-203.
35. Huber, M.T. and T. Compton, *The human cytomegalovirus UL74 gene encodes the third component of the glycoprotein H-glycoprotein L-containing envelope complex.* J Virol, 1998. **72**(10): p. 8191-7.
36. Huber, M.T. and T. Compton, *Intracellular formation and processing of the heterotrimeric gH-gL-gO (gCIII) glycoprotein envelope complex of human cytomegalovirus.* J Virol, 1999. **73**(5): p. 3886-92.
37. Humbel, B.M. and M. Müller, *Freeze substitution and low temperature embedding*, in *Science of Biological Specimen Preparation*, M. Müller, et al., Editors. 1985, SEM Inc., AMF O´Hare: Chicago, USA. p. 175-183.
38. Johnson, R.A., et al., *Human cytomegalovirus up-regulates the phosphatidylinositol 3-kinase (PI3-K) pathway: inhibition of PI3-K activity*

inhibits viral replication and virus-induced signaling. J Virol, 2001. **75**(13): p. 6022-32.
39. Kato, A., et al., *Herpes simplex virus 1-encoded protein kinase UL13 phosphorylates viral Us3 protein kinase and regulates nuclear localization of viral envelopment factors UL34 and UL31.* J Virol, 2006. **80**(3): p. 1476-86.
40. Kattenhorn, L.M., et al., *Identification of proteins associated with murine cytomegalovirus virions.* J Virol, 2004. **78**(20): p. 11187-97.
41. Klupp, B.G., et al., *Pseudorabies virus UL36 tegument protein physically interacts with the UL37 protein.* J Virol, 2002. **76**(6): p. 3065-71.
42. Klupp, B.G., H. Granzow, and T.C. Mettenleiter, *Effect of the pseudorabies virus US3 protein on nuclear membrane localization of the UL34 protein and virus egress from the nucleus.* J Gen Virol, 2001. **82**(Pt 10): p. 2363-71.
43. Kremer, J.R., D.N. Mastronarde, and J.R. McIntosh, *Computer visualization of three-dimensional image data using IMOD.* J Struct Biol, 1996. **116**(1): p. 71-6.
44. Krosky, P.M., M.C. Baek, and D.M. Coen, *The human cytomegalovirus UL97 protein kinase, an antiviral drug target, is required at the stage of nuclear egress.* J Virol, 2003. **77**(2): p. 905-14.
45. Krosky, P.M., et al., *The human cytomegalovirus UL44 protein is a substrate for the UL97 protein kinase.* J Virol, 2003. **77**(14): p. 7720-7.
46. Ksiazek, T.G., et al., *A novel coronavirus associated with severe acute respiratory syndrome.* N Engl J Med, 2003. **348**(20): p. 1953-66.
47. Kuhn, D.E., C.J. Beall, and P.E. Kolattukudy, *The cytomegalovirus US28 protein binds multiple CC chemokines with high affinity.* Biochem Biophys Res Commun, 1995. **211**(1): p. 325-30.
48. Kurner, J., et al., *New insights into the structural organization of eukaryotic and prokaryotic cytoskeletons using cryo-electron tomography.* Exp Cell Res, 2004. **301**(1): p. 38-42.
49. Lepault, J., et al., *Organization of double-stranded DNA in bacteriophages: a study by cryo-electron microscopy of vitrified samples.* Embo J, 1987. **6**(5): p. 1507-12.
50. Liu, Y. and B.J. Biegalke, *The human cytomegalovirus UL35 gene encodes two proteins with different functions.* J Virol, 2002. **76**(5): p. 2460-8.
51. Marschall, M., et al., *The protein kinase pUL97 of human cytomegalovirus interacts with and phosphorylates the DNA polymerase processivity factor pUL44.* Virology, 2003. **311**(1): p. 60-71.
52. Marschall, M., et al., *Cellular p32 recruits cytomegalovirus kinase pUL97 to redistribute the nuclear lamina.* J Biol Chem, 2005. **280**(39): p. 33357-67.
53. Mettenleiter, T.C., *Herpesvirus assembly and egress.* J Virol, 2002. **76**(4): p. 1537-47.
54. Mettenleiter, T.C., *Budding events in herpesvirus morphogenesis.* Virus Res, 2004. **106**(2): p. 167-80.
55. Michel, D. and T. Mertens, *The UL97 protein kinase of human cytomegalovirus and homologues in other herpesviruses: impact on virus and host.* Biochim Biophys Acta, 2004. **1697**(1-2): p. 169-80.
56. Michel, D., et al., *Functional regions of the human cytomegalovirus protein pUL97 involved in nuclear localization and phosphorylation of ganciclovir and pUL97 itself.* J Gen Virol, 1998. **79 (Pt 9)**: p. 2105-12.
57. Michel, M., T. Hillmann, and M. Müller, *Cryosectioning of plant material frozen at high pressure.* J Microsc, 1991. **163**: p. 3-18.

58. Mocarski, E. and C.T. Courcelle, *Cytomegaloviruses and their replication*, in *Fields Virology*, D.M. Knipe, et al., Editors. 2001, Lippincott Williams & Wilkins: Philadelphia, Pa. p. 2629-2673.
59. Moor, H. and M. Höchli. *The influence of high-pressure freezing on living cells*. in *7th Int. Congress of Electron Microscopy*. 1970.
60. Moor, H. and U. Riehle. *Snap-freezing under high pressure: a new fixation technique for freezeetching*. in *4th European Reg. Conf. of Electron Microscopy* 1968.
61. Moss, B., *Poxviridae: The Viruses and their Replication*, in *Fields Virology*, D. Knipe and P.M. Howley, Editors. 2001, Lippincott Williams & Wilkins: Philadelphia, Pa. p. 1849-2883.
62. Müller, M. and H. Moor. *Cryo-fixation of suspensions and tissues by propane jet freezing and high-pressure freezing*. in *42nd Ann. Meet. Electron Microsc.Soc. Am.* 1984. San Francisco: San Francisco Press, Inc, San Francisco.
63. Muranyi, W., et al., *Cytomegalovirus recruitment of cellular kinases to dissolve the nuclear lamina.* Science, 2002. **297**(5582): p. 854-7.
64. Murk, J.L., et al., *Influence of aldehyde fixation on the morphology of endosomes and lysosomes: quantitative analysis and electron tomography.* J Microsc, 2003. **212**(Pt 1): p. 81-90.
65. Murphy, E., et al., *Reevaluation of human cytomegalovirus coding potential.* Proc Natl Acad Sci U S A, 2003. **100**(23): p. 13585-90.
66. Newcomb, W.W., F.L. Homa, and J.C. Brown, *Involvement of the portal at an early step in herpes simplex virus capsid assembly.* J Virol, 2005. **79**(16): p. 10540-6.
67. Newcomb, W.W., et al., *Cell-free assembly of the herpes simplex virus capsid.* J Virol, 1994. **68**(9): p. 6059-63.
68. Palade, G.E., *A study of fixation for electron microscopy.* J Exp Med, 1952. **95**(3): p. 285-98.
69. Prichard, M.N., et al., *Human Cytomegalovirus UL97 Kinase Is Required for the Normal Intranuclear Distribution of pp65 and Virion Morphogenesis.* J Virol, 2005. **79**(24): p. 15494-502.
70. Rand, A., *Atlas Shrugged*. 35th Anniversary Edition ed. 1957, New York, USA: Penguin Putnam Inc.
71. Reimer, L., *Transmission Electron Microscopy*. 2nd ed, ed. P.W. Hawkes. Vol. 36. 1989, Berlin, Germany: Springer-Verlag.
72. Reynolds, A.E., et al., *Ultrastructural localization of the herpes simplex virus type 1 UL31, UL34, and US3 proteins suggests specific roles in primary envelopment and egress of nucleocapsids.* J Virol, 2002. **76**(17): p. 8939-52.
73. Riehle, U. and M. Höchli, *The theory and thechnique of high-pressure freezing*, in *Freeze-Etching Technique and Application*, E.L. Benedetti and P. Favard, Editors. 1973, Société Francaise de microscopie Eléctronique: Paris, France. p. 31-60.
74. Risco, C., et al., *Endoplasmic reticulum-Golgi intermediate compartment membranes and vimentin filaments participate in vaccinia virus assembly.* J Virol, 2002. **76**(4): p. 1839-55.
75. Roffman, E., et al., *Putative site for the acquisition of human herpesvirus 6 virion tegument.* J Virol, 1990. **64**(12): p. 6308-13.
76. Roizman, B. and D. Knipe, *Herpes simplex viruses and their replication*, in *Fields Virology*, D. Knipe and P.M. Howley, Editors. 2001, Lippincott-Raven Publishers: Philadelphia, PA. p. 2399-2460.

77. Rupp, B., et al., *Conditional cytomegalovirus replication in vitro and in vivo.* J Virol, 2005. **79**(1): p. 486-94.
78. Sanchez, V., et al., *Accumulation of virion tegument and envelope proteins in a stable cytoplasmic compartment during human cytomegalovirus replication: characterization of a potential site of virus assembly.* J Virol, 2000. **74**(2): p. 975-86.
79. Schierling, K., et al., *Human cytomegalovirus tegument protein ppUL35 is important for viral replication and particle formation.* J Virol, 2005. **79**(5): p. 3084-96.
80. Schmolke, S., et al., *The dominant phosphoprotein pp65 (UL83) of human cytomegalovirus is dispensable for growth in cell culture.* J Virol, 1995. **69**(10): p. 5959-68.
81. Shimoni, E. and M. Muller, *On optimizing high-pressure freezing: from heat transfer theory to a new microbiopsy device.* J Microsc, 1998. **192 (Pt 3)**: p. 236-47.
82. Simpson-Holley, M., et al., *Identification and Functional Evaluation of Cellular and Viral Factors Involved in the Alteration of Nuclear Architecture during Herpes Simplex Virus 1 Infection.* J Virol, 2005. **79**(20): p. 12840-51.
83. Sinzger, C., et al., *A simple and rapid method for preparation of viral DNA from cell associated cytomegalovirus.* J Virol Methods, 1999. **81**(1-2): p. 115-22.
84. Smith, J.D. and E. De Harven, *Herpes simplex virus and human cytomegalovirus replication in WI-38 cells. I. Sequence of viral replication.* J Virol, 1973. **12**(4): p. 919-30.
85. Sodeik, B., M.W. Ebersold, and A. Helenius, *Microtubule-mediated transport of incoming herpes simplex virus 1 capsids to the nucleus.* J Cell Biol, 1997. **136**(5): p. 1007-21.
86. Spaderna, S., et al., *Deletion of gpUL132, a structural component of human cytomegalovirus, results in impaired virus replication in fibroblasts.* J Virol, 2005. **79**(18): p. 11837-47.
87. Studer, D., M. Michel, and M. Muller, *High pressure freezing comes of age.* Scanning Microsc Suppl, 1989. **3**: p. 253-68; discussion 268-9.
88. Studer, D., et al., *Vitrification of articular cartilage by high-pressure freezing.* J Microsc, 1995. **179 (Pt 3)**: p. 321-32.
89. Tooze, J., et al., *Progeny vaccinia and human cytomegalovirus particles utilize early endosomal cisternae for their envelopes.* Eur J Cell Biol, 1993. **60**(1): p. 163-78.
90. Varnum, S.M., et al., *Identification of proteins in human cytomegalovirus (HCMV) particles: the HCMV proteome.* J Virol, 2004. **78**(20): p. 10960-6.
91. Wagner, M., et al., *Comparison between human cytomegalovirus pUL97 and murine cytomegalovirus (MCMV) pM97 expressed by MCMV and vaccinia virus: pM97 does not confer ganciclovir sensitivity.* J Virol, 2000. **74**(22): p. 10729-36.
92. Walther, P. and A. Ziegler, *Freeze substitution of high-pressure frozen samples: the visibility of biological membranes is improved when the substitution medium contains water.* J Microsc, 2002. **208**(Pt 1): p. 3-10.
93. White, D.L., et al., *The chemical nature of osmium tetroxide fixation and staining of membranes by x-ray photoelectron spectroscopy.* Biochim Biophys Acta, 1976. **436**(3): p. 577-92.
94. Wild, P., et al., *Impairment of nuclear pores in bovine herpesvirus 1-infected MDBK cells.* J Virol, 2005. **79**(2): p. 1071-83.

95. Wild, P., et al., *Enhanced resolution of membranes in cultured cells by cryoimmobilization and freeze-substitution.* Microsc Res Tech, 2001. **53**(4): p. 313-21.
96. Williams, R.C., *High-resolution electron microscopy of the particles of tobacco mosaic virus.* Biochim Biophys Acta, 1952. **8**(3): p. 227-44.
97. Winkler, M., S.A. Rice, and T. Stamminger, *UL69 of human cytomegalovirus, an open reading frame with homology to ICP27 of herpes simplex virus, encodes a transactivator of gene expression.* J Virol, 1994. **68**(6): p. 3943-54.
98. Wolf, D.G., et al., *Distinct and separate roles for herpesvirus-conserved UL97 kinase in cytomegalovirus DNA synthesis and encapsidation.* Proc Natl Acad Sci U S A, 2001. **98**(4): p. 1895-900.
99. Wolfstein, A., et al., *The inner tegument promotes herpes simplex virus capsid motility along microtubules in vitro.* Traffic, 2006. **7**(2): p. 227-37.

6 Acknowledgments

First I want to thank Paul Walther for accepting me as PhD student and giving me the freedom to work independently. You were a great mentor and an excellent friend.

Many thanks go to Thomas Mertens for guidance, great support and funding over these years. I highly appreciated your constructive criticism in our discussions

I further want to thank all my colleagues in both the EM and the virology lab for their support.

I would also like to thank all external collaborators for their support and discussions: Michael Winkler in Kiel; Brigitte Rupp, Zsolt Ruzsics and Ulrich Koszinowski in Munich; Jacomine Krijnse-Locker, Heidelberg; Frank Fleischer and Volker Schmidt in Ulm and Michael Mach in Erlangen.

I am also very grateful to Martin Müller, formerly in Zürich, for the discussions during my studies and my diploma thesis. I learned a lot about science and life.

As greatest reverence I have to offer to an author that has changed my vision of life, I am proud to state:

"I SWEAR BY MY LIFE AND MY LOVE OF IT THAT I WILL NEVER LIVE FOR THE SAKE OF ANOTHER MAN, NOR ASK ANOTHER MAN TO LIVE FOR MINE."

[70]

For Zorica I just want to summarise my feelings by a quote, since plain words are not enough:

"…there was still one response, the greatest, that she had missed. She thought: To find a feeling that would hold, as their sum, as their final expression, the purpose of all the things she loved on earth… To find a consciousness like her own, who would be the meaning of her world, as she would be of his… " [70]

This is what I found in you.